
**Performance Analysis of Si-Based Ultra-Shallow Junction
Photodiodes for UV Radiation Detection**

PROEFSCHRIFT

ter verkrijging van de graad van doctor
aan de Technische Universiteit Delft,
op gezag van de Rector Magnificus prof. ir. K.C.A.M. Luyben,
voorzitter van het College voor Promoties,
in het openbaar te verdedigen op maandag 15 april 2013 om 15:00 uur

door

Lei SHI

Master of Science in Electrical Engineering
geboren te Harbin, China.

Dit proefschrift is goedgekeurd door de promotor:

Prof. dr. ir. A. J. P. Theuwissen

Copromotor

Dr. S. Nihtianov

Samenstelling promotiecommissie:

Rector Magnificus,	voorzitter
Prof. dr. ir. A. J. P. Theuwissen	Technische Universiteit Delft, promotor
Dr. S. Nihtianov	Technische Universiteit Delft, copromotor
Prof. dr. K. Ozanyan	The University of Manchester
Prof. dr. ir. J.P.H. Benschop	Universiteit Twente
Prof. dr. G.Q. Zhang	Technische Universiteit Delft
Prof. dr. ir. G.C.M. Meijer	Technische Universiteit Delft
Dr. F. Scholze	Physikalisch-Technische Bundesanstalt

Lei Shi,
Performance Analysis of Si-Based Ultra-Shallow Junction Photodiodes for UV
Radiation Detection,
Ph.D. Thesis, Delft University of Technology,
with summary in Dutch.

ISBN: 978-94-6186-142-9

Printed by:
Ipskamp Drukkers B.V.
Josink Maatweg 43
7545 PS Enschede
The Netherlands

Copyright © 2013 by Lei Shi
Cover design: Lei Shi

All rights reserved. No part of this publication may be reproduced or distributed in any form or by any means, or stored in a database or retrieval system, without the prior written permission of the author.

PRINTED IN THE NETHERLANDS

To my parents

Table of Contents

Chapter 1 Introduction.....	1
1.1 Application challenges.....	1
1.2 Main questions.....	2
1.3 A potential solution.....	3
1.4 Objectives.....	3
1.5 Organization of the thesis.....	3
References.....	6
Chapter 2 Si-Based UV Photodiodes.....	8
2.1 Short overview of UV photodetectors.....	8
2.2 Silicon photodiodes.....	10
2.2.1 Basic photodiode structure.....	10
2.2.2 Operating principle.....	11
2.2.3 Important optical characteristics.....	11
2.3 Main challenge of Si-based photodiodes in UV photon detection.....	13
2.4 Theoretically attainable responsivity of Si-based photodetectors in the UV spectral range.....	14
2.5 Ideal model of Si-based photodiodes.....	15
2.6 Performance of state-of-the-art silicon UV detectors.....	17
2.7 Si-based pure boron photodiode (PureB-diode) technology.....	22
2.7.1 Typical electrical performance.....	24
2.7.2 Optical performance in the EUV spectral range.....	25
2.8 Summary.....	26
References:.....	28
Chapter 3 Surface Properties of PureB-diodes.....	31
3.1 Pure boron CVD technology and diode fabrication.....	31
3.2 Surface oxidation.....	33
3.3 Uniformity of the amorphous boron (α -boron) coverage.....	35
3.4 Post-processing thermal annealing.....	37
3.5 Summary.....	37

References:.....	39
Chapter 4 Surface Charge-Collection Efficiency (CCE) of PureB-Diodes..	40
4.1 Optical test setup.....	40
4.2 DUV/VUV optical performance of PureB-diodes	40
4.3 Surface charge-collection effect.....	42
4.3.1 Surface charge-collection phenomenon of PureB-diodes.....	42
4.3.2 Doping-gradient-induced surface charge collection effect.....	46
4.4 Summary	51
References:.....	53
Chapter 5 Response Time Characterization and Series Resistance Optimization.....	55
5.1 High surface sheet resistance	55
5.2 Response time versus variational irradiation area.....	57
5.3 Series resistance optimization.....	62
5.4 Summary	66
Reference:	67
Chapter 6 Stability Characterization	68
6.1 Possible UV-induced defects in silicon photodiodes	68
6.2 Optical performance stability.....	68
6.2.1 DUV/VUV stability	68
6.2.2 EUV stability	74
6.2.3 Optical performance stability versus surface charge-collection effect.....	76
6.2.4 Photon-emission current induced instability.....	77
6.3 Dark current degradation	82
6.4 Summary	87
Reference:	89
Chapter 7 Robustness to Detrimental Working Conditions	92
7.1 Carbon contamination in vacuum	92
7.2 Hydrogen radical (H^*) cleaning	93
7.2.1 Filament-enhanced H^* generation system.....	94
7.2.2 Plasma-generated H^* technique	96

7.3 Stability investigation under H [*] exposure	98
7.3.1 Robustness of the diode active area	98
7.3.2 H [*] -induced defects along the diode perimeter	101
7.4 Improved passivation	108
7.5 Summary	111
Reference:	112
Chapter 8 Conclusions.....	114
8.1 Strategies for creating high-performance Si-based photodiodes.....	114
8.2 Major research achievements.....	115
8.3 Ongoing and potential future work	116
Reference:	119
Summary	120
Samenvatting	123
Appendix	127
List of Publications.....	128
Acknowledgements	131
About the Author.....	133

Chapter 1 Introduction

1.1 Application challenges

Nowadays, many scientific and industrial applications demand high performance ultraviolet (UV) photodetectors [1][2]. Such applications are: medical imaging (280 nm – 400 nm spectral range) [3], protein analysis and DNA sequencing (240 nm – 300 nm spectral range) [4], forensic analysis (250 nm – 300 nm spectral range) [5], disinfection and decontamination (240 nm – 280 nm spectral range) [6], space observation [7], etc.

One of the most challenging applications of UV radiation detection is in the microelectronics industry. According to the International Technology Roadmap for Semiconductors (ITRS) [8], deep-UV (DUV)* [9] lithography systems, which use an ArF excimer laser with a radiation wavelength of 193 nm, will remain the “work horse” of lithography for many years ahead, together with 13.5 nm extreme-UV (EUV) lithography. Thus, a growing interest in UV radiation detection at wavelengths between 1 nm and 200 nm (DUV/VUV/EUV spectral ranges) has been significantly triggered by advances in lithography equipment, since several sensors are used for optimizing the imaging performance. Therefore, the development and the fabrication of high-performance detectors for UV radiation are becoming important to the future of nanoelectronics manufacturing.

The **key requirements** of such sensors are:

High UV sensitivity

To achieve high sensitivity, any quantum efficiency loss due to photon reflection/absorption in the front window of the detector, or recombination of photo-generated carriers in the detector, should be prevented. Therefore, for semiconductor-based UV detectors, the optical performance can be strongly affected by the capping layer thickness, material purity and doping techniques.

High stability

The stability of the performance is essential when using UV detectors in applications such as lithography systems. For instance, in next-generation lithography systems, the detectors should offer long-term radiation hardness, since they will receive very high levels of exposure reaching 100 kJ/cm² DUV exposure,

*: Divisions of the UV spectral range are listed in the Appendix on p.127. [9]

and 1 MJ/cm² EUV exposure. At the same time, the detectors are mounted in difficult to reach locations and operated under special conditions (in vacuum for EUV system). Therefore, in order to avoid high maintenance costs and throughput decline, the detectors should operate reliably within the performance specifications during the lifetime of the machine, which is 10 years.

High speed

In a lithography machine, the frequency of the pulsed-light source can be relatively high, while the duration of the pulses can range from a few picoseconds to a few hundred nanoseconds. This means that UV detectors in alignment and dose control systems must have a high operational speed in order to react to each light pulse.

In addition to the basic factors mentioned above, ***durability in detrimental environments*** also has to be considered. In many applications, the sensitive surface of a UV detector is affected by harsh conditions that can deteriorate the electrical/optical performance. For example, in IC fabrication, when the photoresist reacts to UV light, it releases hydrocarbons, such as C₂H₂, which might cause a carbon layer to form on the active area of the detector, reducing the sensitivity of the device. Removing the contaminants appears to be an aggressive process for the detector itself. Thus, the sensor needs to be covered with dedicated capping layers which protect the sensitive area during the cleaning process without deteriorating its optical performance, for example, by absorbing UV photons.

Furthermore, an ***IC-compatible technology*** for producing the photodiodes is also highly preferred. In this way, not only the electronic interface circuit but also other sensors (such as integrated temperature sensors used to compensate the temperature dependence of the detector output signal) can be integrated on a single chip to realize a smart sensor system.

1.2 Main questions

A broad literature study on commercially available state-of-the-art UV detector technologies showed that no single UV detector can fulfill all the key requirements listed above in the full UV range. While a few promising solutions have already been reported in the EUV spectral range, in the VUV and DUV ranges the performance of the existing detectors is quite unsatisfactory. (More details of this comparative study are presented in Chapter 2).

This conclusion leads to the following two questions:

- (i) is there a semiconductor-based photodetector structure which can provide high and stable optical performance over the full UV range, and especially in the DUV/VUV range?
- (ii) which of the currently available semiconductor technologies can provide such a structure?

1.3 A potential solution

A newly developed silicon-based ultra-shallow junction photodiode (PureB-diodes) fabricated by a pure boron chemical vapor deposition (CVD) technology [10], has demonstrated a near-theoretical responsivity in the EUV spectral range (the measured responsivity at a 13.5 nm wavelength is 0.265 A/W) [11][12][13][14]. This superior optical performance is realized by: unique nanometer-thin boron capping layer; nanometer-deep p-n junction; defect-free doping technique. Due to these promising features, PureB-diode technology is considered to be a promising solution for developing advanced UV photodetectors.

1.4 Objectives

The objective of the thesis is to investigate theoretically and experimentally the performance of Si-based PureB-diodes as radiation detectors in the full UV spectral range. The main research topics are:

- ◆ Investigation of the surface charge collection mechanism within the highly doped p^+ silicon region of PureB-diodes;
- ◆ Stability characterization of PureB-diodes under VUV/EUV radiation;
- ◆ Durability evaluation of PureB-diodes in detrimental working conditions for potential industrial applications;
- ◆ Presenting a strategy for designing a high performance Si-based photodiode for UV radiation.

1.5 Organization of the thesis

In Chapter 2, state-of-the-art Si-based UV detectors are reviewed and compared based on a proposed ideal model of Si-based photodiodes. The main advantages of PureB-diodes are presented.

In Chapter 3, the basic fabrication process, the device structure and notably the surface properties of PureB-diodes are introduced in detail.

In Chapter 4, the optical sensitivity of PureB-diodes is characterized in DUV/VUV spectral range. Moreover, distinctive high surface charge-collection efficiency (CCE) within the highly doped p^+ silicon region of PureB-diodes is validated.

In Chapter 5, the impact of the series resistance on the response time of PureB-diodes is studied and solutions for its optimization are proposed, while maintaining good optical UV sensitivity.

In Chapter 6, the radiation hardness of PureB-diodes is evaluated in the DUV/VUV and EUV spectral ranges. Mechanisms behind the radiation-induced degradation are analyzed. Possible solutions for designing high-stability Si-based DUV/VUV and EUV photodiodes are discussed.

In Chapter 7, with a focus on certain industrial applications, the durability of PureB-diodes in detrimental working conditions is evaluated. The damage mechanism is studied and improved device structures are proposed.

Lastly, in Chapter 8 the conclusions of the presented research work are drawn and suggestions are made for future work.

The basic structure of this thesis is described in Fig. 1.1.

Chapter 1 Introduction

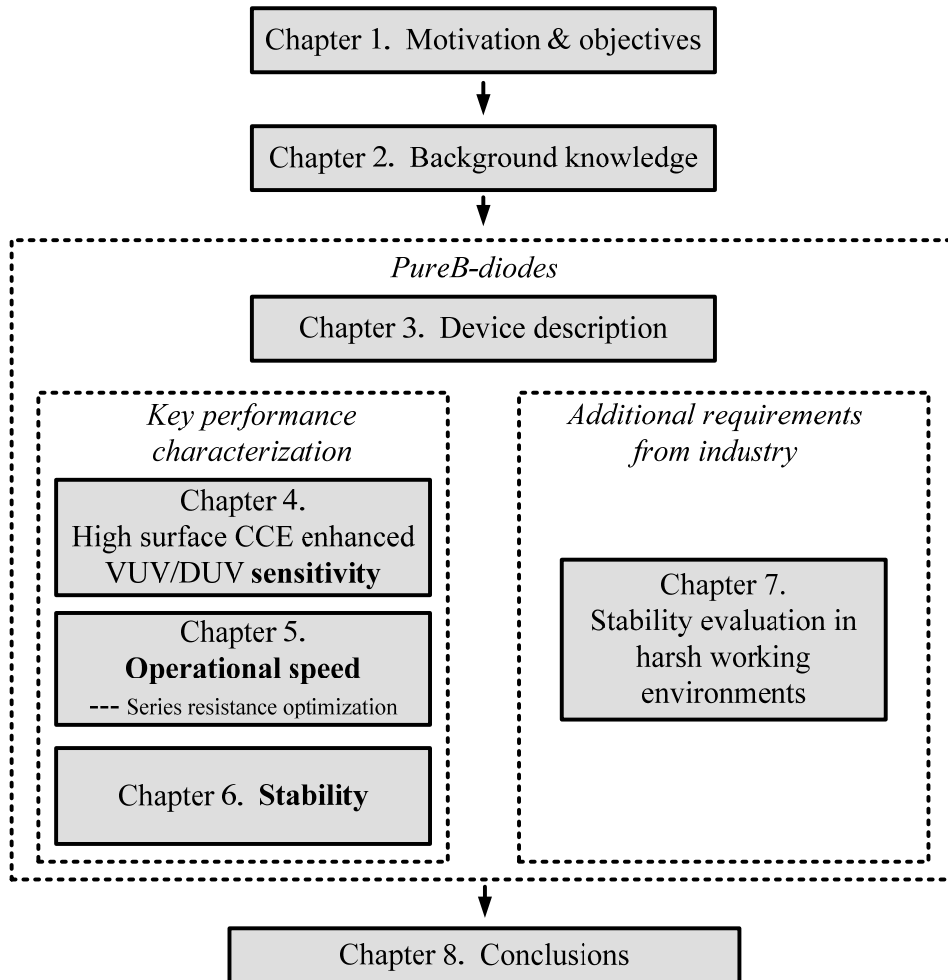


Fig. 1.1 Basic structure of the thesis

References

- [1] E. Monroy, F. Omnès and F. Calle, “Wide-bandgap semiconductor ultraviolet photodetectors”, *Semiconductor Science and Technology*, vol. 18, no. 4, pp. 33-51, Apr. 2003.
- [2] M. Razeghi and A. Rogalski, “Semiconductor ultraviolet detectors”, *J. Appl. Phys.*, vol. 79, no. 10, pp. 7433-7473, Jan. 1996.
- [3] W. Grundfest, “Overview of medical applications and cardiovascular intervention”, *Proc. Quantum Electronics and Laser Science Conference*, pp. 187, May 1999.
- [4] A. Karczewska and A. Sokolowska, “Materials for DNA sequencing chip”, *Abstract book of 3rd International Conference on Novel Applications of Wide Bandgap Layers*, pp. 176, June 2001.
- [5] W.A. Smith and K.P. Lam, “Exploratory analysis of UV-Vis absorption spectra”, *Proc. 3rd International Congress on Image and Signal Processing (CISP2010)*, pp. 3359-3363, Oct. 2010.
- [6] G. Knight, “Monitoring of ultraviolet light sources for water disinfection”, *Proc. 39th IEEE Industry Applications Conference*, pp. 1016-1018, Oct. 2004.
- [7] P. E. Malinowski et al., “10 μm pixel-to-pixel pitch hybrid backside illuminated AlGaIn-on-Si imagers for solar blind EUV radiation detection”, *Proc. IEEE International Electron Devices Meeting (IEDM)*, pp. 348-351, Dec. 2010.
- [8] International Technology Roadmap for Semiconductors: Lithography, 2007 Edition. Available at: <http://www.itrs.net>.
- [9] ISO 21348, Process for Determining Solar Irradiances. Available at: http://www.spacewx.com/ISO_solar_standard.html.
- [10] F. Sarubbi, L. K. Nanver and T. L. M. Scholtes, “CVD delta-doped boron surface layers for ultra-shallow junction formation”, *ECS Transactions*, vol. 3, no. 2, pp. 35-44, Nov. 2006.
- [11] F. Sarubbi, L. K. Nanver, T. L. M. Scholtes, S. N. Nihtianov and F. Scholze, “Pure boron-doped photodiodes: a solution for radiation detection in EUV lithography”, *Proc. IEEE 38th European Solid-State Device Research Conference (ESSDERC)*, pp. 278-281, Sep. 2008.
- [12] L. Shi, F. Sarubbi, S. N. Nihtianov, L. K. Nanver, T. L. M. Scholtes and F. Scholze, “High performance silicon-based extreme ultraviolet (EUV) radiation detector for industrial application”, *Proc. 35th Annual Conference of the IEEE Industrial Electronics Society (IECON)*, pp. 1891-1896, Nov. 2009.
- [13] F. Scholze, H. Rabus and G. Ulm, “Mean energy required to produce an electron-hole pair in silicon for photons of energies between 50 and 1500 eV”, *J. Appl. Phys.*, vol. 84, no. 5, pp. 2926-2939, Sept. 1998.

- [14] F. Scholze, H. Henneken, P. Kuschnerus, H. Rabus, M. Richter and G. Ulm
“Determination of the electron-hole pair creation energy for semiconductors from the
spectral responsivity of photodiodes”, *Nuclear Instruments and Methods in Physics
Research*, vol. 439, no. 2-3, pp. 208-215, 2000.

Chapter 2 Si-Based UV Photodiodes

In this chapter, first a comparative overview of all existing ultraviolet (UV) photodetectors is presented based on the performance requirements defined in Chapter 1. The subsequent analyses are restricted to silicon-based devices, due to their superior characteristics. The optical performance of commercially available state-of-the-art Si-based UV photodiode is reviewed, and their advantages and drawbacks are summarized in comparison with a proposed ideal model of Si-based photodiode. It has been found that a recently developed silicon-based ultra-shallow junction diode, fabricated by a pure boron (PureB) CVD technology, best fits the structure of the ideal model, and provides excellent opportunities for the design and fabrication of high-sensitivity radiation-hard photodiodes in the full UV spectral range.

2.1 Short overview of UV photodetectors

Fig. 2.1 shows a classification diagram of the existing UV photodetectors together with key arguments (*in italics*) which lead to the conclusion that silicon photo detectors are the superior option. The arguments provided are derived from the performance requirements defined in Chapter 1: high sensitivity, high operational speed, high stability, compact design, and IC-compatibility.

As illustrated in Fig. 2.1 [1][2], photoelectric-based detectors are more attractive than photographic-based detectors due to their higher sensitivity, better linearity and higher operational speed. On the second step of the diagram, semiconductor-based devices are chosen for their high stability and outstanding linearity. On the next step, photovoltaic detectors provide advantages in terms of sensitivity and operational speed, compared to photoconductive detectors. The last choice is made between devices based on silicon and wide-band gap (WBG) semiconductors (diamond, SiC, III-nitrides, and some III-V compounds). The final conclusion is that Si-based photodetectors are superior with respect to performance, cost and IC-compatibility.

It is important to clarify that WBG semiconductor materials have some inherent advantages, such as high-strength chemical-bond structures and intrinsic visible-blindness. This is why in the past decades, WBG semiconductors became attractive for making UV photodetectors, especially for harsh working conditions [2][3]. However, there are still a number of reasons why the full potential of WBG semiconductor-based devices cannot be exploited sufficiently. For example:

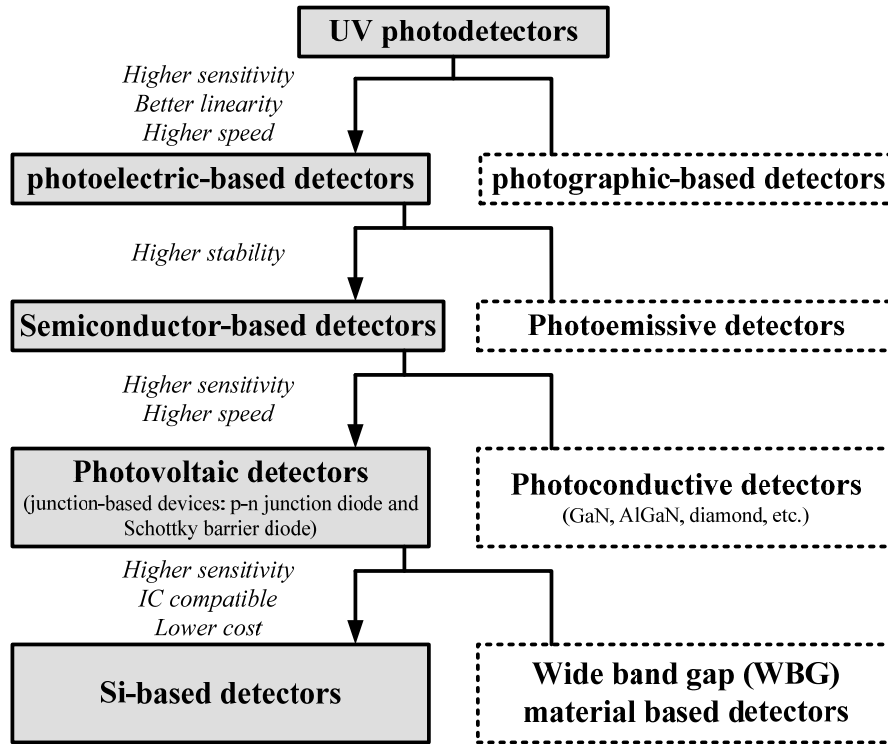


Fig. 2.1 Classification of solid-state UV photodetectors [1][2].

High activation energy of dopants: Very large quantities of the doping impurities are needed to achieve reasonable carrier concentrations, and this leads to a severe reduction of the carrier mobility [2].

Undeveloped technology: Another challenge is the lack of a reliable technology for the fabrication of contacts [2][3]. In this field, the major difficulty is the realization of low-resistance ohmic contacts. This is related to two main limitations: the large barrier heights associated with most metalizations, and the above-mentioned low doping levels.

Poor crystal quality: The lack of high-quality substrates for homoepitaxy or other lattice-matched substrates leads to materials with a high density of dislocations and grain boundaries [2][3]. These structural defects induce deleterious effects on the device performance, such as an enhancement of visible detection and leakage currents. Although impressive improvements have been achieved in making high quality bulk of WBG materials (Such as SiC and GaN) [4][5][6], as is shown in Table 2.1, silicon still offers an unrivaled cost advantage.

In short, although WBG semiconductors show attractive advantages and may become popular materials in the future, currently, for most applications of interest, silicon holds the dominant position in UV-detector fabrication.

TABLE 2.1 COST OF TYPICAL WBG MATERIAL SUBSTRATES COMPARING WITH SILICON [7]

Substrate material	Bulk GaN	SiC	Sapphire	Silicon
Available wafer size	2'' to 3''	4'' to 6''	Up to 8''	Any size
Cost [€/cm ²]	100	10	1	0.1

2.2 Silicon photodiodes

Due to their simple structure and the excellent linearity of the transfer characteristic (output current versus incident light), photodiodes have become the most commonly used Si-based photodetectors [1][8]. In this section, the device structure and the basic operation principle of Si-based photodiodes are reviewed.

2.2.1 Basic photodiode structure

Photodiodes are fabricated based on single crystal silicon wafers similar to those used for the manufacturing of integrated circuit components. One major difference is that photodiodes require a high quality (i.e. low concentration of defects) silicon substrate, which is important for achieving high optical sensitivity [1][8].

Fig. 2.2 shows three basic structures of Si-based photodiodes: Schottky barrier diode, n-on-p junction diode and p-on-n junction diode [1]. The Schottky barrier diode is built by a metal-on-semiconductor junction; the p-on-n (p-n) and n-on-p (n-p) junction diodes are formed at the boundary between p-type and n-type semiconductor, which are created in a single crystal by doping.

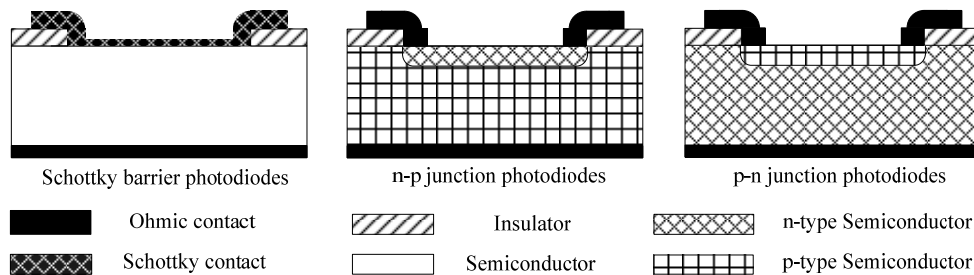


Fig. 2.2 Basic structures of Si-based photodiodes.

2.2.2 Operating principle

The working principle of Si-based photodiodes is explained based on a p-n (the p-region is above the n-region) junction diode structure. A typical cross section of a p-n junction photodiode is presented in Fig. 2.3a in more detail. An n-type silicon substrate is the starting material. A highly doped p⁺ layer is formed on the front surface of the device by thermal diffusion or ion implantation with the appropriate doping material. The interface between the p⁺ region and the n-type silicon substrate is known as a p-n junction. To avoid undesirable absorption of the incident radiation, the front metal contact is normally placed at the edge of the active junction area to form what is often referred to as a “ring electrode”. The entire back is coated with a contact metal. For a p-on-n photodiode, as shown in Fig. 2.3a, the front contact is the anode and the back contact is the cathode. Coating layers can be optionally deposited on the photodiode surface for protection or to serve as pass-band filters /anti-reflection layers.

Photodiodes are usually operated under zero bias voltage or reverse bias voltage in a “current source” mode. A reverse bias voltage is a negative voltage on the anode with respect to the cathode (depicted in Fig. 2.3a). When incident photons are absorbed in silicon, a major phenomenon is to transfer their energy to electrons and in this way to create electron-hole pairs. If this happens in the depletion region, the photon-generated charge is separated by the built-in electric field (E_{bi}) and is collected in the form of external photocurrent by connecting the photodiode to a closed electric loop. Fig. 2.3b presents a typical I-V curve of a photodiode with illumination (photocurrent) and without illumination (dark current). An equivalent electric model of a photodiode is shown in Fig. 2.3c: besides an “ideal diode”, I_p refers to the dark current (leakage current); I_p is the photocurrent under illumination; and I_n is the noise current. Next, C_j is the junction capacitance; R_{sh} is the shunt resistance; R_s is the series resistance; and R_L is the load.

2.2.3 Important optical characteristics

Responsivity (R) is normally used to describe the sensitivity of a photodiode. It is defined as the ratio of the photocurrent to the incident light power at a given wavelength. The unit is [A/W] (Ampere per Watt) or [C/J] (Coulomb per Joule).

Quantum efficiency (QE) is defined as the percentage of the photo-generated charge that contribute to the photocurrent. It is related to the responsivity by Eq. (2.1):

$$QE = \frac{R_{Observed}}{R_{ideal}} \quad (2.1)$$

Next to responsivity and quantum efficiency, two other parameters — Noise Equivalent Power (NEP) and Detectivity (D) — are introduced to evaluate the

minimum detectable light power of the photodiode. The NEP is the optical input power for which the signal-to-noise ratio is equal to one. D^* is the reciprocal of NEP [1][2].

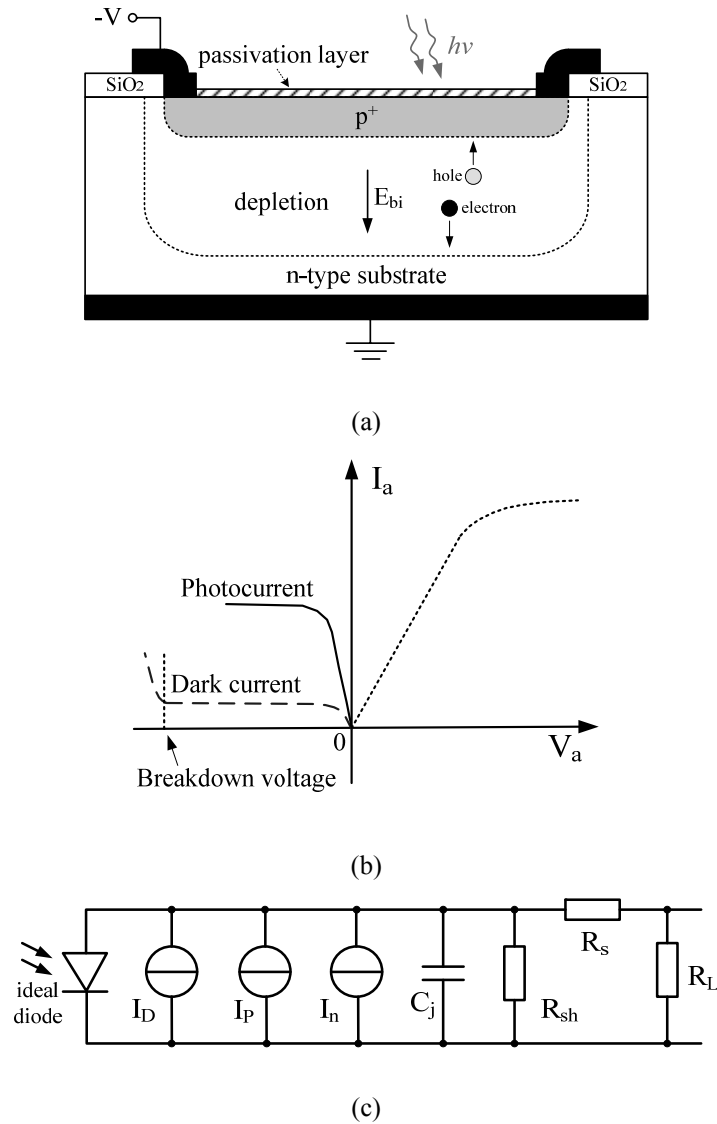


Fig. 2.3 (a) Cross section of a typical Si-based photodiode and the basic photo-generated charge-collection mechanism; (b) I-V characteristic of a photodiode, V_a is the anode voltage and I_a is the anode current; (c) equivalent electric model of a photodiode.

2.3 Main challenge of Si-based photodiodes in UV photon detection

Fig. 2.4a shows the attenuation length (penetration depth) of UV light in silicon [8][9][10]. The most challenging part of the UV spectral range for Si-based photodetectors is between 100 ~ 300 nm (DUV and part of the VUV spectral ranges), since the attenuation length of photons from these spectral ranges in silicon (and

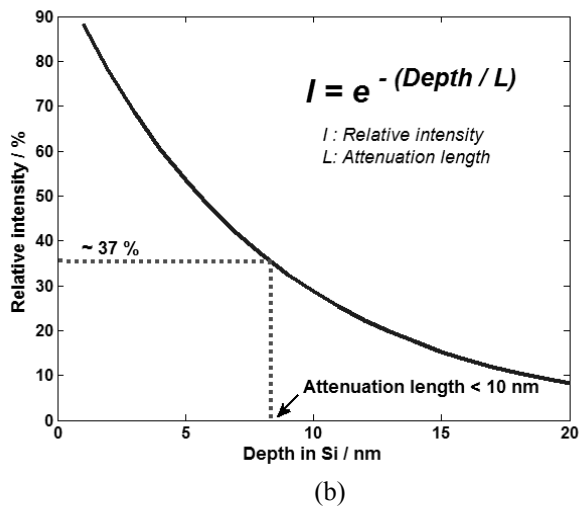
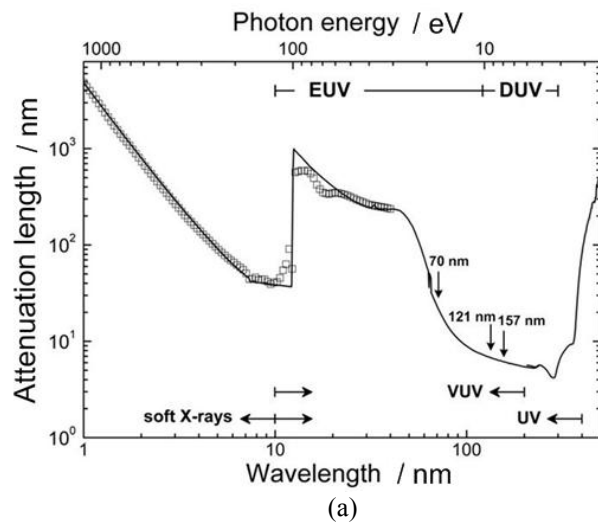


Fig.2.4 (a) Attenuation length (penetration depth) in Si vs. incident radiation wavelength/photon energy [8][9][10]; (b) The relation between the incident DUV radiation intensity and depth in Si, 'L' (in the insert equation) is the attenuation length. Fig.2.4a is reproduced based on Fig. 7, on page 213 of [8].

practically in most of other solid-state materials) is extremely small: less than 10 nm. This means that more than 60% of the incident photons are absorbed in the first 10 nm in silicon, as depicted in Fig. 2.4b. For conventional Si-based p-n junction photodiodes, with junction depth much greater than 10 nm, all the incident photons are absorbed before they reach the depletion region. The photon-generated electron-hole pairs are not separated and they eventually recombine without producing external photocurrent. Therefore, it is very difficult to achieve a high DUV/VUV responsivity with conventional deep junction Si-based photodiodes, which are designed for visible-light detection.

2.4 Theoretically attainable responsivity of Si-based photodetectors in the UV spectral range*

Fig. 2.5 presents the spectral responsivity of an ideal Si-based lossless system (100% quantum efficiency) over the whole UV spectral range [11][12][13]. The upper solid line shows the upper limit set by the internal quantum efficiency of silicon. In the long-wavelength limit (dashed line), one electron per absorbed photon is created; in the short-wavelength limit (dotted line), a constant energy of $W \approx 3.66$ eV is needed to create one electron-hole pair, which leads to a constant responsivity of $R = 1/W \approx 0.273 \text{ A W}^{-1}$. The lower solid line shows the spectral responsivity when the external reflection at the silicon surface is taken into account.

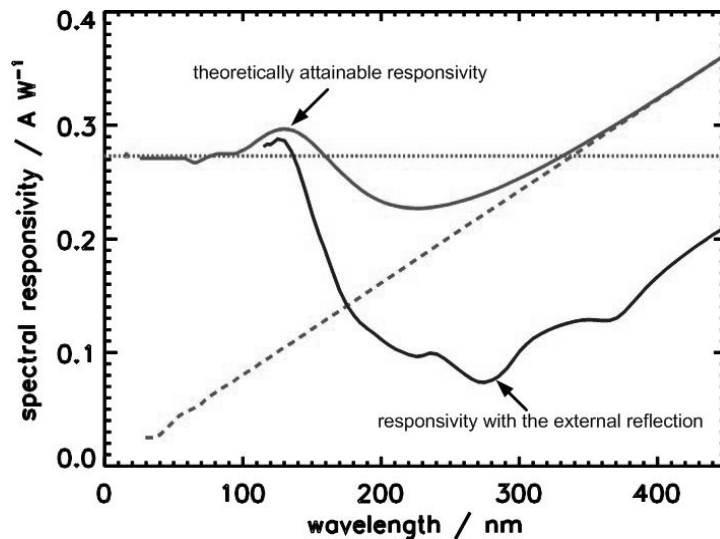


Fig. 2.5 Ideal spectral responsivity of Si-based photodetectors [11][12][13]. *The figure is reproduced from [13].*

*: Section 2.4 was accomplished with the help of Dr. F. Scholze and Dr. A. Gottwald, PTB.

2.5 Ideal model of Si-based photodiodes

As clarified in Chapter 1, the primary performance requirements of a UV photodetector defined in this thesis are: **high sensitivity, high stability and high operational speed (i.e. short response time)**. Regarding these key requirements, an ideal structure of Si-based photodiodes is proposed in this section.

High UV sensitivity

Since responsivity is usually used as a primary factor to determine the sensitivity of a photodetector, the ideal structure should first of all guarantee the theoretically attainable responsivity. The measured photocurrent (Fig. 2.3b) is a result of removing the photo-generated charge from the effective charge-collection zone (which normally is the diode depletion region). As depicted in Fig. 2.6, above the depletion region there are two additional layers: the passivation layer (t_1) and the highly doped Si region (t_2). Obviously, to achieve a maximum responsivity, all photo-generated charge should be created in the effective charge collection zone. Therefore, the passivation and the highly-doped Si regions should be absolutely transparent for the incidence light, or, alternatively, absolutely thin so that no incident photon is lost in these layers. In addition, all photon-generated charge in the charge-collection zone has to be removed from the photodiode. This demands a defect-free p-n junction, which can minimize the recombination of photo-generated charge after the illumination. Moreover, the depletion zone (t_3) has to be sufficiently wide. In this way, no photon can pass through the depletion zone and reach the substrate below it.

The Noise Equivalent Power (NEP) and the Detectivity (D), which represent the

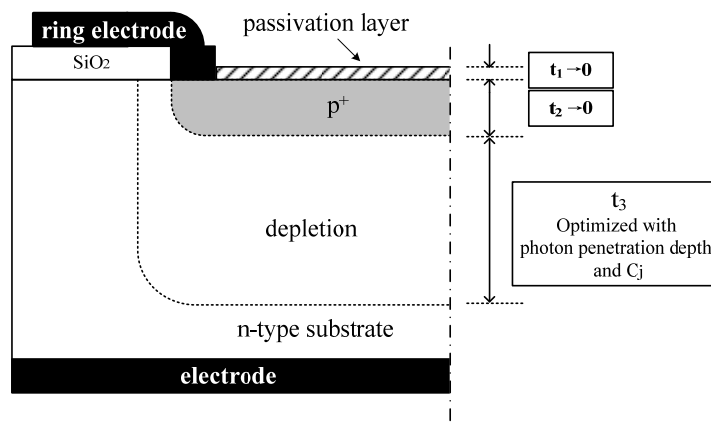


Fig. 2.6 Ideal structure of a Si-based photodiode

minimum detectable light power, depend on the noise level of the photodiode. In the equivalent electric model (see Fig. 2.3c), there are three noise sources: I_n – representing the shot noise which is the statistical fluctuation in both the photocurrent and the dark current, R_{sh} and R_s – generating thermal noise. To eliminate the noise completely, I_n and R_s need to have zero values, and R_{sh} has to be infinitely high.

High operational speed

In many applications, dynamic performance is an important parameter. For a large junction area photodiode, the time constant $R_s \times C_j$ sets the lower limitation of the diode's response time, and consequently the operational speed. Thus, using small values for R_s and C_j is the most direct way to achieve a high operational speed. For a large junction area diode (for example, a circle or square shaped junction area of a few or more mm^2), due to the use of a “ring electrode” forcing the photocurrent to travel horizontally through the layer stack above the p-n junction (p^+ and the passivation layer in Fig. 2.2a) [14][15], R_s is dominated by the resistivity of this stack. Therefore, in the “ideal model” shown in Fig. 2.6, a high conductivity (low sheet resistance) is required for at least one of the layers in the capping stack. A wide depletion helps to reduce the C_j . Besides a larger reverse bias voltage, this can be realized by adding an intrinsic silicon layer between p region and n region (p-i-n diode structure).

High stability

Since any radiation-induced defect in the photodiode's depletion region can lead to a recombination of the photon-generated charge, a UV-radiation-hard p-n junction is a prerequisite for fabricating high stability UV photodiodes.

In addition, to maintain a stable optical performance, the layer stack above the depletion zone needs to have a fixed potential with respect to the ring electrode. Varying this potential will result in parasitic-internal electric fields, which, if opposing the electric field in the depletion zone, might divert part of the photon-generated charge carriers in the wrong direction. Subsequently the diverted charge carriers will eventually recombine and will be lost, leading to lower internal quantum efficiency (IQE) and deteriorated responsivity. For example, one commonly observed phenomenon which leads to varying of the surface potential is when the top passivation layer is charged as a result of the external photoelectron emission effect: when the incident high energy photons reach the surface of the device, electrons are kicked out resulting in excess of holes and hence the surface being positively charged. [16][17]. To prevent the creation of a surface positive charge, the escaped electrons need to be compensated by electrons from the ring electrode. To facilitate and speed up this process, again as in the case with the high operational speed, the sheet resistance of the stack above the p-n junction needs to be low.

Based on above analysis, an ideal structure of Si-based UV photodiodes which is optimized for high sensitivity, high stability and high operational speed can be summarized in Fig. 2.6, Fig. 2.7 and Table 2.2.

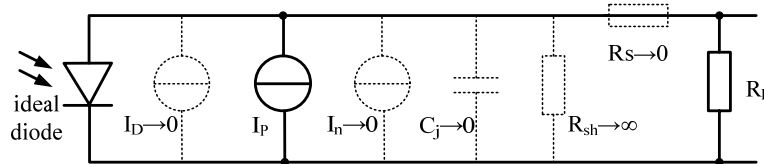


Fig. 2.7 equivalent circuit of an ideal photodiode.

TABLE 2.2 MAIN CHARACTERISTICS OF AN IDEAL SILICON-BASED PHOTODIODE.

Key requirement	Related diode features	Ideal structure
Responsivity	Passivation layer thickness	0
	Junction depth	0
	Depletion width	Optimized by the photon attenuation length
Detectivity	Dark current	0
	Shunt resistance	∞
Operational speed	Series resistance	0
	Junction capacitance	0
Stability	Passivation layer	Oxide-free, high-conductivity

2.6 Performance of state-of-the-art silicon UV detectors

In the following section, the optical performance of representative Si-based UV photodiodes is reviewed. In comparison with the proposed ideal model, the advantages and drawbacks of different diode structures are summarized.

Schottky barrier diode

Compared to other diode structures, the Schottky barrier diode meets the minimum junction depth criterion: the depletion region starts from the Si surface. This “zero-depth” depletion region is in accordance with the ideal structure presented in Fig. 2.6. Also, the conductive metal layer on the diode surface prevents the creation of parasitic electric fields due to charging, and in this way provides very high stability of the responsivity. However, the strong absorption in the metal

capping layer, which is required for the creation of the Schottky barrier, significantly reduces the responsivity throughout the UV spectral range. Fig. 2.8 shows a High Resolution Transmission Electron Microscopy (HRTEM) image of a state-of-the-art PtSi-nSi Schottky barrier diode published in [18]. This diode is fabricated on *n*-type Si (100) wafers. The Pt films are deposited by magnetron sputtering in an ordinary high vacuum system in Ar plasma, and the silicide is formed after deposition annealing. The resulting films, which were less than 10-nm-thick, were partially epitaxially to the (100) silicon, forming an abrupt, contamination-free, laterally uniform interface between the PtSi film and the silicon substrate [18].

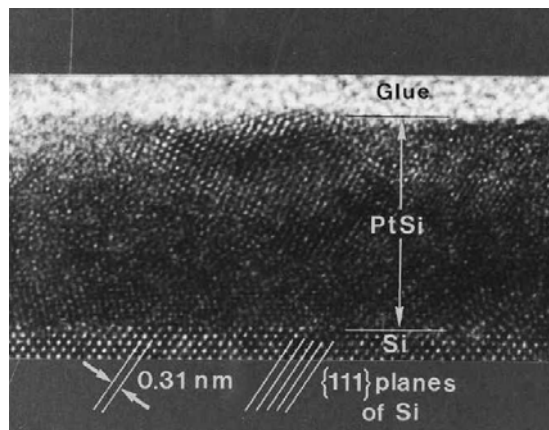


Fig. 2.8 Micrograph of the transverse section of a 7.5-nm thick PtSi film on Si (100). Reprinted with permission from [18], Copyright [1996], American Institute of Physics.

The spectral responsivity of this PtSi-nSi Schottky Barrier Photodiodes is illustrated in Fig. 2.9. It is important to point out that the measured responsivity in the wavelength range from 100 nm to 300 nm (DUV/VUV range) is only about 0.02 A/W, which is much lower than the ideal value of Si-based devices [11][12][18].

Besides the low responsivity, the low breakdown voltage and the high dark current are also limiting factors for the use of Schottky barrier photodiodes in applications where high reverse bias voltage (for reducing the value of the junction capacitance) and/or low dark current are required.

On the other hand, as discussed above, a superior radiation hardness of this PtSi-nSi Schottky barrier photodiode has been observed (presented in Fig. 2.10 [19]). Compared with two commercially available n-p/p-n junction photodiodes, while exposed to radiation with 150-nm wavelength, negligible responsivity degradation is reported. This is achieved by maintaining a fixed electric potential of the metal capping layer and reading the photocurrent from the silicon substrate [18].

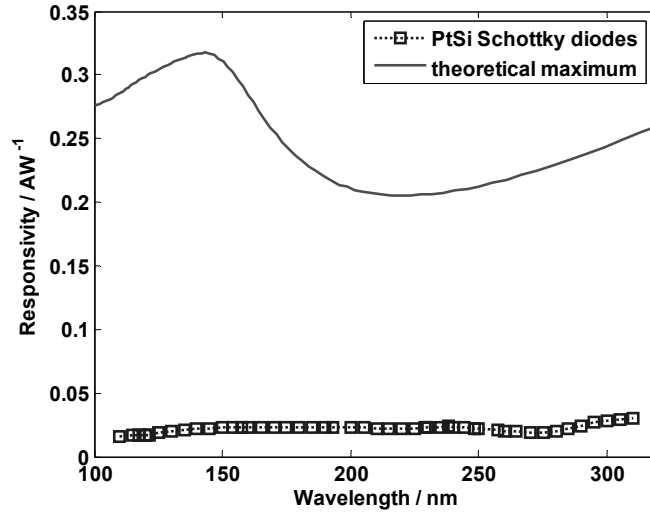


Fig. 2.9 Spectral responsivity of a PtSi Schottky photodiode [11][12][18].

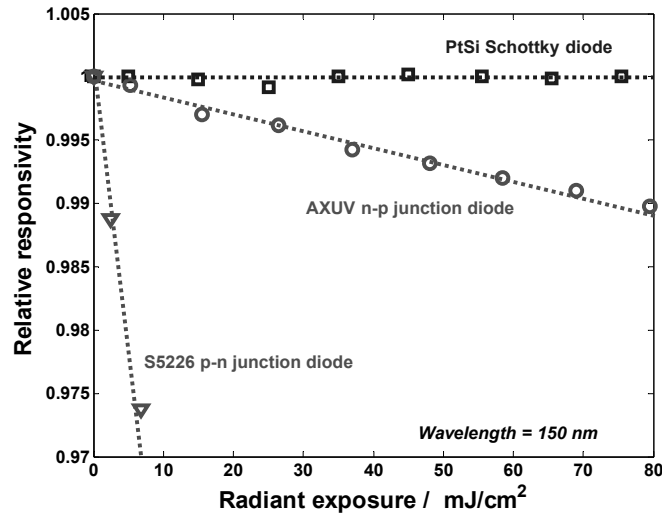


Fig. 2.10 Optical performance stability of a PtSi Schottky barrier diode compared with a commercial p-n diode (Hamamatsu, S5226) and an n-p diode (IRD, AXUV). Data is quoted from [19].

n-on-p junction diode

Currently n-on-p silicon photodiodes are the most commonly used UV photodetectors (especially in the wavelength range below 300 nm), since they can

profit from the natural positive charging of the capping silicon oxide layer created during production. During operation, this positive charge is maintained by the photoelectron emission effect [16]. A result of the positive charge is an electric field which helps to separate part of the photo-generated charge and directs the minority carriers (holes in this case) into the depletion zone. In this way, the highly doped n^+ region partly becomes an active (or at least semi-active) region, and the effective charge-collection zone is extended from the depletion region towards the detector surface. This effect reduces the thickness of the highly doped silicon region (t_2 in the ideal model, as shown in Fig. 2.6). Therefore, the positive charge in the oxide improves the charge-collection efficiency (CCE) near the diode surface and provides good responsivity even with deeper n-p junctions.

However, a disadvantage of this structure is the reduced responsivity in the EUV and VUV ranges due to the optical properties of the oxide passivation layer, and the need for a critical processing step to nitride the Si-SiO₂ interface, without which the photodiodes show very poor radiation hardness [20].

The IRD AXUV/UVG photodiodes have an n-on-p structure with a nitrated passivating SiO₂ surface layer (AXUV: ~ 5 nm, UVG: ~ 160 nm, [19]). A typical cross section of this kind of n-p junction photodiode is shown in Fig. 2.11 [20]. The measured responsivity of IRD AXUV/UVG photodiodes is presented in Fig. 2.12

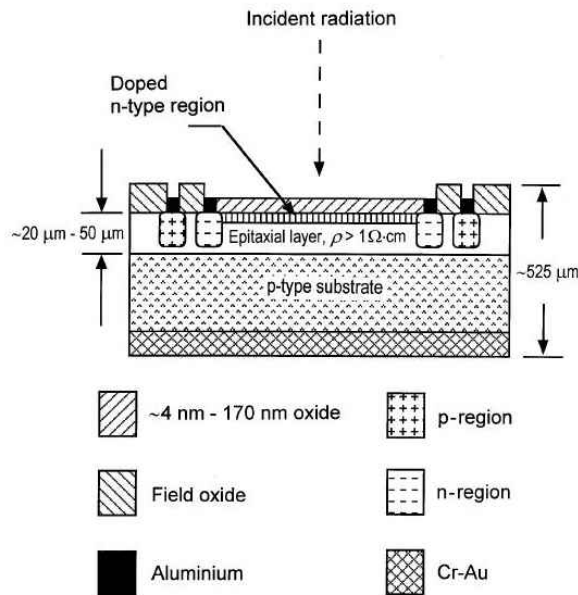


Fig. 2.11 Cross-section of AXUV/UVG Si-based photodiodes. [20] The figure is reproduced by permission of IOP Publishing.

[19][20]. It can be seen in Fig. 2.12 that the VUV responsivity of the AXUV/UVG photodiodes in the wavelength range between 150 nm and 300 nm is much higher than that of the PtSi-nSi Schottky photodiode. The variation of the spectral responsivity at different wavelengths, which is especially distinctive for the UVG device, is caused by interference effects in the comparatively thick oxide passivation layer [20].

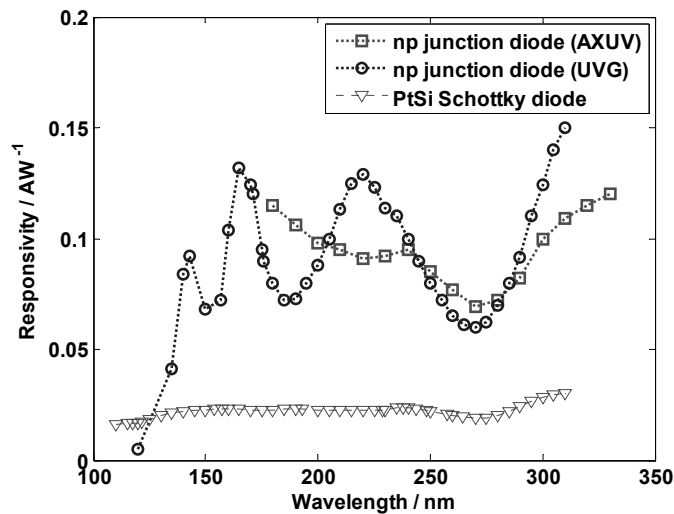


Fig. 2.12 Spectral responsivity of AXUV (reported by NIST) and UVG (reported by PTB) silicon photodiodes in the 120 nm to 330 nm spectral range (the comparison device is the PtSi Schottky photodiode shown in Fig. 2.6.) [19][20].

The responsivity degradation of the IRD UV photodiodes is illustrated in Fig. 2.13 [20]. For a prolonged exposure to a 193-nm ArF laser source, a noticeable decrease in the responsivity is observed when the total exposure level reaches 200 kJ/cm² [20]. It can be clearly seen that due to a positive photoelectron emission-induced charging of the diode surface, the measured responsivity first increases. However, with a further increase of the exposure level, a drop of the responsivity has been measured. One possible explanation is: while exposed to UV radiation, the UV-induced damage along the Si-SiO₂ interface of the photodiode (creating dangling bonds which may trap the photo-generated minority carriers) increases. When this kind of damage becomes dominant, it starts to affect negatively the surface CCE, and consequently the responsivity. It is important to mention that since the circumstances of the experiment are not well known to us, we do not exclude the possibility that part of the degradation of responsivity may have been caused by radiation-induced surface contamination [21][22].

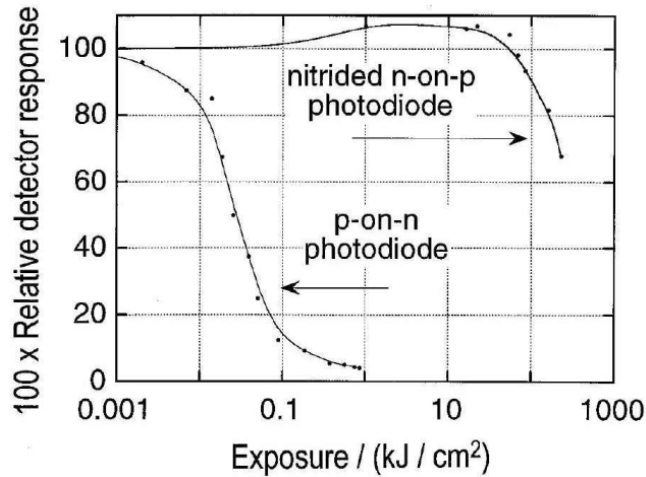


Fig. 2.13 Degradation of one of the UVG photodiodes during prolonged exposure to a pulsed laser at $\lambda=193$ nm. Also plotted is the corresponding degradation of a p-on-n silicon photodiode. [20] *The figure is reproduced by permission of IOP Publishing.*

p-on-n junction diode

For p-on-n junction diodes, the photoelectron emission-induced positive charge on the diode surface creates an electric field which acts against the built-in voltage in the depletion region. This electric field directs the photo-generated minority carriers (electrons) in direction opposite to the p-n junction, and reduces the chance to be collected. Consequently, a poor stability in the DUV/VUV range has been observed with conventional p-on-n junction photodiodes (shown in Figs. 2.10 and 2.13).

In Table 2.3, the performance of representative state-of-the-art Si-based UV photodiodes is summarized. Based on this overview, we can conclude that there is no commercially available Si-based UV detector performing well throughout the UV spectrum, specially in DUV/VUV range.

2.7 Si-based pure boron photodiode (PureB-diode) technology

A newly developed boron-doped ultra-shallow p^+n junction photodiode (PureB-diode) has been recently introduced as a competitive candidate for the EUV spectral range applications [17][25]. Fig. 2.14a shows a cross section of this photodiode. The technology used to produce the photodiode is based on the formation of an ultra-shallow p^+n junction by using a pure boron chemical vapor deposition (PureB CVD). With the PureB CVD process a nanometer-thin amorphous boron (α -boron) layer and a delta-like B-doped layer on Si substrates can be grown. In addition, a defect-

TABLE 2.3 PERFORMANCE OVERVIEW OF REPRESENTATIVE COMMERCIALY AVAILABLE SI-BASED UV DETECTORS.

Diode structure	Schottky	n-on-p			p-on-n
		IRD AXUV	IRD SXUV ^(a)	IRD UVG	
Commercially available devices	ETH PtSi-nSi	IRD AXUV	IRD SXUV ^(a)	IRD UVG	Hamamatsu (S5226)
EUV sensitivity (A/W) @ 13.5 nm	~ 0.2 ^(b)	~ 0.265	~ 0.23	Unknown	Unknown
Stability under EUV	Unknown ^(c)	Not stable	Good	Unknown	Unknown
DUV/VUV sensitivity (A/W) @ 193 nm	~ 0.03	~ 0.1	~ 0.01	~ 0.137	~ 0.1
DUV/VUV sensitivity (A/W) @ 157 nm	~ 0.02	~ 0.1	< 0.01	Unknown	Unknown
DUV/VUV sensitivity (A/W) @ 121 nm	≤ 0.02	Unknown	< 0.01	< 0.05	Unknown
Stability under DUV/VUV	Good	Not stable	Unknown	Acceptable	Not stable
References	[18][19]	[19][20][23][24]	[23][24]	[19][20]	[19]

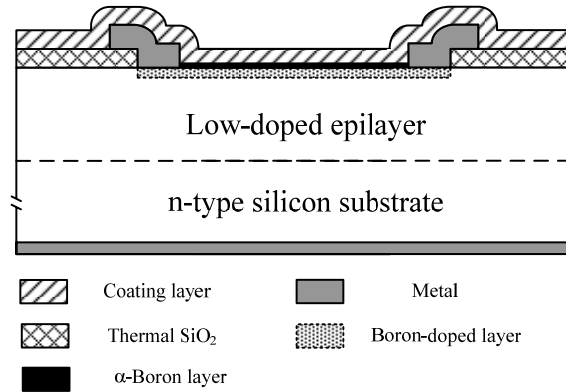
(a) SXUV: Si-based n-on-p junction photodiodes with nitride metal silicide front window;

(b) Value from measurement at PTB (*personal communication with Dr. F. Scholze*);

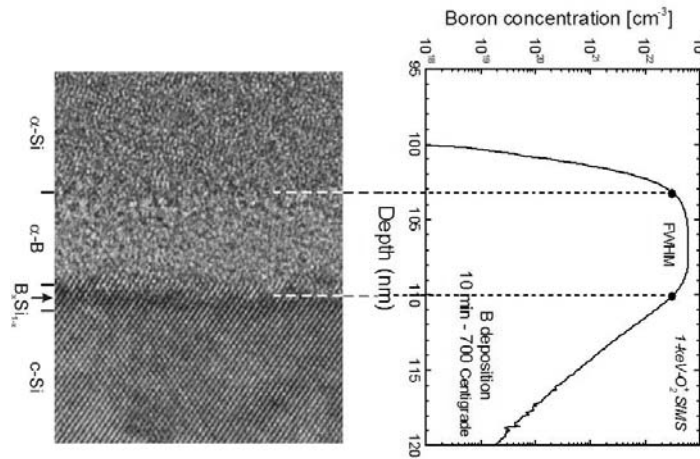
(c) Stability proven only in the VUV range [19].

free interface is created between the nanometer-thin α -boron layer and the silicon. Fig. 2.14b shows an HRTEM image of a PureB-layer formed after a 10-min B deposition at 700 °C, in comparison with a Boron Secondary Ion Mass Spectrometry (SIMS) profile [17][25][26][27]. The structure shown in Fig. 2.14 is very close to the ideal structure proposed in Fig. 2.6 due to the minimum thickness of the passivation layer (t_1) and the minimum thickness of the highly doped Si region (t_2). The extremely ultra-shallow junction is expected to enhance the sensitivity to UV radiation significantly. Moreover, the uniform α -boron coating is expected to act as an oxide-free surface passivation layer, instead of a silicon dioxide layer, which can improve the optical stability of the PureB-diodes by preventing radiation-induced Si-SiO₂ interface damage.

A similar concept of this pure boron CVD process has also been reported in [28].



(a)



(b)

Fig. 2.14 (a) Cross section of PureB-layer diodes; (b) HRTEM image of a PureB-layer formed after a 10-min B deposition at 700 °C compared with a Boron SIMS profile (the measured doping tail is influenced by a knock-on effect due to the extremely high concentration of boron on the surface.). The sample was covered with 20 nm of PVD α -Si for the TEM analysis. *The figure is reproduced based on [17][25][26][27].*

2.7.1 Typical electrical performance

Typical I-V characteristics of PureB-diodes fabricated on a 4-inch, 2 - 5 ohm-cm, n-Si wafer, are shown in Fig. 2.15. The reproducible low dark current and ideal I-V behavior indicate that the above-mentioned PureB-deposition process is a stable and reliable technology for creating defect-free p^+n ultra-shallow junctions. Furthermore, PureB-diodes can uphold a very high breakdown voltage. Extremely low dark current: ~ 1 pA, for a diode with a $300 \times 300 \mu\text{m}^2$ junction area, is observed at a reverse bias voltage as high as -40 V. [13][29]

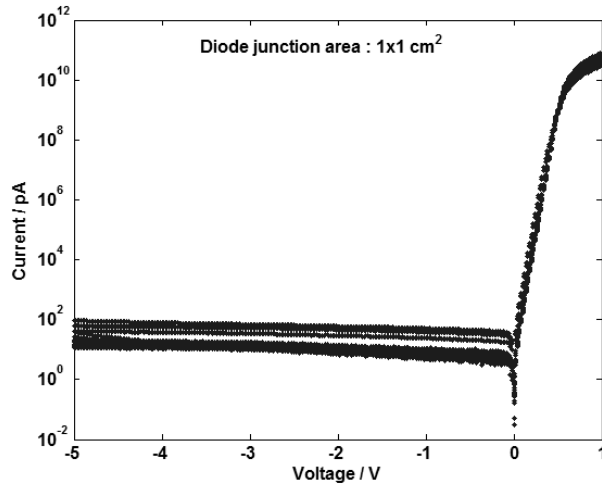


Fig 2.15 I-V characteristics of 24 PureB-diodes (active area is $1 \times 1 \text{ cm}^2$) fabricated on a 4-inch, 2-5 ohm-cm, n-Si wafer [13][29].

2.7.2 Optical performance in the EUV spectral range

All optical tests with PureB-diodes were carried out at PTB (Physikalisch-Technische Bundesanstalt) in Berlin, Germany using the synchrotron radiation storage ring BESSY [30]. Fig. 2.16 presents the measured EUV responsivity (symbols) of a PureB-diode with a 2.5 min B-deposition (α -boron thickness $< 5 \text{ nm}$,

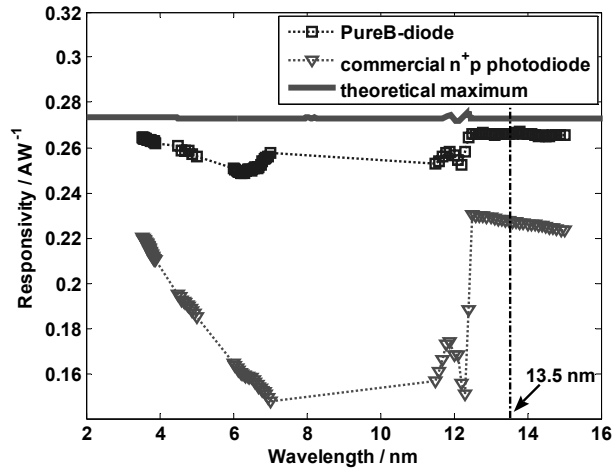


Fig. 2.16 Measured spectral responsivity (symbols) of EUV PureB-diodes with a 2.5 min boron deposition compared with a commercial n^+p photodiode (IRD SXUV) and the theoretically attainable values for an ideal Si-based photodetector [11][12][17][23][25].

pn junction depth < 10 nm) compared with a commercial n^+p photodiode and the theoretically attainable values for an ideal Si-based photodetector. As indicated in the plot, at the 13.5-nm wavelength, the measured responsivity of PureB-diode is about 0.265 A/W, which is very close to that of an ideal lossless system (0.27 A/W, solid line in Fig. 2.16) [11][12][17][25]. This again confirms that the PureB-deposition process can provide ultra-shallow, high-quality, damage-free p^+ -doped active surface layers which can minimize any quantum-efficiency loss due to either recombination of photo-generated carriers or absorption in the front window.

Owing to the above-mentioned advantages, the PureB-diode technology promises to become a solution for creating photodetectors with high and stable sensitivity over the full UV range.

However, a significant drawback of the PureB-diodes is the large sheet resistance (up to 10 k Ω /square) of the layer stack on top of the p-n junction – the anode area [14][15][31]. This high resistance is a result of the nanometer-thin p^+ layer and the relatively high resistivity of the α -boron surface layer, which has also to remain very thin. The high sheet resistance of the anode area may become the dominant contributor to the series resistance, R_s , of the photodiode when the junction area is large (more than a few square millimeters). As already discussed, a larger R_s means a larger time constant and a lower operational speed. These may limit the detection of high-frequency, short-duration UV pulses in some applications, for example in UV lithography. Furthermore, the high surface resistance may lead to the accumulation of photoelectron-emission-induced positive charge on the diode surface, and a consequent deterioration of the stability.

2.8 Summary

In this chapter a comparative study between different existing UV-detector technologies is presented. It has been found that Si-based photodiodes hold a superior position with respect to high sensitivity, simplicity, low costs, and IC-compatibility. Based on the reported DUV/VUV optical performance of state-of-the-art Si-based UV photodiodes, their advantages and drawbacks are evaluated. Schottky barrier diodes have excellent radiation hardness, however their responsivity and resolution are relatively low. The good responsivity of n-on-p junction diodes in the DUV spectral range relies on a positively-charged oxide surface, but this oxide surface also affects the stability and reduces the responsivity in the EUV and VUV spectral ranges. Alternatively, n-on-p photodiodes with a conductive top layer (SXUV detector from IRD, shown in Table 2.3) demonstrate very good responsivity and stability in the EUV range; however, their responsivity significantly drops in the DUV and VUV spectral ranges. Due to the photoelectron emission-induced positive charge on the detector surface, conventional p-on-n

junction photodiodes with an oxide top layer are less stable than both Schottky barrier diodes and n-on-p junction diodes.

Therefore, it is concluded that there is no commercially available semiconductor-based photodetector which can provide a high and stable optical performance over the full UV range. The main performance challenges are in the DUV and VUV spectral ranges, where the penetration depth in silicon is very small, while the photon energy is still sufficiently high to cause photoelectron emission.

This conclusion raises the question: is there a photodetector technology which can provide a device structure close to the proposed ideal model that has a better chance of meeting the key performance requirements defined in Chapter 1?

Regarding the “high-responsivity” requirement, the PureB-diode technology presented in Section 2.7 is in accordance with the proposed ideal structure: the nanometer-deep junction and the nanometer-thin α -boron capping layer provide an inherent ultra-thin absorption window in front of the depletion region. This nanometer-thin absorption window can greatly reduce the unwanted photon loss, which is proven by the near-theoretical responsivity measured at a 13.5-nm wavelength in the EUV spectral range. This unique feature indicates that PureB-diodes can potentially achieve better responsivity than any other commercially available Si-based photodetector over the full UV spectral range. Therefore, the main goal of this research work is to investigate the electrical and optical performance of photodiodes fabricated by the PureB technology and design high-sensitivity, high-stability photodiodes for UV radiation detection.

The research topics covered in the thesis are:

1. Optical performance characterization of PureB-diodes in the DUV and VUV spectral ranges.
2. Investigation of the optical performance and response time of PureB-diodes, related to the high sheet resistance of the surface layers.
3. Stability and robustness study of PureB-diodes in detrimental working conditions.

References:

- [1] M. Razeghi and A. Rogalski, "Semiconductor ultraviolet detectors", *J. Appl. Phys.*, vol. 79, no. 10, pp. 7433-7473, Jan. 1996.
- [2] E. Monroy, F. Omnès and F. Calle, "Wide-bandgap semiconductor ultraviolet photodetectors", *Semiconductor Science and Technology*, vol. 18, no. 4, pp. 33-51, Apr. 2003.
- [3] M. R. Werner and W. R. Fahrner, "Review on materials, microsensors, systems and devices for high-temperature and harsh-environment application", *IEEE Trans. on Industrial Electronics*, vol. 48, no. 2, pp. 249-257, Apr. 2001.
- [4] D. Nakamura et al. "Ultrahigh-quality silicon carbide single crystals". *Nature*, vol. 430, pp. 1009-1012, June 2004.
- [5] M. Kanechika, T. Uesugi, and T. Kachi, "Advanced SiC and GaN power electronics for automotive systems", *Proc. 2010 IEEE International Electron Devices Meeting (IEDM)*, pp. 1351-1354, Dec. 2010.
- [6] P. E. Malinowski et al., "10 μm pixel-to-pixel pitch hybrid backside illuminated AlGaIn-on-Si imagers for solar blind EUV radiation detection", *Proc. 2010 IEEE International Electron Devices Meeting (IEDM)*, pp. 1451-1454, Dec. 2010.
- [7] N. Kaminski and O. Hilt, "SiC and GaN devices - competition or coexistence", *Proc. 7th International Conference on Integrated Power Electronics Systems (CIPS2012)*, pp. 1-11, Mar. 2012.
- [8] G. F. Dalla Betta (Ed.), *Advances in Photodiodes*, Rijeka, Croatia, InTech, 2011.
- [9] E. D. Palik (Ed.), *Handbook of Optical Constants of Solids*, Orlando, Academic Press, 1985.
- [10] Henke data. Available from http://henke.lbl.gov/optical_constants.
- [11] F. Scholze, H. Henneken, P. Kuschnerus, H. Rabus, M. Richter and G. Ulm "Determination of the electron-hole pair creation energy for semiconductors from the spectral responsivity of photodiodes", *Nuclear Instruments and Methods in Physics Research*, vol. 439, no. 2-3, pp. 208-215, 2000.
- [12] F. Scholze, H. Rabus and G. Ulm, "Mean energy required to produce an electron-hole pair in silicon for photons of energies between 50 and 1500 eV", *J. Appl. Phys.*, vol. 84, no. 5, pp. 2926-2939, Sept. 1998.
- [13] L. Shi, S. Nihtianov, L. K. Nanver, F. Scholze, and A. Gottwald, "High-sensitivity high-stability silicon photodiodes for DUV, VUV and EUV spectral ranges," *Proc. SPIE*, vol. 8145, pp. 21-25, Aug. 2011.
- [14] S. Xia, F. Sarubi, R. Naulaerts, S. Nihtianov and L. Nanver, "Response time of silicon photodiodes for DUV/EUV radiation", *Proc. 2008 IEEE Instrumentation and Measurement Technology Conference (I2MTC)*, pp. 1956-1959, May 2008.

- [15] L. Shi, S. Nihtianov, S. Xia, L. K. Nanver, A. Gottwald and F. Scholze, “Electrical and optical performance investigation of Si-based ultrashallow-junction p⁺-n VUV/EUV photodiodes”, *IEEE Transactions on Instrumentation and Measurement*, vol. 61, issue 5, pp. 1268-1277, May 2012.
- [16] R. E. Vest and L. R. Canfield, “Photoemission from silicon photodiodes and induced changes in the detection efficiency in the far ultraviolet”, *Proc. the 10th United States National Conference on Synchrotron Radiation Instrumentation*. vol. 417, pp. 234-240, 1997.
- [17] L. Shi, F. Sarubbi, S. N. Nihtianov, L. K. Nanver, T. L. M. Scholtes and F. Scholze, “High performance silicon-based extreme ultraviolet (EUV) radiation detector for industrial application”, *Proc. 35th Annual Conference of the IEEE Industrial Electronics Society (IECON)*, pp. 1891-1896, Nov. 2009.
- [18] K. Solt, H. Melchior, U. Kroth, P. Kuschnerus, V. Persch, H. Rabus, M. Richter and G. Ulm, “PtSi-n-Si Schottky-barrier photodetectors with stable spectral responsivity in the 120-250 nm spectral range”, *Appl. Phys. Lett.*, vol. 69, no. 24, pp. 3662-3664, 1996.
- [19] P. Kuschnerus, H. Rabus, M. Richter, F. Scholze, L. Werner and G. Ulm, “Characterization of photodiodes as transfer detector standards in the 120 nm to 600 nm spectral range”, *Metrologia*, vol. 35, pp. 355-362, 1998.
- [20] L. R. Canfield, R. E. Vest, R. Korde, H. Schmidtke and R. Desor, “Absolute silicon photodiodes for 160 nm to 254 nm photons”, *Metrologia*, vol. 35, pp. 329-334, Aug. 1998.
- [21] R. Garg, A. Wüest, E. Gullikson, S. Bajt, and G. Denbeaux, “EUV optics contamination studies in presence of selected hydrocarbons”, *Proc. of SPIE*, vol. 6921, no.36, Mar. 2008.
- [22] F. Scholze, R. Klein, and T. Bock, “Irradiation stability of silicon photodiodes for extreme-ultraviolet radiation”, *Appl. Opt.*, vol. 42, no. 28, Oct. 2003.
- [23] F. Scholze, R. Klein and R. Müller, “Characterization of detectors for extreme UV radiation”, *Metrologia*, vol. 43, S6-S10, 2006
- [24] F. Scholze, G. Brandt, R. Müller, B. Meyer, F. Scholz, J. Tümmeler, K. Vogel and G. Ulm, “High-accuracy detector calibration for EUV metrology at PTB”, *Proc. SPIE*, vol. 4688, pp. 680-689, 2002.
- [25] F. Sarubbi, L. K. Nanver, T. L. M. Scholtes, S. N. Nihtianov and F. Scholze, “Pure boron-doped photodiodes: a solution for radiation detection in EUV lithography”, *Proc. IEEE 38th European Solid-State Device Research Conference (ESSDERC)*, pp. 278-281, Sept. 2008.
- [26] F. Sarubbi, T. L. M. Scholtes, and L. K. Nanver, “Chemical vapour deposition of α -boron layers on silicon for controlled nanometer-deep p⁺n junction formation”, *J. Electron. Mater.*, vol. 39, no. 2, pp. 162-173, 2010.

- [27] F. Sarubbi, L. K. Nanver and T. L. M. Scholtes, "CVD delta-doped boron surface layers for ultra-shallow junction formation", *ECS Transactions*, vol. 3, no. 2, pp. 35-44, Nov. 2006.
- [28] US Patent 5 719 414, Photoelectric conversion semiconductor device with insulation film, Feb. 17, 1998.
- [29] L. Shi, L. K. Nanver, A. Šakić, S. Nihtianov, A. Gottwald and U. Kroth, "Optical stability investigation of high-performance silicon-based VUV photodiodes", *Proc. IEEE Sensors2010*, pp. 132-135, Nov. 2010.
- [30] R. Klein, C. Laubis, R. Müller, F. Scholze and G. Ulm, "The EUV metrology program of PTB", *Microelectronic Engineering*, vol. 83, pp. 707-709, 2006.
- [31] L. Shi, L. K. Nanver, A. Šakić, S. Nihtianov, T. Knežević, A. Gottwald and U. Kroth, "Series resistance optimization of high-sensitivity Si-based VUV photodiodes", *Proc. 2011 IEEE Instrumentation and Measurement Technology Conference (I2MTC)*, May 2011.

Chapter 3 Surface Properties of PureB-diodes

Due to the limited attenuation length (penetration depth) of DUV/VUV photons in silicon [1][2], the properties of the PureB-diode surface structure play an important role in its performance. For proper interpretation and analysis of the reported optical experimental data in this thesis, we first discuss the device surface structure based on recent scientific publications and dedicated experimental results.

3.1 Pure boron CVD technology and diode fabrication

The pure boron (PureB) CVD technology was developed at the DIMES (Delft Institute of Microelectronics and Nanotechnology) facilities of Delft University of Technology [3][4]. A micro-image and a schematic cross section of a PureB-diode for DUV/VUV photon detection are shown in Fig. 3.1a [3][4][5].

A low-doped ($< 10^{14} \text{ cm}^{-3}$) epitaxial layer is grown on a 1-10 Ωcm n-type Si (100) substrate. The epilayer thickness sets the breakdown voltage and the junction capacitance of the diodes and can be adjusted for specific applications. An n^+ implantation ($3 \times 10^{15} \text{ cm}^{-2}$ at 40 keV) on the back-side of the wafer is used to provide ohmic contact to the substrate. After the growth of 300 nm of thermal oxide, the diode active area is plasma-etched with soft landing on the Si. Then, α -boron surface layers are selectively deposited into the SiO_2 openings by using a pure boron atmospheric/low-pressure chemical vapor deposition (AP/LPCVD) at 700 °C with di-borane B_2H_6 as the gas source. In Fig. 3.1b, TEM images are shown of a 2.5 min B-layer deposition on a Si(100) substrate (DIMES fabricated sample). As indicated in the images, this technique offers the advantage of thin and uniform boron coverage. A 0.6 μm aluminum physical vapor deposition (PVD) metallization and patterning defines both the outer ring anode contact on the front side and the cathode electrode on the back side. The diode processing is completed with a 400 °C alloy step in forming gas [3][4].

A similar process is used for the fabrication of PureB-diodes in IMEC's 200 mm CMORE line [5]. As depicted in the device cross-sections in Fig. 3.2, IMEC-fabricated PureB-diodes are formed by growing an intrinsic Si-epi layer on top of a highly-doped buried n-layer in a p-type silicon substrate. This complex structure is designed to allow the photocurrent to be read from the cathode of multiple photodiodes on one substrate by electrically isolating the cathodes. In this way the photoelectron emission current does not contribute to the measured photocurrent (this issue is discussed further in Chapter 6). The p^+ layer of the diode is formed by a 2.5-min pure-boron CVD, which is basically similar to the DIMES deposition. In contrast to the DIMES devices, on top of the boron surface layer, there is an additional nanometer-thin TiN layer which is applied to protect the nanometer-thin

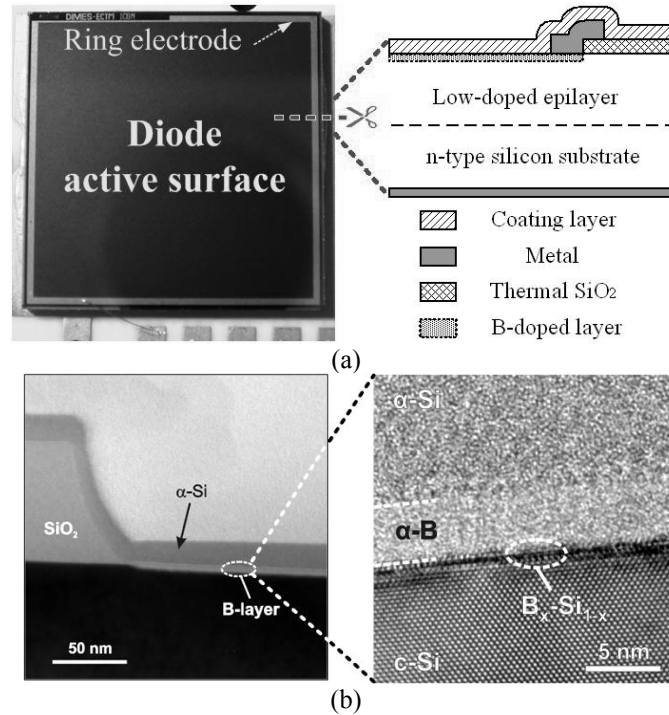


Fig. 3.1 (a) Photo and cross section of DIMES-fabricated PureB-diodes ($1 \times 1 \text{ cm}^2$)[10]; (b) TEM images of a 2.5 min boron deposition on a Si(100) substrate (DIMES sample). The sample was covered with 20 nm of PVD α -Si for the TEM analysis. The figure is reproduced from [3][4][5].

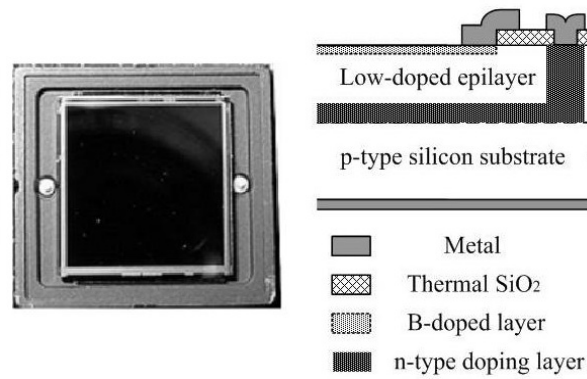


Fig. 3.2 Photo and cross-section of an IMEC-fabricated PureB-diode ($1 \times 1 \text{ cm}^2$) [5].

boron layer in the processing steps that follow the boron deposition, such as the etching step for patterning the metal electrode [5]. The thickness of this extra layer is

between 0.5 to 1.5 nanometers, which can be estimated, for example, by the measured responsivity difference before and after the Ti-L edge (~ 2.7 -nm wavelength in the EUV spectral range).

3.2 Surface oxidation

Optical and physical measurement results confirm the presence of oxide components on the surface of the tested PureB-diode samples, when thin boron coverage is formed. Table 3.1 presents the ellipsometer-measured oxide component on the diode surface of DIMES fabricated PureB-diodes. The results also show that the oxide presence tends to be lower with increased boron layer thickness. A similar result was found with an X-ray Photoelectron Spectroscopy (XPS) measurement: the SiO_x component was measured on the surface of Sample #2, which is shown in Table 3.1. Since no boron oxide was detected on the diode surface by the XPS test, we can conclude that the α -boron layer itself cannot be oxidized after boron deposition.

The UV optical measurement results also show the presence of “oxygen” element in the surface layer stack of PureB-diodes. For example, as illustrated in Fig. 3.3, a measured EUV responsivity undulation around the oxygen absorption edge ($\lambda \approx 2.3$ nm) indicates oxide component on the surface of Sample #2 and Sample #3 (presented in Table 3.1). However, the undulation is too small to predict the exact oxide content.

The oxide-induced effect was observed in the DUV/VUV spectral range, as well. Fig. 3.4 shows the measured DUV/VUV spectral response of PureB-diodes with different boron coverage thicknesses (from less than 1 nm to 12 nm) [6]. As shown in the figure, when the boron coverage is thin (< 1 nm), a significantly higher responsivity is observed in the 130 nm to 160 nm spectral range. Fig. 3.5 shows simulated anti-reflective behavior of SiO_2 layers on Si with different thicknesses.

TABLE 3.1 ELLIPSOMETER MEASURED SURFACE LAYER STACK OF PUREB-DIODE (DIMES SAMPLES) WITH DIFFERENT BORON THICKNESSES.

Diode #	Boron coverage thickness (nm)	Measured equivalent oxide thickness (nm)
#1	< 1 nm	5~6 nm
#2	4 nm	3 nm
#3	12 nm	1~1.5 nm
#4	14 nm	< 1 nm
#5	15 nm	No measurable oxide

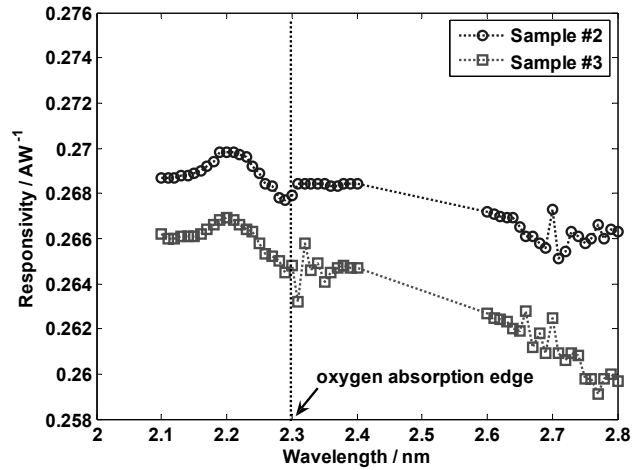


Fig. 3.3 Monitored responsivity undulation around the oxygen absorption edge ($\lambda \approx 2.3$ nm) of PureB-diodes (DIMES samples).

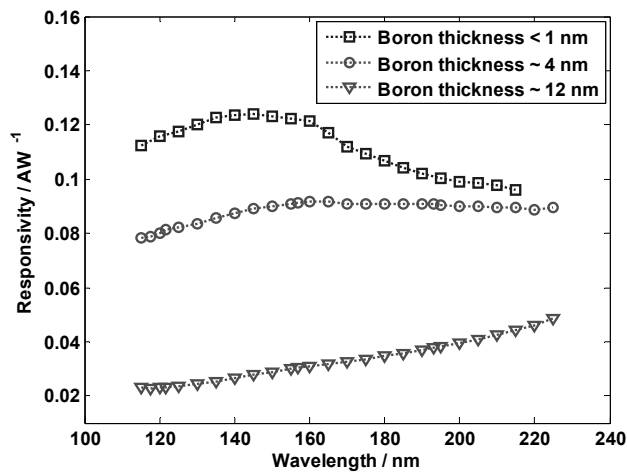


Fig. 3.4. Measured responsivity of PureB-diodes (DIMES samples) with different boron layer thicknesses in the DUV/VUV spectral range. Boron layer thickness was measured by ellipsometry [6].

Each curve has an anti-reflectivity (1-reflectance) enhancement around 130-nm wavelength [1]. This increase will ultimately result in a higher responsivity of the photodiode. The small peak shift between the measurement results and simulation results is probably due to the impure oxide components (not only SiO_2) on the

surface of the PureB-diodes. Therefore, this responsivity enhancement phenomenon can be considered as another indirect indication of the surface oxidation.

Based on the above experimental results, it is probable that a thick enough boron layer will guarantee dense, pin-hole-free coverage. Otherwise, oxygen may diffuse through the thin boron layer, or via pin-holes in the boron layer, to oxidize the underlying silicon surface. At this moment, due to the lack of a sub-nanometer surface analysis technique, this surface oxidation phenomenon has not yet been fully investigated. A possible solution for further analysis could be high-resolution Transmission Electron Microscopy (HRTEM) plus a nanometer-resolution X-ray Photoelectron Spectroscopy (XPS). The former can give an indication of the crystal lattice structure along the diode surface, and the latter can detect the amount of the oxide component within nanometer-deep layer on the diode surface. In this way, the location, structure and quantity of the surface oxide can be analyzed.

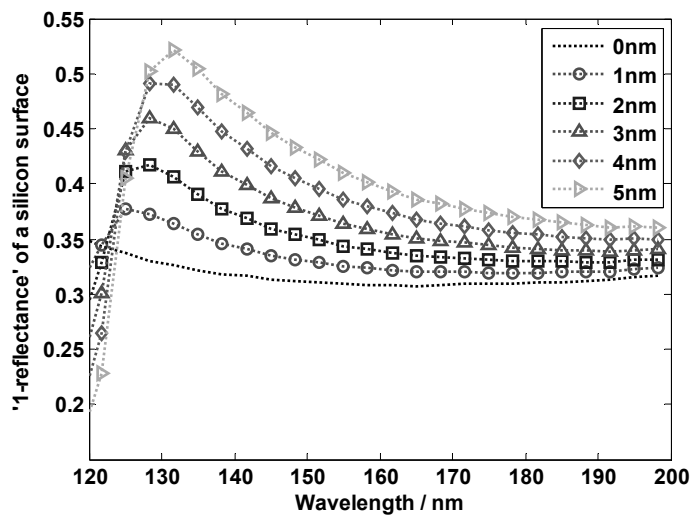


Fig. 3.5 Simulated anti-reflectivity (1-reflectance of a silicon surface) of a 0~5 nm thick SiO₂ layer in the DUV/VUV spectral range [1].

3.3 Uniformity of the amorphous boron (α -boron) coverage

As shown in Fig. 3.4, the VUV radiation is absorbed intensively in the nanometer-thin PureB-layer, which makes the responsivity of the PureB-diodes very sensitive to its thickness. This makes the DUV/VUV responsivity a good indicator of the uniformity of the boron thickness on the diode surface. Fig. 3.6 presents the responsivity uniformity of PureB-diodes with different boron layer thicknesses, at

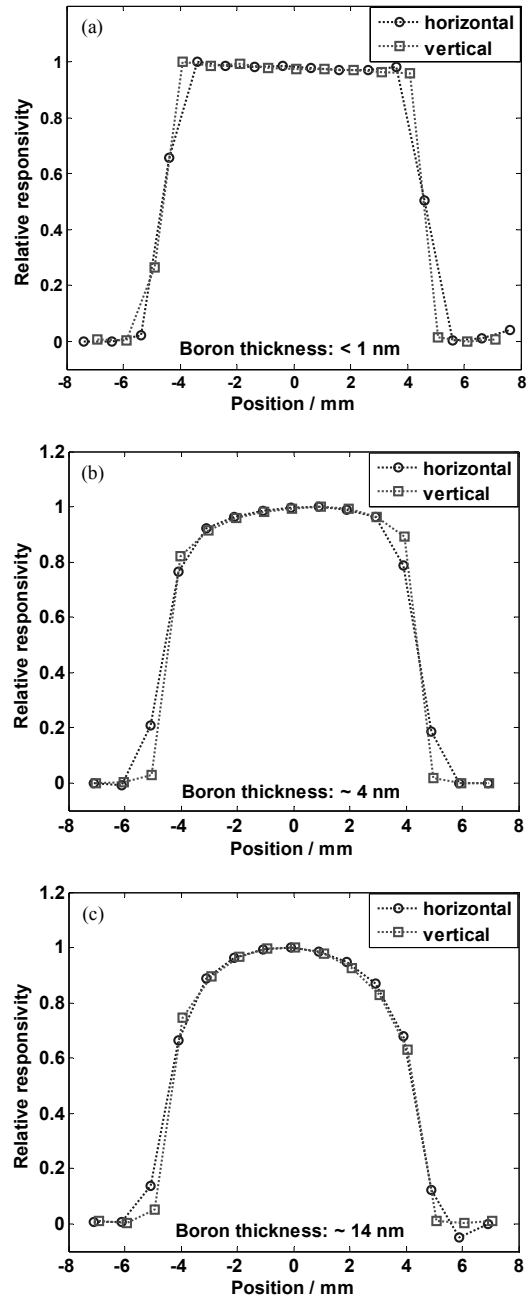


Fig. 3.6 Responsivity uniformity of PureB-diodes (DIMES sample, $1 \times 1\text{ cm}^2$ junction area), at 193 nm wavelength. The boron layer thickness was measured by ellipsometry.

193-nm wavelength. Obviously, a better uniformity is achieved when the boron layer is thinner. However, as mentioned above, too thin boron coverage may lead to oxidations of the diode surface, potentially affecting the performance stability of the photodiodes (details are discussed in Chapter 6).

3.4 Post-processing thermal annealing

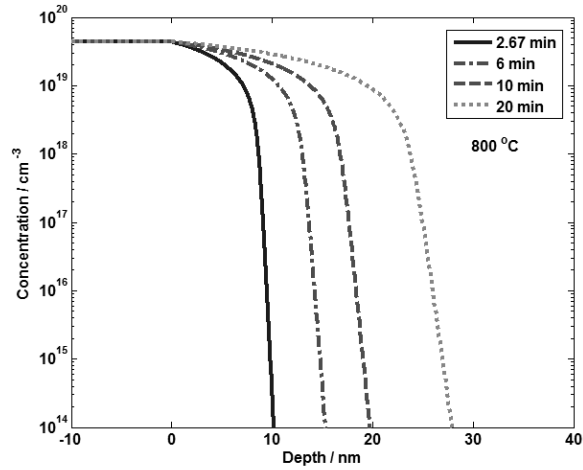
Deeper p-n junction photodiodes are produced by a post-deposition thermal anneal process on the standard ultra-shallow junction PureB-diodes. A thermal “drive-in” can drive the boron dopants into the deeper part of the bulk silicon. By varying the anneal temperature and the “drive-in” time, PureB-diodes with different junction depth can be fabricated. Fig. 3.7 shows simulation results which indicate the relationship between different anneal recipes and the resulting junction depth. By varying the anneal temperature (800 or 900 °C) and time (2 min 40 s to 20 min), the junction depth of the PureB-diode can be well controlled in the range from a few nanometers to hundreds of nanometers [7][8].

3.5 Summary

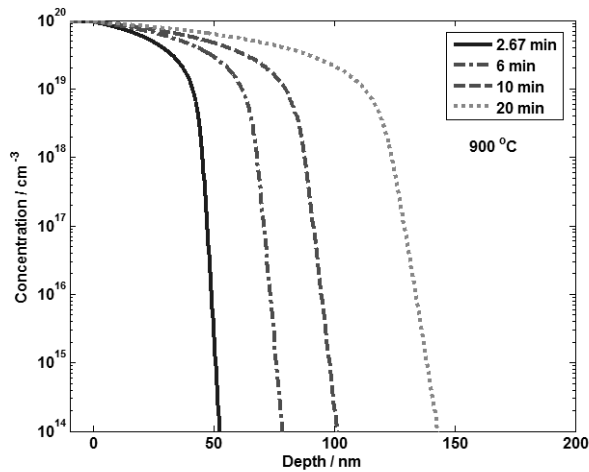
The fabrication process, the device structure, and the surface conditions of PureB-diodes are introduced in this chapter. The nanometer-deep attenuation length of DUV radiation and part of the VUV radiation in most solid materials makes the surface structure and properties of PureB-diodes extremely important for understanding and analyzing the DUV/VUV optical performance. In Table 3.2, the surface properties discussed in this chapter and the optical/electrical performance they may affect are summarized.

TABLE 3.2 SURFACE PROPERTIES OF PUREB-DIODE AND THE RELATED OPTICAL/ELECTRICAL PERFORMANCE

Surface property	Related optical/electrical performance	Related Chapter
Surface oxidation	Optical stability	Chapter 6
Boron thickness/uniformity	Sensitivity; Optical stability	Chapter 4, 6
Junction depth	Sensitivity; Optical stability; response time	Chapter 4, 5, 6



(a)



(b)

Fig. 3.7 Simulation results of the PureB-diode junction depth (active boron concentration vs. depth) with different anneal temperatures and times: (a) $800\text{ }^{\circ}\text{C}$ and (b) $900\text{ }^{\circ}\text{C}$. The arsenic bulk doping is $N_{As} = 1 \times 10^{12}\text{ cm}^{-3}$ [8].

References:

- [1] E. D. Palik (Ed.), *Handbook of Optical Constants of Solids*, Orlando, Academic Press, 1985.
- [2] Henke data. Available from: http://henke.lbl.gov/optical_constants.
- [3] F. Sarubbi, T. L. M. Scholtes, and L. K. Nanver, "Chemical vapour deposition of α -boron layers on silicon for controlled nanometer-deep p^+n junction formation", *J. Electron. Mater.*, vol. 39, no. 2, pp. 162-173, 2010.
- [4] F. Sarubbi, L. K. Nanver and T. L. M. Scholtes, "CVD delta-doped boron surface layers for ultra-shallow junction formation", *ECS Transactions*, vol. 3, no. 2, pp. 35-44, Nov. 2006.
- [5] L. Shi, S. Nihtianov, L. Haspeslagh, F. Scholze, A. Gottwald and L. K. Nanver, "Surface-charge-collection-enhanced high-sensitivity high-stability silicon photodiodes for DUV and VUV spectral ranges", *IEEE Trans. on Electron Devices*, vol. 59, no. 11, pp. 2888 – 2894, Nov. 2012.
- [6] L. Shi, F. Sarubbi, L. K. Nanver, U. Kroth, A. Gottwald and S. Nihtianov, "Optical performance of B-layer ultra-shallow-junction silicon photodiodes in the VUV spectral range", *Proc. Eurosensors XXIV*, Sept. 2010.
- [7] L. Shi, L. K. Nanver, A. Šakić, S. Nihtianov, T. Knežević, A. Gottwald and U. Kroth, "Series resistance optimization of high-sensitivity Si-based VUV photodiodes", *Proc. 2011 IEEE Instrumentation and Measurement Technology Conference (I2MTC)*, May 2011.
- [8] L. Shi, S. Nihtianov, S. Xia, L. K. Nanver, A. Gottwald and F. Scholze, "Electrical and optical performance investigation of Si-based ultrashallow-junction p^+n VUV/EUV photodiodes", *IEEE Transactions on Instrumentation and Measurement*, vol. 61, no. 5, pp. 1268-1277, May 2012.

Chapter 4 Surface Charge-Collection Efficiency (CCE) of PureB-Diodes

In this chapter, a distinctive surface charge collection process in the highly-doped p^+ region of PureB-diodes is validated experimentally and explained theoretically, based on a physical model of the doping-gradient-induced internal electric field [1]. It is irrefutable that, besides the ultra-shallow p^+n junction, this newly discovered beneficial doping-gradient-induced surface charge collection effect is the main factor for achieving the superior DUV/VUV responsivity demonstrated by the PureB-diodes.

4.1 Optical test setup

All optical tests presented in the following parts of this thesis were carried out at the EUV- and UV/VUV- synchrotron radiation beamlines of PTB (Physikalisch-Technische Bundesanstalt) in Berlin, Germany [2][3][4][5]. As shown in Fig. 4.1a, two detector arrays were assembled in a metal package. The positioning of the sample and the electrical contacts with the diodes were realized with a fixture mounted on an x-y stage. During each test, the detectors were in an ultra-high vacuum environment with residual gas pressures below 10^{-5} Pa.

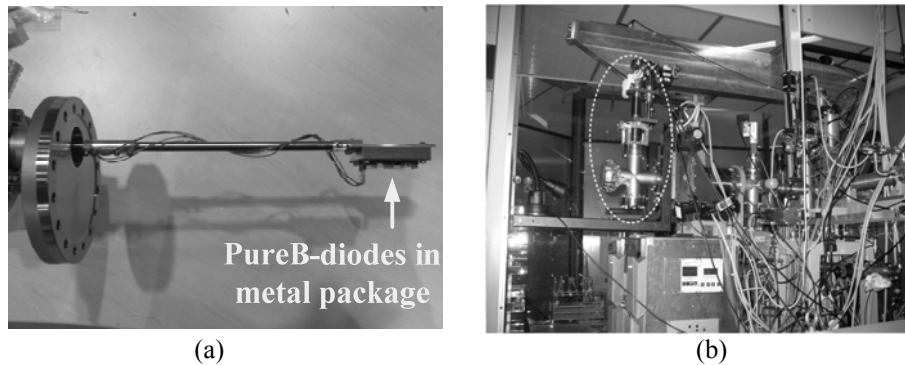


Fig. 4.1 (a) Mounting of two detector arrays on a PTB x-y positioning stage; (b) the high-accuracy DUV/EUV metrology setup at PTB (test samples were assembled in the vacuum chamber indicated by the dashed circle).

4.2 DUV/VUV optical performance of PureB-diodes

As discussed in the previous chapters, PureB-diodes are reported to have an outstanding optical performance in the extreme-ultraviolet (EUV) spectral range (a near-theoretical responsivity of 0.265 A/W was measured at 13.5-nm wavelength)

[6][7][8][9]. The relatively large attenuation length of EUV photons (according to Fig. 2.4a, the attenuation length in silicon at 13.5 nm is larger than 500 nm [10][11]) makes the impact of the thin boron layer and the shallow junction depth on the responsivity of PureB-diodes negligible. That is why, for this particular spectral range, the PureB-diodes structure can be assumed as ideal. However, in the more challenging DUV and part of the VUV spectral ranges (wavelengths between 100 nm and 300 nm), the photon attenuation length in Si is only a few nanometers [10][12], which means that a significant part of the photons will be absorbed in the first few nanometers below the device surface. So, a high DUV/VUV sensitivity of PureB-diodes will be a good indicator of their superior optical performance over the entire UV spectral range.

Fig. 4.2 shows the responsivity of a DIMES made PureB-diode compared with other commercially available state-of-the-art photodiodes in the DUV/VUV spectral range (wavelengths from 100 nm to 220 nm) [13][14][15][16][17]. This PureB-diode was fabricated by a 2 min 40 s boron deposition which forms a roughly 2 nm boron coverage and a less than 10 nm junction depth. The measured responsivity is in the order of 0.1 A/W or higher [16]. This confirms that the ultra-thin pre-absorption stack, which is composed of the nanometer-thin boron layer and the nanometer-thin p^+ region, can greatly reduce the undesired photo losses in the front

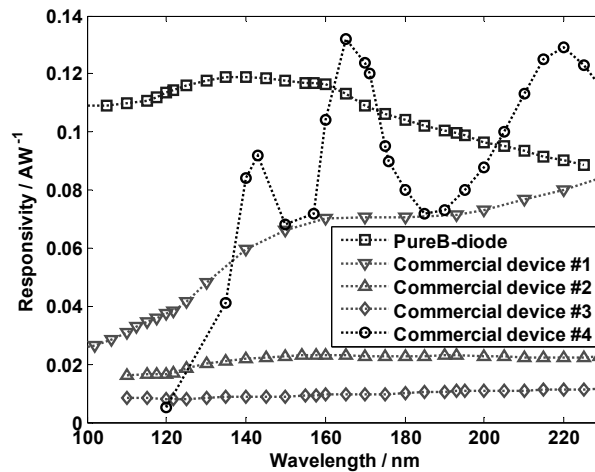


Fig.4.2 Measured responsivity of PureB-diodes in the DUV/VUV spectral range, compared with other state-of-the-art Si-based photodetectors. The measured PureB-diode was fabricated at DIMES (Junction depth: < 10 nm; α -boron: ~2 nm, measured by ellipsometer). Device #1 is an SPD p^+n junction photodiode; device #2 is an ETH PtSi-Schottky photodiode; device #3 is an IRD SXUV n^+p junction photodiode; device #4 is an IRD UVG n^+p junction photodiode. [13][14][15][16][17]

window on top of the effective charge-collection zone (depletion region).

4.3 Surface charge-collection effect

Since the pre-absorption layer thickness of PureB-diodes is already comparable with the attenuation length of DUV/VUV photons in silicon, investigations of the DUV/VUV optical performance will not only provide information about the photodiode responsivity, but will also help to understand the photon-generated charge collection mechanism near the diode surface and its impact on the internal quantum efficiency of PureB-diodes.

4.3.1 Surface charge-collection phenomenon of PureB-diodes

Fig. 4.3 compares the responsivity of the PureB-diode from Fig. 4.2 with the theoretically attainable responsivity of an ideal Si-based photodetector in the DUV/VUV spectral range [8][9]. As indicated in the figure, based on the measured responsivity at 193-nm wavelength (0.0997 A/W) and the theoretical value (0.215 A/W), the quantum efficiency (QE) of this PureB-diode can be calculated as: $QE=0.0997/0.215\approx 0.46$.

Considering the measured near 100% quantum efficiency (near theoretical responsivity) of the PureB-diodes at 13.5-nm wavelength (Fig. 2.17), the recombination of the photon-generated charge in the diode depletion region can be

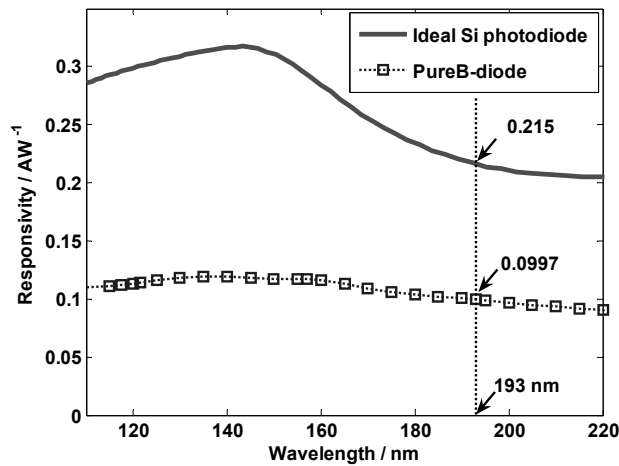


Fig. 4.3 Measured responsivity of PureB-diodes in DUV/VUV spectral range compared with the theoretically attainable values for an ideal Si-based photodetector [8][9]. The measured diode was fabricated at DIMES (junction depth: < 10 nm; α -boron thickness: ~ 2 nm, measured by ellipsometer) [16][17].

assumed as negligible. Besides the possible external reflection induced photon loss on the diode surface, the main reason for this quantum efficiency drop of the PureB-diodes in the DUV/VUV spectral range should be the undesired photon absorption in the α -boron surface layer and the underlying highly doped silicon region (p^+ region).

As illustrated in Fig. 2.4a [10][12], the attenuation length of DUV and part of VUV radiation (wavelength between 100 nm and 200 nm) in silicon is extremely small. For example, at 193-nm wavelength, the photon attenuation length in silicon is only about 5.5 nm [10][12]. To simplify the analysis, we first ignore the photon losses in the 2 nm thin boron top layer and assume that the responsivity drop is only due to the photon absorption in the highly doped silicon region. Based on Eq. (4.1)

$$\text{Absorption coefficient} = e^{-\frac{\text{thickness}}{\text{attenuation length}}} \quad (4.1)$$

and the ratio between the measured responsivity and the theoretical attainable value for 193-nm wavelength (the calculated QE), the equivalent thickness of the highly doped silicon region can be roughly calculated and it is approximately 4.3 nm.

Moreover, as shown in Fig. 4.4, the VUV radiation is also absorbed intensively in the nanometer-thin α -boron layer. Compared to a 4-nm boron-covered PureB-diode, the responsivity of a similar PureB-diode (with 12-nm boron coverage) shows a drop of more than 50% (from 0.09 A/W to less than 0.04 A/W at 193 nm).

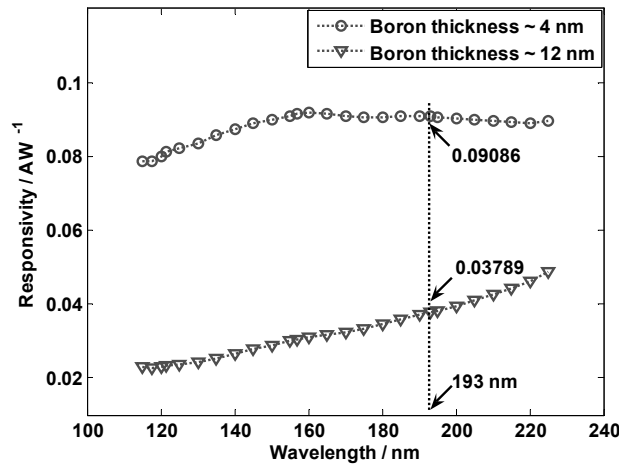


Fig. 4.4 Measured VUV/DUV responsivity of PureB-diodes with different boron thicknesses on the diode's surface. The measured diode was fabricated at DIMES (boron thickness was measured by ellipsometer).

Therefore, considering the additional photon absorption in the 2 nm α -boron layer, the thickness of the highly doped silicon region, which is actually the junction depth of the measured PureB-diode, should be even smaller than 4.3 nm.

On the other hand, as illustrated in Fig. 2.14, a SIMS-measured junction depth of an ultra-shallow junction PureB-diodes is about 10 nm (10^{19} cm⁻³ boron concentration was detected at a depth of 10 nm). It must be mentioned here that due to the extremely high surface-boron-concentration-induced knock-on effect during the SIMS measurement, the real junction depth should be less than 10 nm. As discussed in [18][19], based on simulation results, a 2 min 40 s boron deposition will deliver a junction depth of about 5 nm.

Thus far, even without taking the external reflection into account, we encounter a discrepancy between the calculated equivalent junction depth (<4.3 nm) based on the optical results, and the measured junction depth. This leads us to the idea that, possibly, in the first few nanometers below the silicon surface (the highly-doped p⁺ region), there is a charge-collection phenomenon, which can effectively extend the charge-collection zone (normally within the diode depletion region) toward the diode surface.

However, ultra-shallow junction devices cannot provide reliable information about the surface phenomena and their effect on the responsivity, since the depletion region (the conventional effective charge-collection zone) is too close to the diode surface. The real contribution of the surface charge-collection effect in the nanometer-thin p⁺ region to the measured responsivity is difficult to distinguish. In order to further investigate this surface charge-collection phenomenon, additional experiments were performed using devices with deeper p-n junctions.

As discussed in Chapter 3, deeper junction PureB-diodes can be formed by a thermal anneal after the boron deposition [18]. Fig. 4.5 shows the DUV/VUV responsivity of a deeper junction PureB-diode (DIMES sample). This device was fabricated by a 20 min anneal at 900 °C, and the simulated junction depth was around 150 nm (see Fig. 3.4) [18]. Normally, due to the nanometer attenuation length of DUV/VUV photons in silicon, for conventional silicon-based photodiodes, a junction depth of more than 100 nm means extremely low responsivity in the DUV and part of the VUV spectral range (wavelength between 100 nm and 300 nm).

However, as illustrated in Fig. 4.5, relatively high responsivity (around 0.05 A/W) was measured on the deep junction photodiode. This is about 50% of the responsivity of ultra-shallow junction devices without extra dopant “drive-in” [17][18]. A similar phenomenon has been observed in the EUV range [20]. Fig. 4.6 shows a fairly high responsivity ($\geq 85\%$ of the theoretical maximum around 13.5 nm [8][9]) measured on the same 150 nm deep junction device. The measured responsivity is significantly higher than the values calculated based on the absorption coefficient of 150 nm silicon layer [10][11].

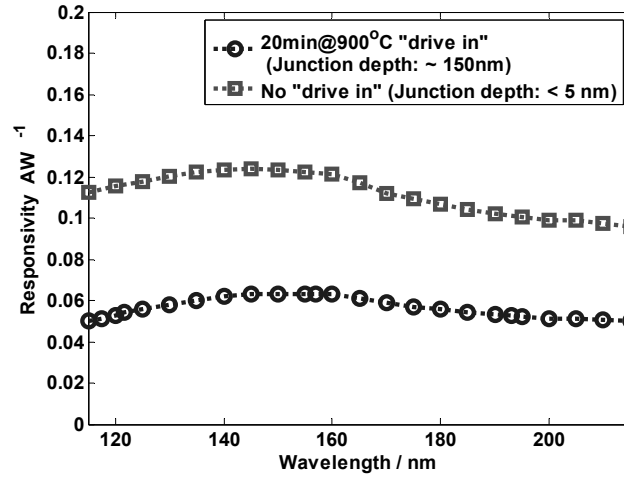


Fig. 4.5 Responsivity of PureB-diodes with different junction depths [17][18]. (Capping layer stack: deep junction, <1 nm boron + ~ 9 nm oxide; shallow junction: <1 nm boron + ~ 4 nm oxide. Measured by ellipsometer)

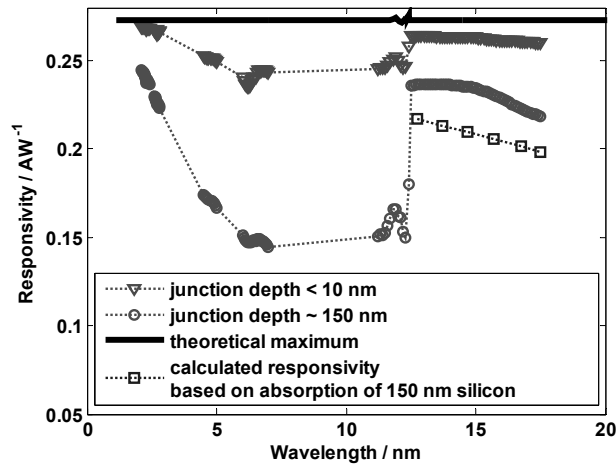


Fig. 4.6 Responsivity of the PureB-diodes (DIMES sample) with different junction depths compared to the theoretically attainable values for a Si-based photodiode, and the calculated responsivity based on the absorption coefficient of 150 nm Si [8][9][10][11][20].

Based on all these presented evidences, it is clear that, in addition to the shallow p-n junction, the outstanding DUV/VUV sensitivity of PureB-diodes is also

enhanced by a distinctive high surface charge collection process in the highly-doped p^+ region.

4.3.2 Doping-gradient-induced surface charge collection effect

The surface charge collection effect of photodiodes is not a completely new concept.

As early as 1979, a primitive design strategy, which intend to use the doping-profile-induced electric field to improve the optical sensitivity, had been proposed in [1]: “For a *p-on-n* silicon photodiodes, which is accomplished by diffusing *p*-type impurities into an *n*-type substrate, if a profile of the diffused impurity gradually decreases from the surface toward the junction, an internal built-in electric field would be induced in the diffused layer by the impurity gradient. The built-in electric field would cause optically excited carriers to drift toward the junction in shorter times than in the case of diffusion. In this way, it is helpful for to enhance the effective collection of photo-generated carriers.” But, due to the technique limitations at that time, device optical performance had suffered from many other unfavorable factors, such as diffusion-induced defects and the large junction depth. Therefore, no such photodiode, which could benefit from the doping-gradient-induced surface charge collection effect, had been practically made.

In [8][21][22], a continuous (and monotonous) charge collection efficiency as a function of depth had been modeled by the X-ray spectroscopy researchers using diode-like detectors for energy dispersive detection of single photons. As shown in Fig. 4.7, this charge collection model mainly involves three physical aspects: photon absorption positions (determined by the attenuation length); extension of the photo-generated charge cloud (R , in the figure); probability of photo-generated electrons at a certain depth to be effectively collected (charge collection efficiency, CCE) [22]. The essential point of this theory is the supposed long life-time of minority carriers: they diffuse in all directions but do not get lost. Eventually, just by chance, some of them enter the depletion region and are collected. However, no beneficial electric field is considered in this charge-collection model.

By combining the above mentioned two surface charge collection mechanisms, the observed charge collection phenomenon of PureB-diodes could be explained as follows: in the first few nanometers below the silicon surface, where the vast majority of the DUV/VUV photons are absorbed, a doping-gradient-induced internal electric field is created in the highly-doped p^+ silicon region. As illustrated in Fig. 4.8, this beneficial electric field (E_i) will separate the photo-generated carriers in the same manner as the built-in electric field (E_{bi}) in the diode depletion region, with the only difference being that the chance of recombination may be higher in the non-depleted region. Moreover, since the pure boron deposition and the subsequent thermal drive-in are both damage-free processes, it is plausible that the recombination in the p^+ layer is relatively small and consequently a long life-time of

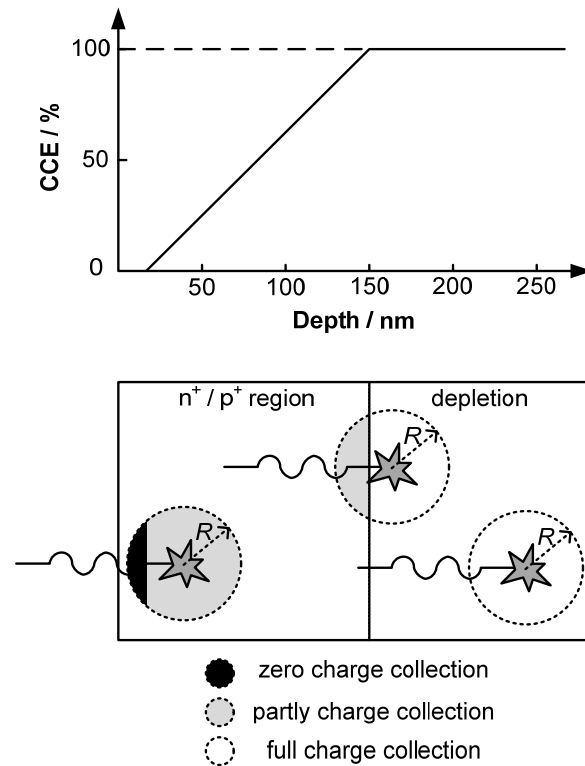


Fig. 4.7 Surface charge-collection theory introduced in [21][22]. Schematic plot of the charge collection efficiency CCE (top), compared with the schematic diagram of the photon absorption and charge collection in photodiodes (bottom) [22]. *The figure is reproduced by permission of IOP Publishing.*

minority carriers in this region should be expected. As a result, the effective charge-collection zone (normally within the diode depletion region) is extended toward the diode surface. Therefore, a higher responsivity can be achieved and a smaller equivalent junction depth is calculated.

Such a beneficial charge-collection effect is believed to be accomplished by the unique doping profile in the p^+ region of the PureB-diode: (i) the high doping gradient in the p^+ layer induces an internal electric field which has the same direction as the electric field in the depletion region; (ii) the amorphous boron capping layer, which plays a role as a dopant source, ensures that there will be no roll-off of the doping profile at the surface. This effect is otherwise often observed in, for example, implanted junctions (as shown in Fig. 4.9 [23]), and gives an undesirable reversal of the electric field direction at the surface.

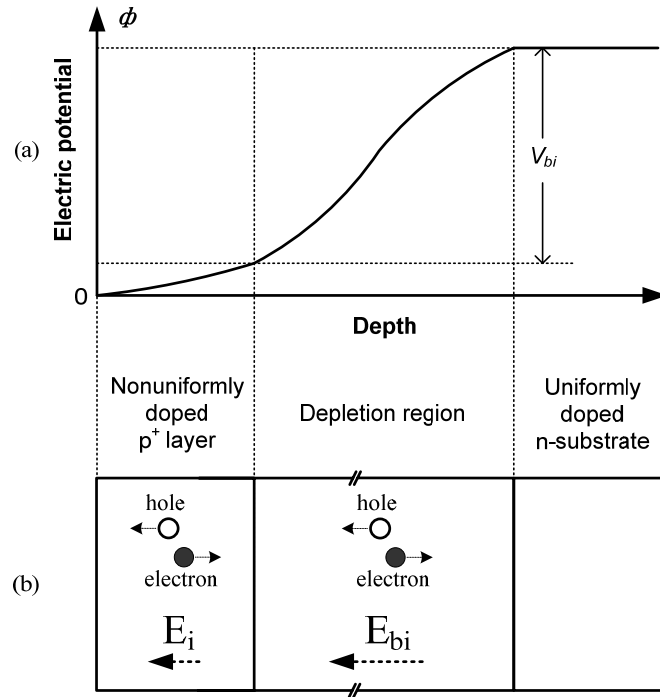


Fig. 4.8 (a) Schematic plot of the electric potential over depth of PureB-diodes (V_{bi} : the built-in voltage of a p-n junction), compared with (b) schematic diagram of the doping-gradient enhanced charge collection effect.

In Fig. 4.10a and b, the simulated doping profiles and the doping gradient induced internal electric field are shown for boron-doped junctions under different annealing conditions.

From the measured response (Fig. 4.11), the photo-generated carrier attenuation-length in p⁺ Si can be extracted based on Eq. (4.2), which expresses the number of carriers reaching the depletion edge:

$$y = y_0 \times e^{-\left(\frac{x}{L}\right)} \quad (4.2)$$

where y_0 is the initial number of photo-generated carriers, x is the depth from the silicon surface to the p⁺ region, and L is the attenuation length of photo-generated carriers due to the recombination in silicon. The carrier recombination rate may vary with the doping concentration, but in this simplified approximation a constant recombination rate is assumed in the p⁺ region.

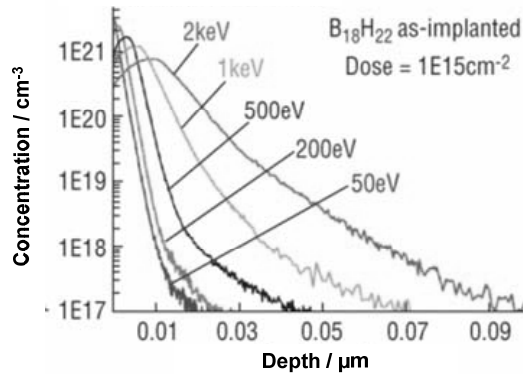


Fig. 4.9 Example of SIMS profiles of B₁₈H₂₂ implanted into c-Si. A significant roll-off of the doping profile at the surface was measured. *Figure is reproduced based on [23]*

The number of carriers reaching the depletion region can be assumed to be proportional to the measured photocurrent and consequently the photodiode responsivity. The exponential fitting curves of the measured responsivity of PureB-diodes with different junction depths (shown in Fig. 4.11) indicate that in the p⁺ region, the carrier attenuation-length is in the order of 400 nm to 500 nm with the DIMES devices and 700 nm to 1100 nm with the IMEC devices. Such a large attenuation-length indicates that although the electron-hole pairs are mainly generated in the nanometer-deep non-depleted p⁺ Si surface by DUV/VUV photons benefiting from the high doping-gradient-induced internal electric field and the defect-free doping process, most of the photo-generated carriers still can reach the hundreds of nanometers-deep depletion region without significant recombination in the p⁺ Si layer.

Possible explanations for the measured differences of the “photo-generated carrier attenuation-length” between the DIMES and IMEC photodiodes, shown in Fig.4.11, are: 1. Uncertainties of the “effective thermal anneal time” which affect the accuracy of the junction depth estimation; 2. Lower defect density of the IMEC samples in the p⁺ region; 3. Samples may have small difference in the capping layer thickness.

Further evidence of the presence of this beneficial charge-collection effect was also found during the optical performance stability tests. Details are discussed in Chapter 6.

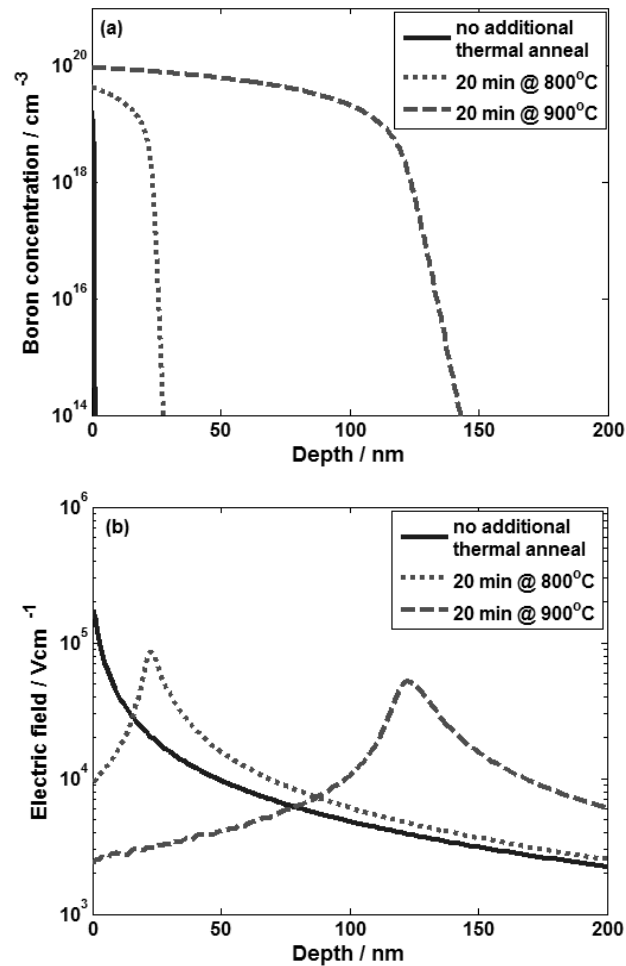
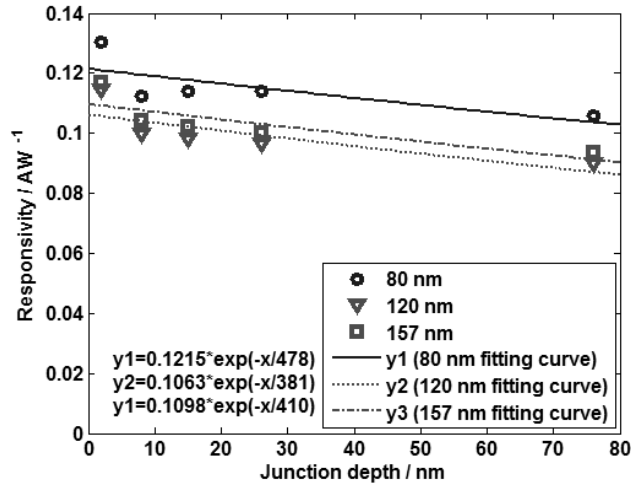


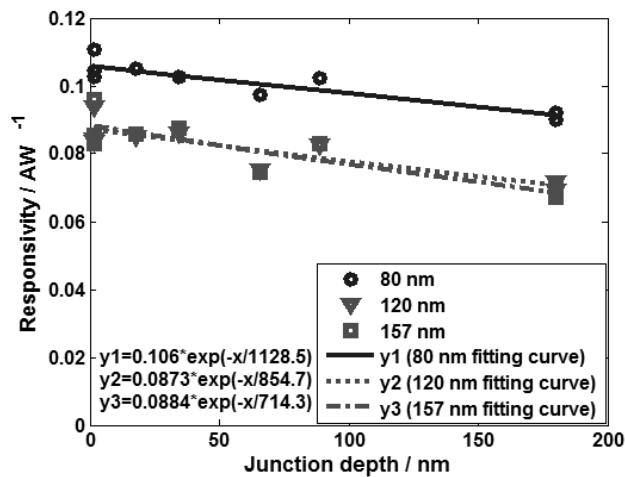
Fig. 4.10 (a) Simulated boron doping profile of PureB-diodes with different anneal temperatures; (b) simulated internal electric field corresponding to the different boron doping profiles. The maximum value of this electric field is found at the steepest part of the doping profile. Simulations were performed with Synopsys MEDICI™ software. [17]

To summarize, this observed high surface charge-collection efficiency (CCE) is ensured by several exceptional properties of PureB-diodes:

- (i) a damage-free p⁺ region up to the diode surface [24][25][26];
- (ii) a steep doping profile created in the p⁺ region;
- (iii) no doping profile roll-off at the diode surface.



(a)



(b)

Fig. 4.11 Measured responsivity of PureB-diodes with different junction depths, at 80nm, 120nm and 157nm wavelengths. (a) DIMES samples: the capping layer stacks were 1~1.5 nm boron layer and 1~2 nm parasitic oxide; (b) IMEC samples: capping layer stacks are 1~2 nm boron layer and 0.5~1.5 nm TiN passivation layer. [17]

4.4 Summary

Based on the reported experimental results and the above analysis, it becomes irrefutable that the α -boron capping layer of PureB-diodes acts as an ample source of

boron dopants, and therefore prevents a surface roll-off of the doping concentration, which is inevitable by other alternative doping techniques. Owing to such unique doping profile beneath the diode surface and the doping-gradient induced beneficial electric field in the p^+ region, PureB CVD technology gives the fabricated photodiodes effective charge collection up to the device surface, even if the p-n junction itself is quite deep. It has been demonstrated that, besides the “ultra-shallow junction”, an optimized doping profile plus a damage-free doping technique could be an alternative way to reduce the equivalent thickness of the pre-absorption layer on top of the photodiode effective charge-collection zone. This observed doping-profile-enhanced surface charge-collection effect offers significant opportunities for designing a high-sensitivity photodiode when an “ultra-shallow junction” is difficult to apply, when, for example, a low surface sheet resistance is the primary goal. In addition, it also enhances the compatibility of Pure-B CVD technology with standard Si processing, and becomes one of the inherent advantages of these silicon-based photodiodes when it comes to fabricating fully-integrated DUV/VUV smart-sensor systems.

References:

- [1] Hirobumi Ouchi, Toji Mukai, Tatsuya Kamei, Masahiro Okamura, "Silicon p-n junction photodiodes sensitive to ultraviolet radiation", *IEEE Trans. on Electron Devices*, vol. 26, no. 12, pp. 1965 – 1969, Dec. 1979.
- [2] A. Gottwald, U. Kroth, M. Richter, H. Schöppe and G. Ulm, "UV and VUV detector-based radiometry at the Metrology Light Source", *Meas. Sci. Technol.*, vol. 21, no. 12, 2010.
- [3] A. Gottwald, U. Kroth, M. Krumrey, M. Richter, F. Scholze and G. Ulm, "The PTB high-accuracy spectral responsivity scale in the VUV and X-ray range", *Metrologia*, vol. 43, pp. 125-129, 2006.
- [4] F. Scholze, R. Klein and R. Müller, "Characterization of detectors for extreme UV radiation", *Metrologia*, vol. 43, pp. 6-10, 2006.
- [5] F. Scholze, G. Brandt, R. Müller, B. Meyer, F. Scholz, J. Tümmeler, K. Vogel and G. Ulm, "High-accuracy detector calibration for EUV metrology at PTB", *Proc. SPIE*, vol. 4688, pp. 680-689, 2002.
- [6] F. Sarubbi, L. K. Nanver, T. L. M. Scholtes, S. N. Nihtianov and F. Scholze, "Pure boron-doped photodiodes: a solution for radiation detection in EUV lithography", *Proc. IEEE 38th European Solid-State Device Research Conference (ESSDERC)*, pp. 278-281, Sept. 2008.
- [7] L. Shi, F. Sarubbi, S. N. Nihtianov, L. K. Nanver, T. L. M. Scholtes and F. Scholze, "High performance silicon-based extreme ultraviolet (EUV) radiation detector for industrial application", *Proc. 35th Annual Conference of the IEEE Industrial Electronics Society (IECON)*, pp. 1891-1896, Nov. 2009.
- [8] F. Scholze, H. Rabus, and G. Ulm, "Mean energy required to produce an electron-hole pair in silicon for photons of energies between 50 and 1500 eV," *J. Appl. Phys.*, vol. 84, no. 5, pp. 2926–2939, Sept. 1998.
- [9] F. Scholze, H. Henneken, P. Kuschnerus, H. Rabus, M. Richter and G. Ulm, "Determination of the electron-hole pair creation energy for semiconductors from the spectral responsivity of photodiodes", *Nuclear Instruments and Methods in Physics Research*, A 439, 208-215, 2000.
- [10] Henke data. Available from: http://henke.lbl.gov/optical_constants.
- [11] NIST data. Available from: <http://physics.nist.gov>.
- [12] E. D. Palik (Ed.), *Handbook of Optical Constants of Solids*, Orlando, Academic Press, 1985.
- [13] M. Richter, U. Kroth, A. Gottwald, C. Gerth, K. Tiedtke, T. Saito, I. Tassy and K. Vogler, "Metrology of pulsed radiation for 157-nm lithography", *Appl Opt.*, vol. 41, no. 34, pp. 7167-7172, Dec. 2002.

- [14] L. R. Canfield, R. E. Vest, R. Korde, H. Schmidtke and R. Desor, "Absolute silicon photodiodes for 160 nm to 254 nm photons", *Metrologia*, vol. 35, p. 329-334, 1998.
- [15] K. Solt, H. Melchior, U. Kroth, P. Kuschnerus, V. Persch, H. Rabus, M. Richter and G. Ulm, "PtSi-n-Si Schottky-barrier photodetectors with stable spectral responsivity in the 120-250 nm spectral range", *Appl. Phys. Lett.*, vol. 69, no. 24, pp. 3662-3664, Dec. 1996.
- [16] L. Shi, F. Sarubbi, L. K. Nanver, U. Kroth, A. Gottwald and S. Nihtianov, "Optical performance of B-layer ultra-shallow-junction silicon photodiodes in the VUV spectral range", *Proc. Euroensors XXIV*, Sept. 2010.
- [17] L. Shi, S. Nihtianov, L. Haspeslagh, F. Scholze, A. Gottwald and L. K. Nanver, "Surface-Charge-Collection-Enhanced High-Sensitivity High-Stability Silicon Photodiodes for DUV and VUV Spectral Ranges", *IEEE Trans. on Electron Devices*, vol. 59, no. 11, pp. 2888 – 2894, Nov. 2012.
- [18] L. Shi, L. K. Nanver, A. Šakić, S. Nihtianov, T. Knežević, A. Gottwald and U. Kroth, "Series resistance optimization of high-sensitivity Si-based VUV photodiodes", *Proc. 2011 IEEE Instrumentation and Measurement Technology Conference (I2MTC)*, May 10-12, 2011.
- [19] A. Šakić et al., "Boron-layer silicon photodiodes for high-efficiency low-energy electron detection", *Solid-State Electronics*, vol. 65-66, pp. 38-44, Nov.-Dec. 2011.
- [20] L. Shi, L. K. Nanver, C. Laubis, F. Scholze and S. Nihtianov, "Electrical performance optimization of a silicon-based photodiode with near-theoretical quantum efficiency", *Proc. TRANSDUCERS2011*, Jun. 2011.
- [21] F. Scholze, M. Procop, "Modeling the response function of energy dispersive X-ray spectrometers with silicon detectors", *X-Ray Spectrometry*, vol. 38, no. 4, pp. 312-321, Aug. 2009.
- [22] R. Hartmann, P. Lechner, L. Strüder, F. Scholze, G. Ulm, "The radiation entrance window of pn junction detectors", *Metrologia*, vol. 32, no. 6, pp. 491-494, 1995.
- [23] L. A. Marquis et al., "Characterization of octadecaborane implantation into Si using molecular dynamics," *Phys. Rev. B*, vol. 74, no. 20, 2006.
- [24] L. K. Nanver, T. L. M. Scholtes, F. Sarubbi, W.B. de Boer, G. Lorito, A. Sakic, S. Milosavljevic, C. Mok, L. Shi, S. Nihtianov and K. Buisman, "Pure-boron chemical-vapor-deposited layers: a new material for silicon device processing", *Proc. 18th International Conference on Advanced Thermal Processing of Semiconductors (RTP2010)*, pp. 136-139, Sept.- Oct. 2010.
- [25] F. Sarubbi, L. K. Nanver and T. L. M. Scholtes, "High effective Gummel number of CVD boron layers in ultrashallow p⁺n diode configurations", *IEEE Trans. Electron Devices*, vol. 57, no. 6, pp. 1269-1278, 2010.
- [26] F. Sarubbi, L. K. Nanver and T. L. M. Scholtes, "CVD delta-doped boron surface layers for ultra-shallow junction formation", *ECS Transactions*, vol. 3, no. 2, pp. 35-44, Nov. 2006.

Chapter 5 Response Time Characterization and Series Resistance Optimization

Together with the superior UV sensitivity, the optically optimized structure (nanometer-thin boron coverage, nanometer-deep junction and the “ring electrode”) results in a high sheet resistance (R_{sheet}) on the surface of PureB-diodes. Such a high R_{sheet} is expected to result in an unpredictable charge removal time of the photodiodes when the area and/or the position of the incident light spot are different. In this chapter, the dependence of the response time of PureB-diodes on the size and location of the illuminated area is studied. To improve the response speed, a series resistance optimization is presented by modifying the diode structure.

5.1 High surface sheet resistance

As discussed in the previous chapters, to guarantee maximum internal quantum efficiency, and hence maximum sensitivity, the absorption of the incident radiation has to be prevented before it reaches the effective charge-collection zone (normally the depletion region of photodiode), where the photo-generated charge is separated and collected [1]. In particular, when the penetration depth of the incident radiation in silicon is extremely small, as is the case in the DUV and part of the VUV spectral ranges (Fig. 2.4), it is important that the charge-collection zone of the photodiode (the depletion region) is as close to the device optical surface as possible [2]. PureB-diodes meet this requirement with their ultra-thin boron coverage and ultra-shallow p^+n junction.

However, an ultra-shallow junction results in a very thin top layer with possibly high sheet resistance (R_{sheet}). In the case of PureB-diodes with p^+ boron doping of the top 1-10 nm of the Si surface, the R_{sheet} is $\sim 10 \text{ k}\Omega/\text{sq}$ or more [1][3][4], depending on the exact processing scheme. Depositing an additional conductive layer on the photodiode-sensitive surface (to be used as one of the diode electrodes) inevitably leads to undesirable absorption of the incident radiation, and hence reduces the sensitivity. Instead, the electrode (typically made of aluminum) is placed at the edge of the active area to form what is often referred to as a “ring electrode”, as indicated in Fig. 3.1 and 5.1 [4][5][6]. For PureB-diodes with a large active area, this high surface R_{sheet} induced by the ultra-shallow junction dominates the series resistance (R_s) of the device, and affects the electrical and optical performance of the PureB-diodes in the following respects:

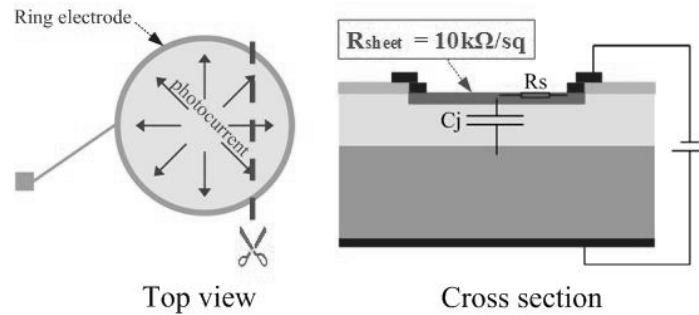


Fig. 5.1 Schematic of a Si-based p^+n photodiode with a ring electrode and an ultra-shallow junction. [4][6]

1. Unpredictable response time

Previous studies [7][8][9] show that the R_s of a photodiode under DC-irradiation, when dominated by the R_{sheet} , is not affected by the size of a photodiode with a round sensitive area, but is affected by the size and the location of the illuminated area [8], as presented in Fig. 5.2 and Eq. (5.1) and (5.2) [8][9]. On the other hand, the junction capacitance C_j is defined only by the junction area and the depletion region width, since the photo-generated charge, regardless of where it was initially created, spreads almost instantly over the whole junction area. This has led to the concern that the photodiode time constant τ , which is the product of R_s and the C_j

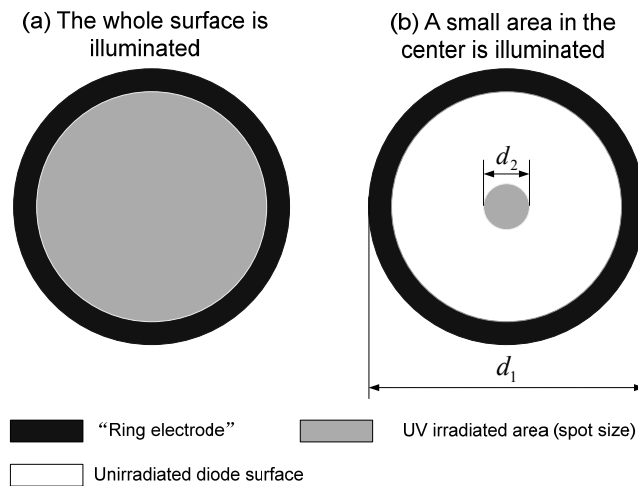


Fig. 5.2 Different sizes of the illuminated area.

(shown in Eq. 5.3), will also be affected by the size and location of the illuminated area. Since this time constant poses a lower limit to the response time, variations in R_s may lead to an unpredictable response time [4][5].

$$R_s = \frac{R_{sheet}}{8\pi} \quad (\text{related to Fig. 5.2 a}) \quad (5.1)$$

$$R_s = \frac{R_{sheet}}{8\pi} \left[1 + 4 \ln \left(\frac{d_1}{d_2} \right) \right] \quad (\text{related to Fig. 5.2 b}) \quad (5.2)$$

$$\tau = R_s C_j \quad (5.3)$$

2. Low operational speed

As presented in [4][5], the photocurrent, which is caused by the photo-generated electron-hole pairs separated in the depletion region, travels through the thin top-layer with a relatively large R_{sheet} . Eq. (5.1) shows that—for a fully illuminated diode, i.e. $d_1=d_2$ (Fig. 5.2a)—the series resistance, which is produced by the sheet resistance, does not depend on the sensitive area of the photodiode. However, the junction capacitance scales with the sensitive area. That is why large-area diodes have a larger time constant, and hence a lower operational speed, which may affect the detection of high frequency UV pulses.

5.2 Response time versus variational irradiation area

To study the relation between the response time for pulsed irradiation and the irradiation area, the dynamic performance of an ultra-shallow junction PureB-diode (DIMES sample, with an 11 mm² circular-shaped active area) was experimentally verified. For this purpose a simple test setup for measuring the time constant of the photodiode was created. In the test setup, a green light emitting diode (LED) was chosen as the light source [4][5]. The penetration depth of green light (wavelength 520 nm ~ 565 nm) in silicon is approximately 1 μm, which is close to the penetration depth of EUV radiation (13.5 nm) in silicon ~ 0.7 μm. Two lenses were applied during the test to focus the light emitted by the LED onto a point. By moving the photodiode we can vary the size and the location of the illuminated area. The LED was driven by a pulsed signal with a frequency of 100 kHz; the pulse duration was 100 ns. The photodiode readout circuit is shown in Fig. 5.3 [4][5]. Essentially, it is a trans-impedance amplifier with a time constant of 1 ns.

Experimental results are presented in Fig. 5.4 a and b. It can be seen that the measured time constants are similar even when the light spot has different sizes and locations. The time constant extracted from the measurement is about 98 ns. To

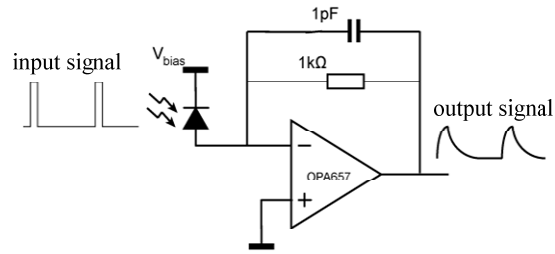
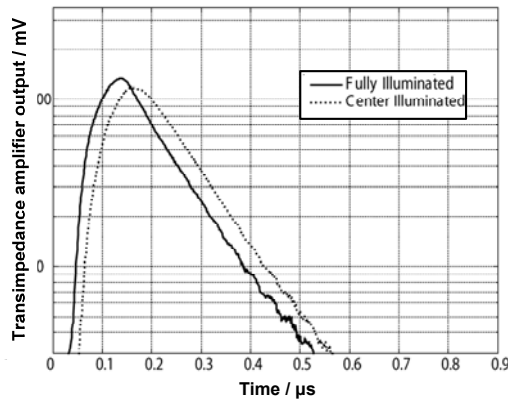
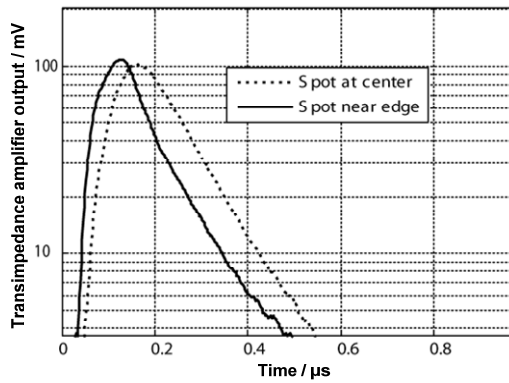


Fig. 5.3 Readout circuit schematic. [4][5]



(a)



(b)

Fig 5.4 Measured photodiode response to a pulse radiation input (a) when the illuminated area sizes are different and (b) when the illuminated spot positions are different. [4][5]

better understand the experimental results, a couple of SPICE simulations were carried out based on the distributed RC network shown in Fig. 5.5, which is believed to represent the photo-generated charge-transfer process much more accurately than the lumped-parameters model of the photodiode. If the illuminated area is circular and concentric with the diode, the symmetry can help to simplify the model. Then the photodiode can be divided into a number of rings, each of which is modeled by an RC-network (Fig. 5.5) [4][5]. The values of the resistances and the capacitances are derived from Eq. (5.4) and (5.5):

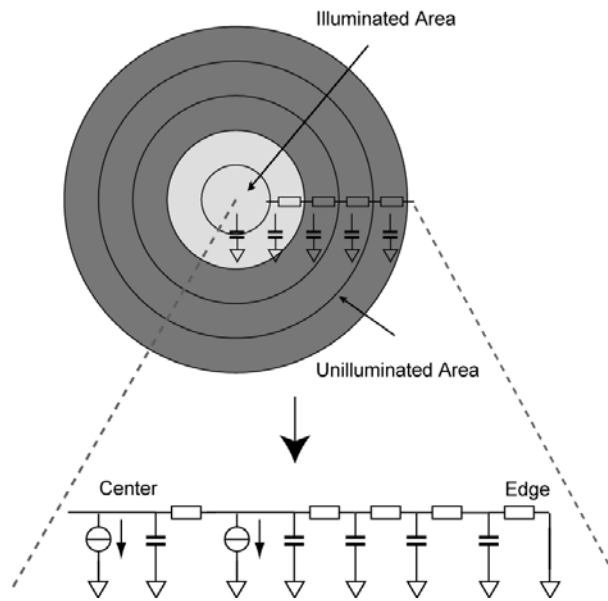


Fig. 5.5 The equivalent circuit when a shallow junction photodiode is partially illuminated. [4][5]

$$R_{ij} = \frac{R_{sheet}}{2\pi} \ln\left(\frac{r_i}{r_j}\right), \text{ with } R_{sheet} = 10k\Omega \quad (5.4)$$

$$C_i = C_{diode} \left(\frac{r_i^2 - r_{i-1}^2}{r_{diode}^2} \right), \text{ with } C_{diode} = 100pF \quad (5.5)$$

where R_{ij} is the resistances between two nodes and C_i is the capacitance representing one ring in the RC-network. r_i and r_j are the corresponding radii of each ring.

When the irradiation intensity is uniform over the photo-sensitive area, if a ring is illuminated, a current source is added to the node of the RC network corresponding to the area of that ring. The value of the current is proportional to the area of the ring.

The simulation results of two cases are shown in Fig. 5.6. The duration of the current pulse in the simulation was 100ns. As can be seen from the plot in Fig. 5.6, with a logarithmic scale for the current, after an initial short period (~0.1 us), the two current curves transform into straight parallel lines. This basically means that the time constants in both cases—central illumination and full illumination—are the same. This result agrees well with the above-mentioned experimental results [4][5].

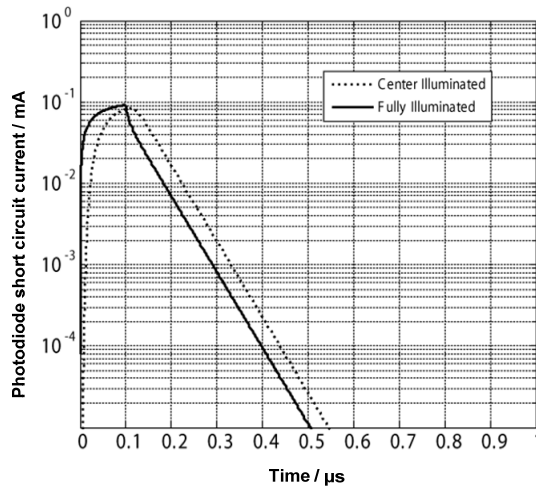


Fig. 5.6 Simulated photodiode short circuit output current with SPICE. [4][5]

This result can be understood in the following way: when the illumination stops, the already generated charge tends to spread itself rapidly over the junction capacitance of the photodiode toward a “balance state”. A “balance state” means that the charge distribution gradient over the junction area is caused only by the high surface sheet resistance, and is no longer a result of the spot location and size. To verify this process, an additional SPICE circuit simulation is performed based on the same model shown in Fig. 5.5. In this simulation, for both cases—central illumination and full illumination—the voltage of each node (shown in Fig. 5.7) was

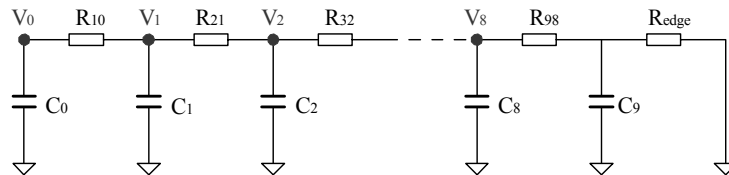
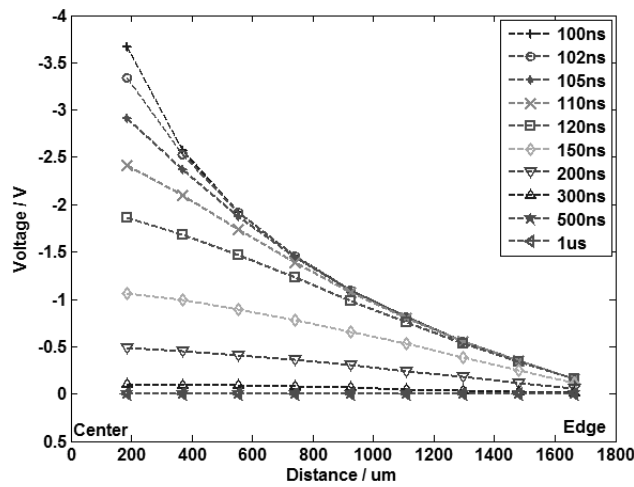


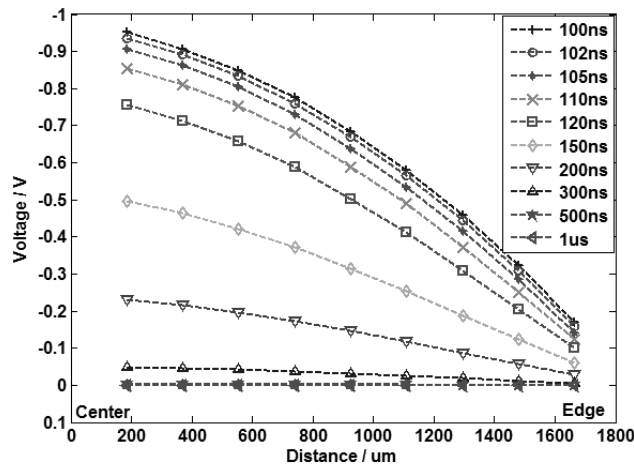
Fig. 5.7 Circuit model for the SPICE simulation.

measured at different moments after exposure. Then, the voltage distribution on the photodiode at different moments after exposure has been plotted in Fig. 5.8 a and b. The voltage value at any point is proportional to the photo-generated charge stored at this point. This means that the voltage distribution shown in Fig. 5.8 follows the same trend as the photo-generated charge distribution.

As shown in Fig. 5.8a, just after the central illumination, the voltage is much higher in the center than at the edge. As a result, most of the photo-generated charge



(a)



(b)

Fig. 5.8 Voltage distribution after (a) center illumination and (b) after full illumination.

is located in the central area at this moment. In the full-illumination case, the voltage, and consequently the photo-generated charge, is more evenly spread throughout the surface of the diode. Only 20ns after illumination, the voltage distribution curves start to follow the same trend for both cases, which can be considered as the “balanced state” mentioned above. This analysis result agrees well with Fig. 5.6, where during the first ~20ns after illumination, the fully illuminated curve maintains a higher slope than the center-illuminated one. This indicates that just after illumination, the fully illuminated surface has more photo-generated charge at the edge than the center-illuminated case. Therefore, photo-generated charge near the edge can easily be taken away by the nearby ring electrode. This is the behavior previously observed for DC illumination [7]. For pulsed irradiation, a “balanced state” is achieved 20ns after the pulse. The two curves are in parallel with each other, which means the time constant for both cases is now the same.

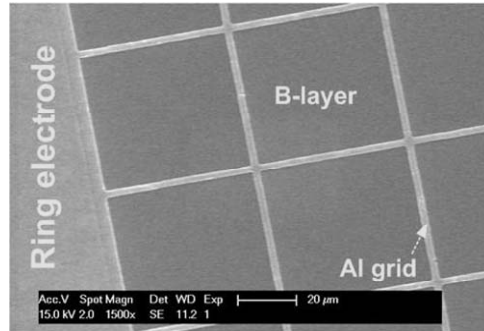
Based on the experimental results, it is clear that when the exposed area/location is different on the diode surface, the high surface sheet resistance will affect the time constant of PureB-diodes only within a very short time (for example, during the first 20ns) after the illumination. In practical applications, this rapid process is negligible.

5.3 Series resistance optimization

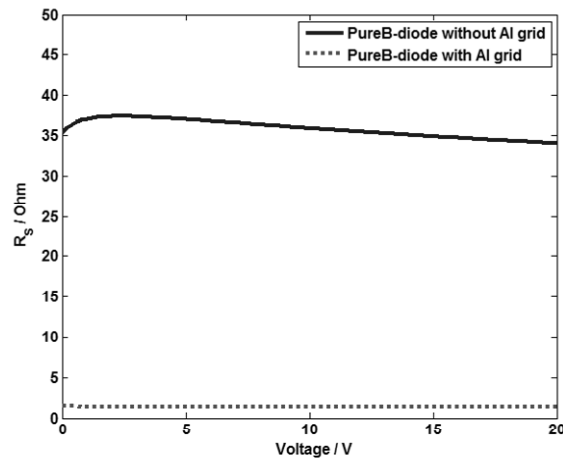
As discussed above, the response time of the PureB-diodes is limited by R_s and C_j . Therefore, with smaller values of C_j and R_s , a higher operational speed can be achieved. The junction capacitance can be adjusted by varying the thickness of the low-doped epi-layer and the doping profile. However, technology and production-cost limitations need to be considered when optimizing the process in this direction. Subsequently, what remains to be considered is the reduction of R_s . Two strategies have been chosen to optimize the R_s of the PureB-diodes: (i) an extended anode electrode; (ii) a deeper junction.

1. Extended anode electrode

The first solution is to improve the anode electrode layout. Fig. 5.9 shows the SEM image of an extended anode electrode, which is achieved by patterning an aluminum grid directly on the deposited boron layer [4][6][10]. With 3- μm wide Al-grid lines and a pitch of 50 μm , the R_s of the diode, and consequently the response time, are both reduced by more than ten times, as indicated in Fig. 5.9b [4]. On the other hand, the effective detection area is reduced due to the added metal grid, which blocks the incident VUV radiation. Compared to the bare diode, a drop in the responsivity is observed both in the VUV and EUV spectral ranges, as shown in Fig. 5.10 a and b. In addition to the drop in sensitivity, the metal grid also deteriorates the local non-uniformity of the sensitivity. For applications which require a high uniformity of responsivity, an extended electrode is not a suitable option.



(a)

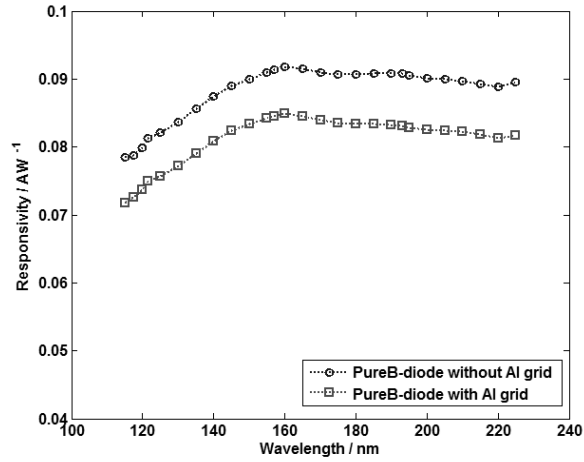


(b)

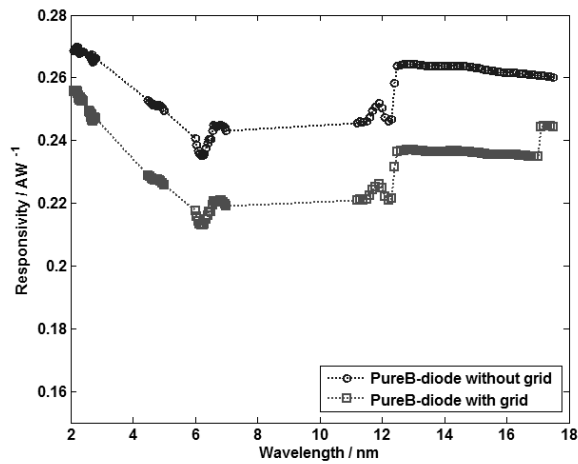
Fig. 5.9 (a) Photograph of the Al-grid and the ring electrode; (b) series resistance vs. reverse bias voltage of PureB-diodes with/without an extended Al grid, measured by impedance analyzer at 1 MHz. During the measurement, both the series resistance (R_s) and the junction capacitance (C_j) were extracted as a function of the bias voltage. The results prove that R_s of PureB-diodes is only slightly dependent of the reverse bias voltage.

2. Deep junction

Another solution for reducing R_s is to increase the depth of the boron doped p^+n junction by a thermal anneal step after the boron layer deposition, which drives the boron dopants further into the silicon. Table 5.1 presents the relationship between different anneal recipes and the resulting junction depth [4][6]. As already introduced in Chapter 3, by varying the anneal temperature (800 °C to 900 °C) and time (10 min to 20 min), the junction depth of the PureB-diode can be sufficiently controlled in the range from a few nanometers to hundreds of nanometers. Over the examined range, the corresponding R_{sheet} varies from ~ 10 k Ω /sq down to ~ 200 Ω /sq



(a)



(b)

Fig. 5.10. Measured responsivity of PureB-diodes with/without an extended anode electrode (Al-grid) in the: (a) VUV, (b) EUV spectral ranges. [4]

when a 160 s deposition at 700 °C is extended with a 20 min anneal at 900 °C [6]. It can be seen in Fig. 5.11 that the measured R_s continues to decrease as the “drive-in” time/temperature is increased. After a 20 min anneal at 900 °C, the R_s is about 10 times smaller than the ultra-shallow junction devices (reduced from $\sim 50\Omega$ to $\sim 5\Omega$), with the same $1\times 1\text{cm}^2$ junction area [4][6].

As already discussed in Chapter 4, due to the beneficial steep doping profile under the surface of PureB-diode, a very high surface charge-collection efficiency

TABLE 5.1 ANNEAL RECIPES VS. SIMULATED JUNCTION DEPTH [6]

Anneal Recipes	Simulated Junction Depth
No anneal	<5 nm
10 min @ 800°C	~ 20 nm
30 min @ 850°C	>30 nm
20 min @ 900°C	~150 nm

The simulations were performed with Taurus TSUPREM-4™.

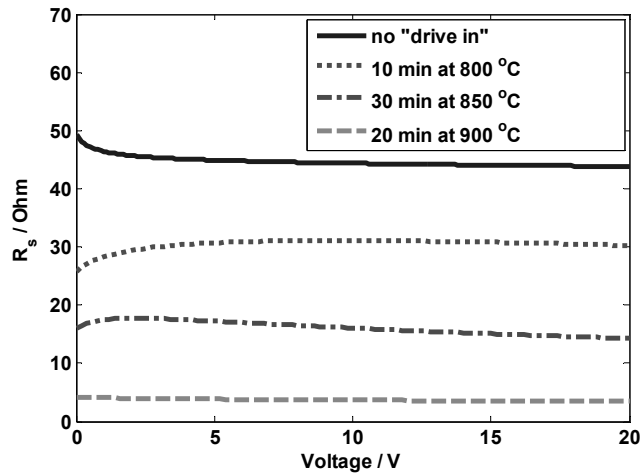


Fig. 5.11 Series resistance vs. reverse bias voltage of PureB-diodes fabricated with different anneal recipes. (R_s is measured by impedance analyzer at 1 MHz.) [4]

(CCE) was found in the boron-doped p^+ surface layer. Based on this unique feature, the photon-generated charge can be collected effectively in the highly doped p^+ Si layer close to the surface, allowing a still high VUV/EUV responsivity to be achieved with deeper junction PureB-diodes (~50% of the responsivity of ultra-shallow junction devices, shown in Fig. 4.5).

As illustrated in Fig. 4.5 and Fig. 5.10, for achieving a similar series resistance level ($R_s < 5 \Omega$, shown in Fig. 5.9b and Fig. 5.11), the ultra-shallow junction devices with additional extended anode electrode have the advantage in DUV/VUV sensitivity. In contrast, the deeper junction PureB-diode can guarantee a high local uniformity of the responsivity.

5.4 Summary

Two negative effects related to a high surface sheet resistance have been studied, including unpredictable response times and high series resistance. Experimentally it has been demonstrated that different illumination spot areas/locations can only slightly affect the response time of PureB-diodes with a high surface sheet resistance. In practical applications, the influence is negligible. Moreover, by improving the structure of the PureB-diodes either by creating an extended anode with the help of an aluminum grid, or by extra thermal annealing, the sheet resistance—consequently the series resistance—of the diode’s surface can be effectively reduced. Although PureB-diodes with an aluminum grid have a higher responsivity for the same series resistance level, the local non-uniformity of the sensitivity limits the applications of this method. On the other hand, deep junction PureB-diodes can also achieve a reasonably low series resistance, while, owing to the high surface charge-collection efficiency, still maintain a good VUV/EUV responsivity and an excellent uniformity.

Reference:

- [1] L. Shi and S. Nihtianov, "Comparative Study of Silicon-Based Ultraviolet Photodetectors", *IEEE Sensors Journal*, vol. 12, no. 7, pp. 2453-2459, July 2012.
- [2] US Patent 7 586 108, Radiation detector, method of manufacturing a radiation detector and lithographic apparatus comprising a radiation detector, September 8, 2009.
- [3] F. Sarubbi, L. K. Nanver, T. L. M. Scholtes, S. N. Nihtianov and F. Scholze, "Pure boron-doped photodiodes: a solution for radiation detection in EUV lithography", *Proc. IEEE 38th European Solid-State Device Research Conference (ESSDERC)*, pp. 278–281, Sept. 2008.
- [4] L. Shi, S. Nihtianov, S. Xia, L. K. Nanver, A. Gottwald and F. Scholze, "Electrical and optical performance investigation of Si-based ultrashallow-junction p⁺-n VUV/EUV photodiodes", *IEEE Transactions on Instrumentation and Measurement*, vol. 61, issue 5, pp. 1268-1277, May 2012.
- [5] S. Xia, F. Sarubi, R. Naulaerts, S. Nihtianov and L. Nanver, "Response time of silicon photodiodes for DUV/EUV radiation", *Proc. 2008 IEEE Instrumentation and Measurement Technology Conference (I2MTC)*, pp. 1956-1959, May 2008.
- [6] L. Shi, L. K. Nanver, A. Šakić, S. Nihtianov, T. Knežević, A. Gottwald and U. Kroth, "Series resistance optimization of high-sensitivity Si-based VUV photodiodes", *Proc. 2011 IEEE Instrumentation and Measurement Technology Conference (I2MTC)*, May 10-12, 2011.
- [7] F. Scholze, R. K. Klein and R. Müller, "Linearity of silicon photodiodes for EUV radiation" *Proc. SPIE*, vol. 5374, pp. 926–934, 2004.
- [8] G. K. Reeves, "Specific contact resistance using a circular transmission line model," *Solid-State Electron.*, vol. 23, no. 5, pp. 487–490, May 1980.
- [9] N. C. Wyeth "Sheet resistance component of series resistance in a solar cell as a function of grid geometry," *Solid-State Electron.*, vol. 20, no. 7, pp. 629–634, July 1977.
- [10] L. Shi, L. K. Nanver, A. Šakić, S. Nihtianov, A. Gottwald and U. Kroth, "Optical Stability Investigation of High-Performance Silicon-Based VUV Photodiodes," *Proc. IEEE SENSORS2010*, pp. 132-135, Nov. 2010.

Chapter 6 Stability Characterization

The capability of Si-based photodetectors to withstand UV radiation is an unconditional requirement for a variety of industrial applications. A good example can be found in next-generation 13.5-nm lithography systems [1]: UV detectors used to optimize the imaging performance will be exposed to EUV radiation levels as high as 1 MJ/cm^2 [2]. Moreover, since EUV radiation is readily absorbed by air and the detectors must operate under vacuum conditions, in order to minimize maintenance costs and throughput reduction, the photodetectors should not be frequently replaced (preferably used during the lifetime of the machine), which imposes a considerable demand in terms of negligible degradation of the electrical and optical behavior of the photodiodes over a ten-year machine lifetime [2]. Similar requirements for stability and reliability can be found in space applications. In this chapter, after a short discussion about the possible types of UV-induced damage in Si-based photodiodes, the stability performance of PureB-diodes under DUV/VUV and EUV radiation is characterized. A strategy is proposed for creating a UV radiation-hard Si-based photodiode.

6.1 Possible UV-induced defects in silicon photodiodes

Silicon has a relatively low band-gap energy (EG) of about 1.12eV at 300K, which is smaller than the photon energy in the UV spectral range (350 nm - 10 nm). As a result, UV photons can cause ionization damage in Si-based devices [3][4][5]. Examples of defects that are induced by the ionization damage are: oxide-trapped charges and interface states [4]. In semiconductor materials, defects introduce intermediate energy levels in the forbidden band-gap zone and consequently affect the performance of the device [6]. Specific to Si-based photodiodes, such defects could lead to a higher dark current and/or a lower responsivity. As reviewed in Chapter 2, most of the conventional Si-based photodetectors demonstrate insufficient radiation hardness to high-energy photons, especially in the EUV spectral range [7-14]. In order to evaluate the radiation hardness of Si-based PureB-diodes, their electrical and optical performance stability is tested by prolonged UV exposure.

6.2 Optical performance stability

6.2.1 DUV/VUV stability

The VUV radiation hardness of the PureB-diode was characterized by a series of irradiations in the VUV spectral range (107 mJ/cm^2 at 157 nm, 48 mJ/cm^2 at 121 nm, and 28 mJ/cm^2 at 70 nm) [15]. After all exposures, the diode responsivity was

checked over the next few months. The exposed diode was fabricated at DIMES. It has an ultra-shallow junction (junction depth < 10 nm). In addition, less than one nanometer of boron coverage and a 4~5 nanometer parasitic oxide were measured by the ellipsometer on the diode surface, which is similar to “Sample #1” shown in Table 3.1.

During this stability test, the VUV responsivity was measured immediately after each illumination step. As indicated in Fig. 6.1, responsivity degradation was observed after exposure. However, when all the illumination steps had been completed, the responsivity of this PureB-diode recovered slowly with time due to a self-healing process. Such responsivity degradation with a subsequent self-healing process can be explained by the external photoelectron emission effect shown in Fig. 6.2. As already mentioned in Chapter 2, the external photoelectron emission is a common effect for devices exposed to VUV/EUV radiation [16]. When the incident VUV/EUV photons reach the surface of the device, electrons are kicked out resulting in the oxide surface being positively charged (see Fig. 6.2). Such positive charge can induce an unwanted electric field (E_c) under the diode surface which has an opposite direction to the beneficial doping-gradient-induced electric field (E_i) in the p^+ silicon. Considering the nanometer-deep junction of the tested PureB-diode, this positive surface charge and the resulting electric field will affect the charge-collection efficiency within the p^+ region (demonstrated in Chapter 4), and consequently reduce the responsivity of the PureB-diode.

Fig. 6.3 presents the results of a few linear responsivity scans along the surface of

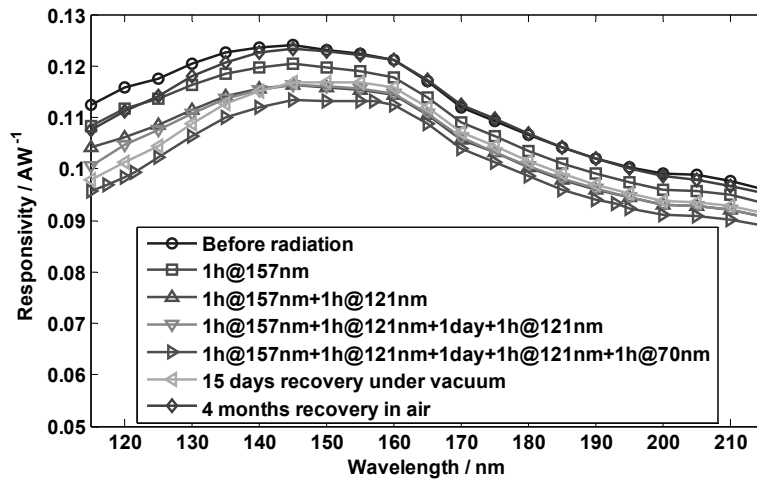


Fig. 6.1 Responsivity degradation of the DIMES-fabricated PureB-diode (junction depth: < 10 nm; ellipsometer-measured capping layer stack: < 1 nm α -boron layer; 4~5 nm parasitic oxide) in the VUV spectral range after a series of VUV irradiations. [15]

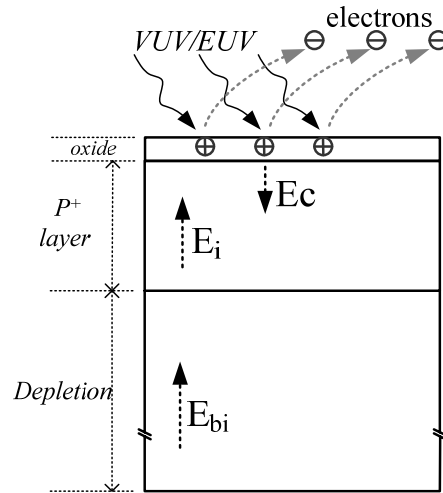


Fig. 6.2 Schematic illustration of the influence of the external photoelectron emission induced positive surface charge on the beneficial “Surface Charge-Collection” effect in the PureB-diode (E_c is the surface-charging-induced electric field; E_i is the doping gradient-induced electric field; and E_{bi} is the built-in electric field in the p-n junction).

the exposed diode at a wavelength of 193 nm. Besides the measured responsivity degradation and the following recovery process within the exposed area, the tendency of the irradiation-induced positive charge to spread and to be discharged, can be clearly distinguished.

To reduce this surface-charging-induced responsivity degradation, PureB-diodes with a new anode layout (ring electrode plus extended aluminum grid) were proposed [15][17][18]. Details on this type of device are shown in Fig. 5.9. As already discussed in Chapter 5, the sheet resistance (R_{sheet}) on the diode surface can be reduced significantly by this extended electrode. A lower R_{sheet} should help to speed up the discharging process of the harmful radiation-induced positive charge, if the discharging is a result of charge flow along the device surface. Consequently, better optical performance stability should be achieved.

Fig. 6.4 a and b present the monitored responsivity degradation of PureB-diodes with the extended anode during a prolonged VUV exposure at a 121-nm wavelength and 157-nm wavelength, respectively. For comparison, another similar PureB-diode with only a “ring-electrode” was measured under the same conditions. As shown in the figures, a responsivity decrease (about 1.5% at 157-nm wavelength; ~ 3.5% at 121-nm wavelength) was observed in both samples. Although the PureB-diode with the extended anode electrode has a relatively small series resistance (see Fig. 5.9), from the experimental results it appears that the stability of this sample has been

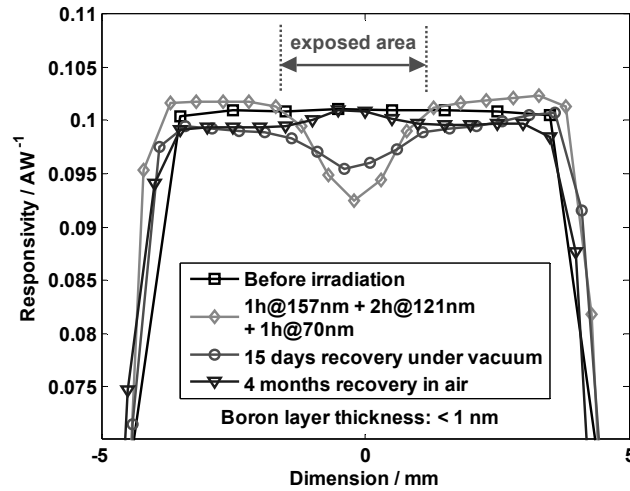
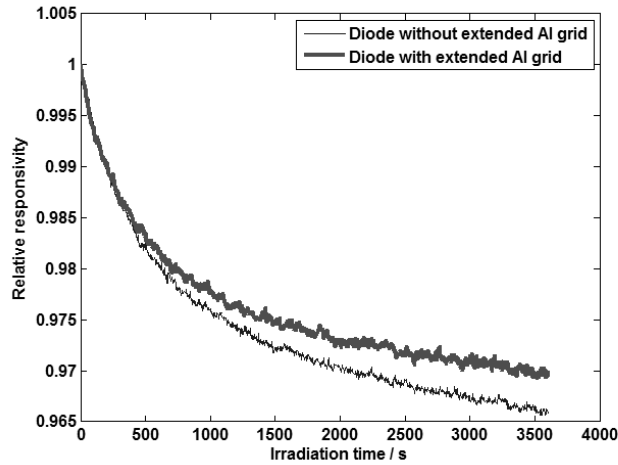


Fig. 6.3 Responsivity of the DIMES-fabricated PureB-diode (junction depth: < 10 nm; ellipsometer measured capping layer stack: < 1 nm α -boron layer; 4~5 nm parasitic oxide) at 193 nm wavelength after a series of VUV irradiations (107 mJ/cm^2 at 157 nm; 48 mJ/cm^2 at 121 nm; and 28 mJ/cm^2 at 70 nm) performed in the central region [15].

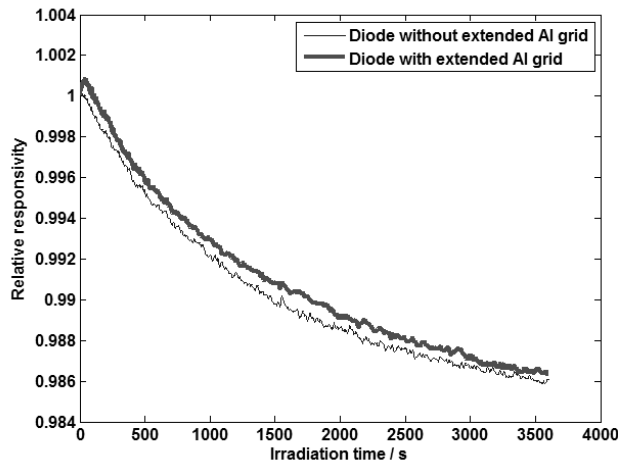
only slightly improved at the 121-nm wavelength. Under 157-nm radiation, no significant difference has been observed between the two samples [18]. The self-healing process of the tested samples is evaluated in Fig. 6.5 a and b. The calculated ratios of the measured responsivity (before irradiation and 5 months after irradiation) show that, compared with the device with only a “ring-electrode”, the PureB-diode with an “grid anode” demonstrated a slightly faster recovery (mainly around 130-nm wavelength) [18].

It is plausible that, with such a grid density (with $3\text{-}\mu\text{m}$ wide aluminum grid lines and a pitch of $50 \mu\text{m} \times 50 \mu\text{m}$, shown in Fig. 5.9), the discharging direction on the diode surface is more vertical than horizontal. In other words, most of the positive charge on the surface is discharged by electrons from the underlying nanometer-deep p^+ region. Only the positive charge near the aluminum grids is compensated by electrons from the extended anode.

Besides the surface charging effect, the radiation-induced Si-SiO₂ interface damage, which cannot be suppressed by an additional metal grid, could be another reason for the responsivity degradation [3][5][19][20]. In principle, for a conventional p-n junction photodiode, the Si-SiO₂ interface defects (dangling bonds) should not affect the responsivity, since this kind of defects are out of the diode depletion, which is normally the effective charge-collection zone. However, as presented in Chapter 4, PureB-diodes have a significant effective charge-collection



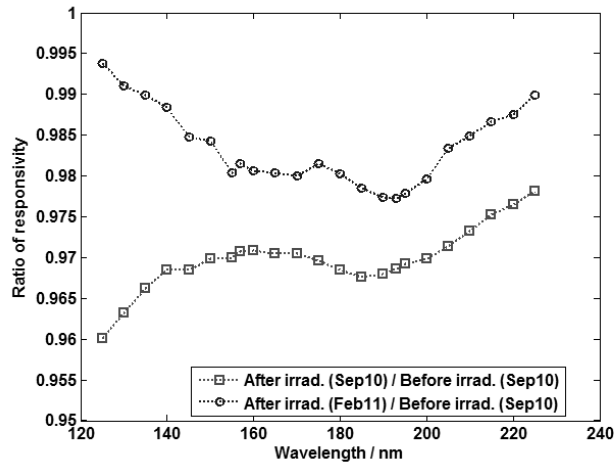
(a)



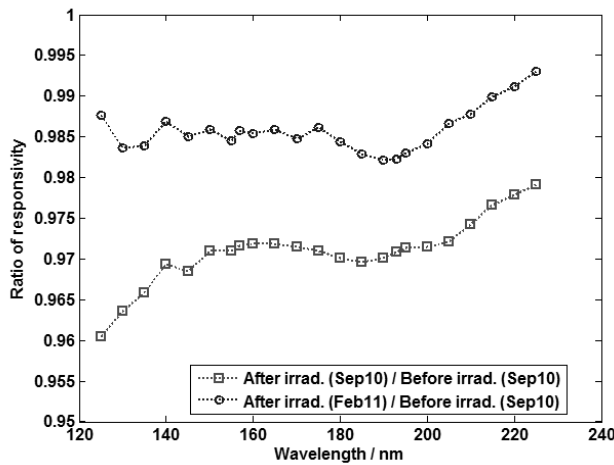
(b)

Fig. 6.4 Monitored responsivity at (a) 121 nm wavelength and (b) 157 nm wavelength of fabricated PureB-diode with/without an extended aluminum grid (junction depth: < 10 nm; ellipsometer measured capping layer stack: ~4 nm α -boron layer; and ~3 nm parasitic oxide) [18].

process starting from the diode surface. Therefore, the radiation-induced Si-SiO₂ interface dangling bonds may play a role as a “recombination center” in the nanometer-thin p⁺ silicon region and lead to unwanted losses of the photon-generated charge. Consequently a lower responsivity will be measured.



(a)



(b)

Fig. 6.5 Ratio of the measured responsivity of the DIMES-fabricated PureB-diode (a) with, and (b) without an additional Al grid, before/after VUV exposure at two different times (Sep. 2010 and Feb. 2011) (junction depth: < 10 nm; ellipsometer measured capping layer stack: ~4 nm α -boron layer; ~3 nm parasitic oxide) [18].

Another phenomenon that should also be pointed out is the initial drop of the responsivity, followed by what appears to be a saturation of the degradation. This saturation could be explained in the following way: when the potential on the diode surface increases by the photoelectron emission effect, the intensity of the emitted electrons drops (as the electrons have to overcome this additional potential barrier),

while the electron flow created by the potential difference between the photodiode surface and the anode increases, which results in an equilibrium of the emitted and received electrons. This electron flow equilibrium stabilizes the potential levels and leads to a stable responsivity with a somewhat lower value.

6.2.2 EUV stability

Similar responsivity degradation behavior of the PureB-diode has also been observed under EUV radiation. Fig. 6.6 shows the measured responsivity before and after a long-term EUV exposure at a 13.5-nm wavelength. After 10kJ/cm² EUV exposure had been received, a nearly 3% responsivity drop was measured on an IMEC-fabricated sample. This sample has an ultra-shallow junction (junction depth < 10 nm) and a capping layer stack with an α -boron layer of a few nanometers and a 1~2 nm TiN layer (calculated by the responsivity difference around the Ti absorption edge (marked in the figure). Similar to the DIMES samples, as presented in Chapter 3, from the responsivity undulation around the oxygen absorption edge ($\lambda \approx 2.3$ nm, see Fig. 3.3), an oxygen element, which indicates a presence of parasitic oxide, can be detected on the surface of IMEC-fabricated PureB-diodes.

The photoelectron-emission induced potential on the diode surface is proportional to the photon energy. Since the photon energy of EUV photons is much larger (for example, the photon energy of a 13.5-nm wavelength is about 91.3 eV), a higher positive surface potential, hence a heavier responsivity degradation, should be expected. However, due to the large attenuation length in silicon (more than 500

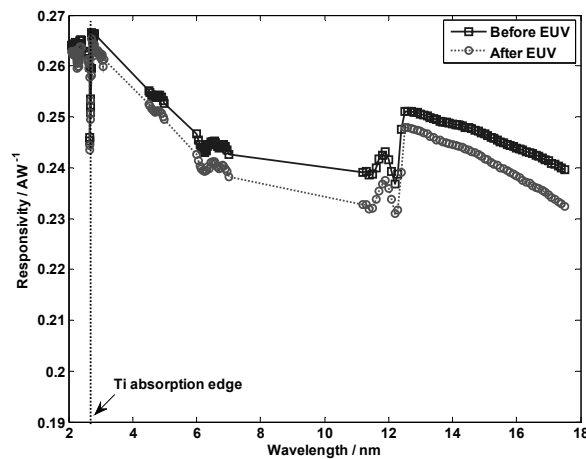


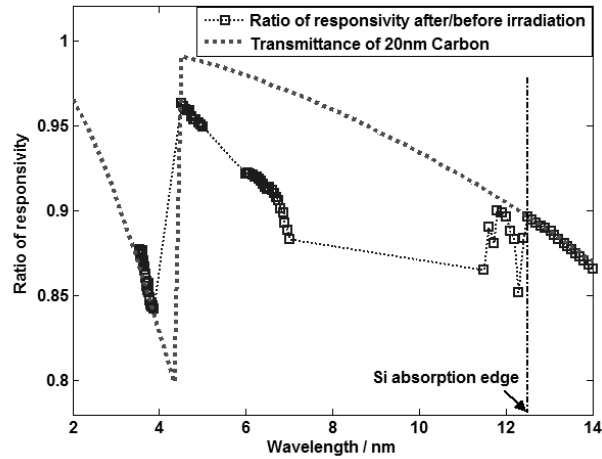
Fig. 6.6 Measured responsivity degradation of an IMEC fabricated PureB-diode in EUV spectral range. The sample has an ultra-shallow junction (junction depth < 10 nm); capping layer stack: few nm α -boron layer and 1~2 nm TiN layer, which is calculated by the responsivity undulation around the Ti absorption edge, and an oxygen element.

nm for a 13.5-nm wavelength [21][22]), most of the incident EUV photons are absorbed in the silicon bulk, which is hundreds of nanometers deep. Therefore, the EUV responsivity of PureB-diode is not very sensitive to the surface condition.

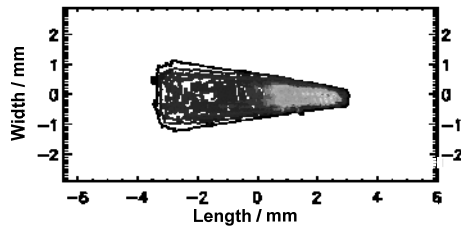
Compared to VUV radiation, EUV photons have a larger attenuation length in conductive material, as well as some metals [21][22]. This allows a thin conductive film covering (instead of the metal grid) to be added on the diode surface to minimize the harmful surface charging effect and further improve the stability of PureB-diodes in the EUV spectral range, especially when the stability is more crucial than sensitivity.

Fig. 6.7 (a) shows the observed EUV responsivity degradation of the DIMES-fabricated PureB-diode after a 24.5-hour prolonged EUV exposure at 13.5 nm (the EUV exposure level was 220 kJ/cm^2) [23]. The sample has a less than 10 nm junction depth, and an additional stack of: 200 nm Si, 100 nm Zr, 6 nm Al. The square-marked curve represents the ratio of responsivity before/after the high-dose exposure. The observed sensitivity degradation comes from a carbon contamination layer formed by the EUV radiation (shown in Fig. 6.7c) [24]. From the height of the carbon absorption edge in the spectrum around 4.3 nm in the plot, it can be calculated that the carbon layer is about 20 nm thick [21][25]. The responsivity ratio plot fits very well with the transmittance curve of a 20-nm-thick carbon layer. Moreover, besides an undulation, there is no significant “jump” shown on the curve before or after the silicon absorption edge ($\sim 12.4 \text{ nm}$ in the figure). This means the “equivalent junction depth” of the exposed sample has not been changed. A stable “equivalent junction depth” indicates that, in the diode p^+ region as well as in the depletion region, there is no EUV-induced defect, which may affect the effective charge-collection process. (On the contrary, as can be seen in Fig. 6. 10, when there is a surface-charge-induced responsivity degradation, a visible “jump” is available around the silicon absorption edge). Therefore, it can be concluded that there is no measurable change in the responsivity due to degradation of the PureB-diode itself.

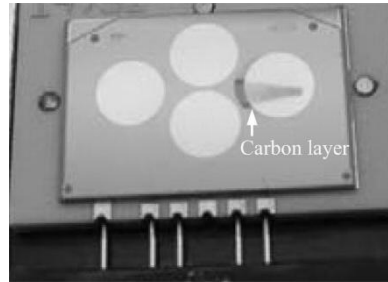
When studying experimentally the radiation hardness of the PureB-diodes, it is important to choose the right exposure levels. Obviously, the 220 kJ/cm^2 exposure level in the reported experiments is much lower than the exposure levels in some industrial applications (for example, the lifetime exposure that EUV photodetectors receive in the next-generation 13.5-nm lithography systems may reach 1 MJ/cm^2 [2]). Creating a 1 MJ/cm^2 exposure level is particularly difficult, as it would require several days’ intensive EUV exposure at the storage ring BESSY II. However, this is not necessary, as any degradation tendency of the tested sample will already present itself at much lower exposure levels. Furthermore, the 220 kJ/cm^2 EUV exposure is achieved within 24.5 hours under intensive radiation (roughly 800 times higher than the radiation intensity in the lithography system), which intensifies any possible



(a)



(b)



(c)

Fig. 6.7 (a) Ratio of responsivity after/before high-dose EUV irradiation (220 kJ/cm^2), compared to the transmittance of a 20-nm carbon layer. (b) Shape of the EUV spot: power density in the high power region (right part) is 3 W/cm^2 (figure was supplied by Dr. F. Scholze, PTB) [10]. (c) carbon contamination layer formed by the irradiation [23].

degradation processes. In this sense, stability after exposure of 220 kJ/cm^2 is sufficient to judge reliably how stable the device is after much higher exposures.

6.2.3 Optical performance stability versus surface charge-collection effect

Fig. 6.8 a and b shows the measured VUV responsivity degradation of PureB-diodes with ultra-shallow junction (junction depth $< 10 \text{ nm}$) and deeper junction (junction depth $> 30 \text{ nm}$), respectively [26]. The surface oxide component (parasitic oxidation) has been validated on both devices by the measured responsivity undulation around the oxygen absorption edge (similar to Fig. 3.3). It can be observed from the degradation curves that, for the same device, a better stability has

been measured under wavelengths where the attenuation length is larger (the attenuation length in silicon at a 70-nm wavelength is > 30 nm [21]). This is in accordance with the fact that for an extremely small attenuation length (< 10 nm) at wavelengths of 121 nm and 157 nm [21], the device performance becomes more dependent on the surface charge-collection process, and consequently more sensitive to the harmful radiation-induced charging/damage along the surface.

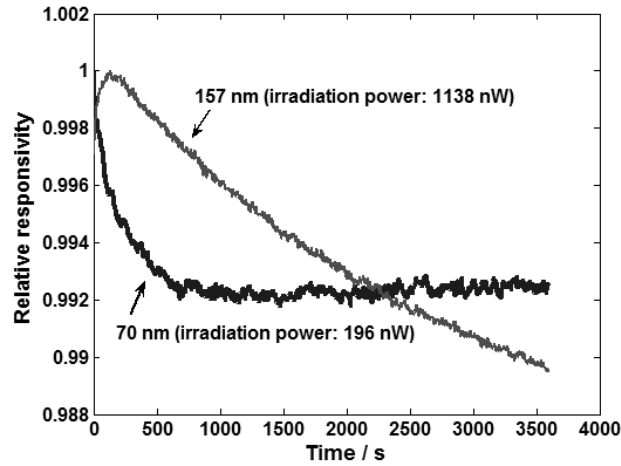
On the other hand, as illustrated in Fig. 6.9, the ultra-shallow junction PureB-diode demonstrates a better stability than the deeper junction one. The same phenomenon has also been observed in the EUV spectral range. Fig. 6.10 presents the responsivity ratio after/before a prolonged exposure at a 13.5-nm wavelength, measured on two PureB-diodes with different junction depths. The total EUV exposure level received is identical ($10\text{kJ}/\text{cm}^2$) on both samples. It can be seen from the figure that the responsivity ratio curve of the ultra-shallow junction device (without the thermal “drive in”) has a smaller “jump” at the silicon absorption edge ($h_2 < h_1$). This means for the same surface charging level (expected for the same EUV dose), the deeper junction device responsivity is more strongly affected by the radiation-induced positive charge on the diode surface. In other words, the deeper junction PureB-diode exhibits a more significant dependence on the surface charge-collection phenomenon than the ultra-shallow junction device.

In addition, as shown in Fig. 6.11, the PureB-diodes with lower parasitic surface oxide content show better optical performance stability. Also considering the measured excellent EUV stability of PureB-diodes with the 100-nm zirconium capping layer (Fig. 6.7), it can be concluded that, to avoid the undesired harmful charging and/or the Si-SiO₂ interface damage, and to achieve a stable sensitivity, an oxide-free and/or high-conductivity surface layer is mandatory.

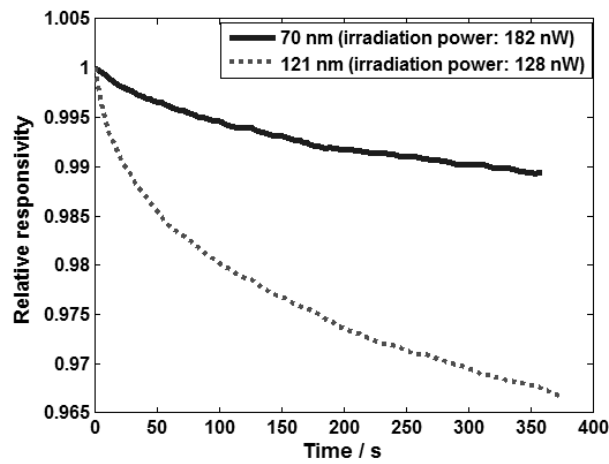
6.2.4 Photon-emission current induced instability

Besides the surface-charging-induced responsivity degradation, the external photoelectron emission effect could also affect the measured photocurrent by introducing a photon-emission current [2]. As shown in Fig. 6.12, when the capping layer is positively charged by UV radiation and the equivalent resistance R between the charged area and the anode is low enough, electrons from the anode will compensate the positive charge, which will result in a photon-emission current (I_{p2} shown in the figure). This extra current will add to the photodiode output signal, which is composed of the dark current I_D and the photocurrent I_{p1} .

In the presence of a less conductive capping layer, the variation of the surface potential and the photon-emission current will affect the response of the detector in pulsed mode. Fig. 6.13 a and b presents the output signal of PureB-diode



(a)



(b)

Fig. 6.8 (a) Monitored responsivity degradation of an ultra-shallow junction PureB-diode (DIMES sample, junction depth < 10 nm) at 70-nm and 157-nm wavelengths. (b) Monitored responsivity degradation of a deeper junction PureB-diode (IMEC sample, after 30 min anneal at 850°C giving a junction depth > 30 nm) at 70-nm and 121-nm wavelengths [26].

The initial increase of the responsivity under 157-nm wavelength radiation is not stochastic, but repeatable on different samples. It can be explained as follows: The strained Si-O-Si bonds in the surface parasitic oxide absorb photons with 7.9 eV energy (157-nm wavelength). The number of strained Si-O-Si bonds decreases by the UV-induced bond alteration ($\equiv \text{Si-O-Si} \equiv (\text{strained}) \xrightarrow{h\nu(7.9\text{eV})} \equiv \text{Si}\cdot + \cdot\text{O-Si} \equiv$). With the decrease of the "Si-O-Si" concentration in the parasitic oxide, the optical absorption of 157-nm wavelength photons weakens, resulting in an enhanced responsivity at the beginning [27][28].

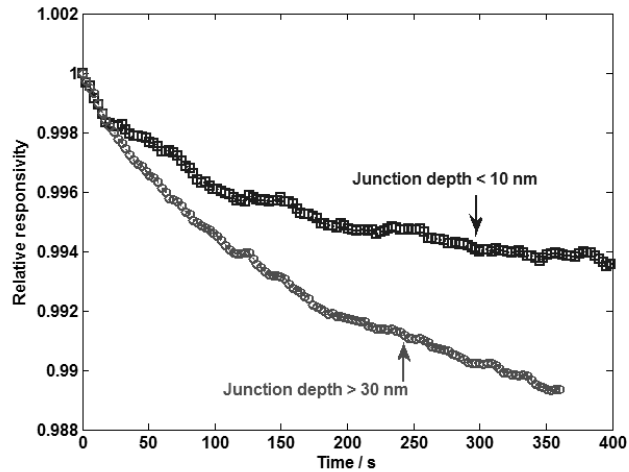


Fig. 6.9 Monitored responsivity degradation of two PureB-diodes (DIMES sample, junction depth < 10 nm; IMEC sample, junction depth > 30 nm) at 70-nm wavelengths (data is from the degradation curves plotted in Fig. 6.8).

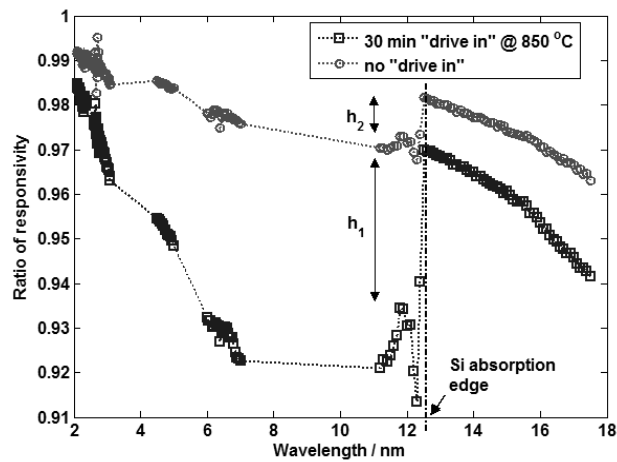


Fig. 6.10 Ratio of responsivity before/after high-dose EUV irradiation (10 kJ/cm^2). The PureB-diode was fabricated by IMEC.

fabricated with different coating layers when periodically exposed to 11.5-nm radiation with 50-second time intervals. The light-gray curves between each signal pulse indicate the dark signal shift due to the slow discharging. As shown in Fig. 6.13a, the positive charge in the less conductive zirconium oxide top layer cannot be quickly compensated for and thus the surface potential will increase continually until

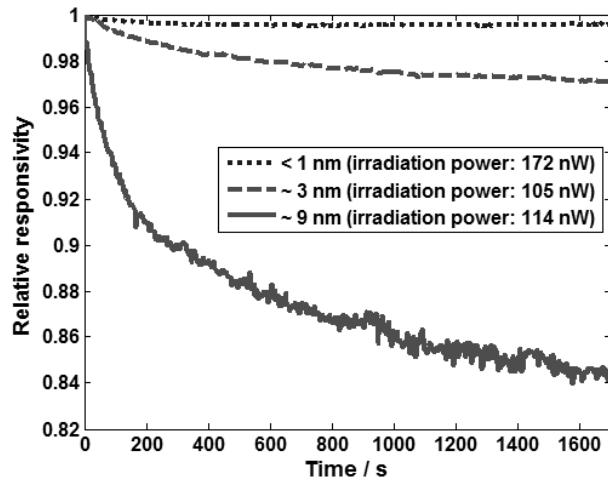


Fig. 6.11 Monitored responsivity degradation of DIMES PureB-diodes with varying parasitic oxide content on the surface, at a 121-nm wavelength. The oxide content was measured by ellipsometry on PureB-diodes with a $1 \times 1\text{ cm}^2$ active area, and is expressed as a thickness in nanometers.

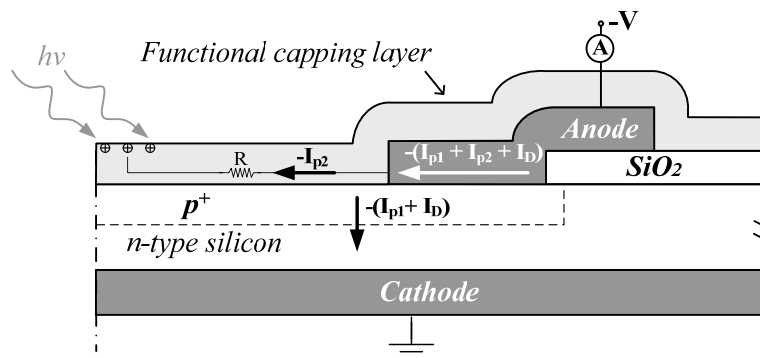
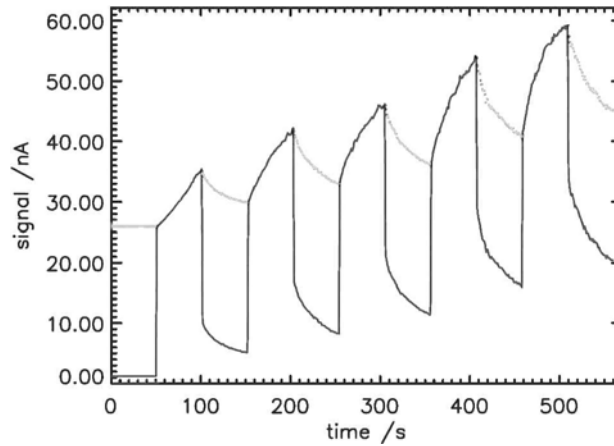
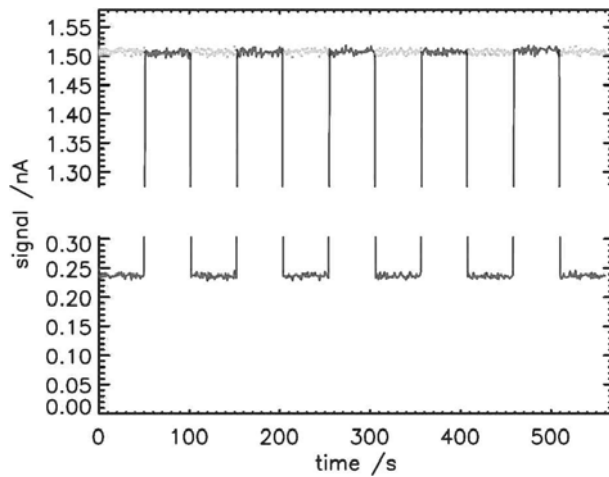


Fig. 6.12 Schematic description of the photoelectron emission effect on a p^+n junction photodiode. The arrows in the picture indicate the flow direction of the electron (R is the equivalent resistance between the charging area and anode; I_{p1} is the photocurrent; I_{p2} is the photon-emission current; and I_D is the dark current).

reaching around 108 V (the photon energy of 11.5-nm wavelength radiation is about 108 eV). Therefore, the compensation current (photon-emission current in Fig. 6.12) and consequently the output signal will have a continuous rising tendency for each irradiation cycle. On the contrary, owing to a much quicker discharging process, the PureB-diode with a conductive surface-layer stack did not reveal any photoelectron emission effect in the pulse response (Fig. 6.13b).



(a)



(b)

Fig. 6.13 Time response plots of two DIMES fabricated PureB-diodes with different capping layers: (a) device with a 100nm zirconium oxide cap layer; (b) device with a 20nm Al + 50nm Zr cap layer. Figures were supplied by Dr. F. Scholze, PTB.

Although a common solution for avoiding the influence of the photon-emission current is to read the signal from the backside electrode (the cathode), this is not a viable option for detector arrays implemented on the same chip with a common backside contact. Therefore, an improved structure has been designed by forming a highly doped n-type buried layer on p-type substrates before the growth of the intrinsic epi-layer (as shown in Figs. 6.14 and 3.2, IMEC fabricated PureB-diodes). In this way, each photodiode is electrically isolated from the neighboring

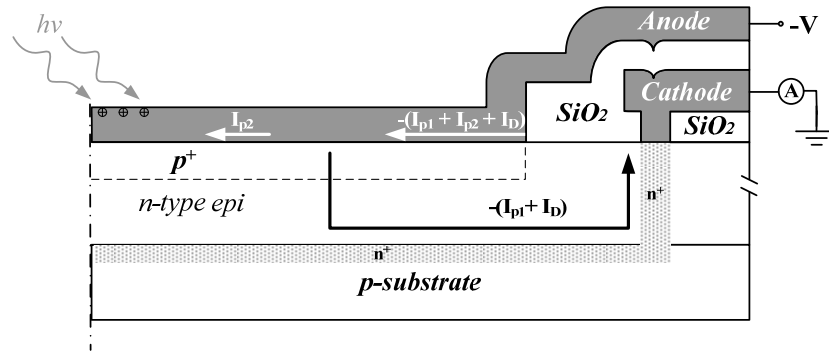


Fig. 6.14 Schematic description of the improved structure of the PureB-diode, which is introduced to reduce photoelectron emission effects in detector array implementations. The arrows in the picture indicate the flow direction of the electron (I_{p1} is the photocurrent; I_{p2} is the photon-emission current; and I_D is the dark current).

photodiodes and the output signal can be read through a separated cathode electrode contact.

6.3 Dark current degradation

As discussed in Section 6.1, besides the responsivity degradation, UV radiation induced defects could also deteriorate the dark current of Si-based photodiodes. As presented in Fig. 6.15, an increase in the dark current level from a few pA to tens of nA at a reverse bias of 7.5 V was observed after 24-hour exposure with a maximum radiation dose of 220 kJ/cm². All exposed samples have an 11 mm² junction area. This dark current degradation was found to be annealed out by thermal treatment at relatively low temperatures, such as ~ 200 °C [29]. As already discussed, the dark current is caused by defects (also called “recombination centers”) within the diode depletion region. Therefore, an increase of the dark current level indicates that more defects are created within the diode depletion region by EUV radiation during the exposure. Fig. 6.16 shows a typical cross-section of a PureB-diode and the possible location of the EUV-induced defects.

The first type of damage may be found in the diode junction area. It is easy to understand that any defect within the junction area may play a role as “recombination center”, which leads to unwanted recombination of photo-generated charge. Therefore, if there is any damage created in the diode junction area after intensive EUV exposure, not only the dark current but also the responsivity of PureB-diodes should be affected. However, as presented in Section 6.2.2 (Fig. 6.7), the measured EUV responsivity remained unchanged after a 24.5 hour prolonged

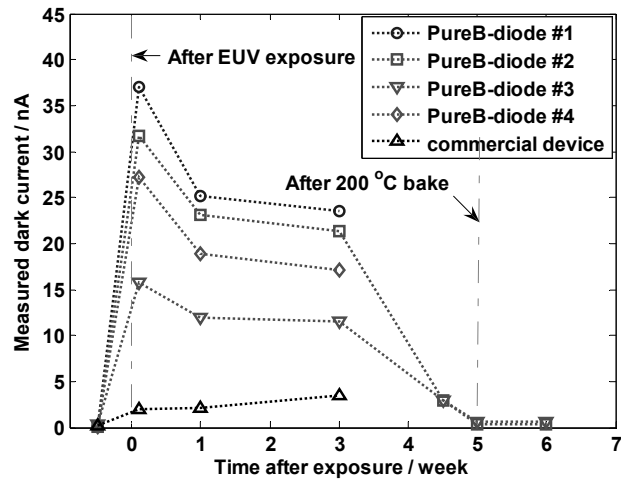


Fig. 6.15 Dark current increase (symbols) of DIMES PureB-diodes measured at different times after a prolonged EUV exposure with a maximum radiation dose of 220 kJ/cm^2 . The junction area of the exposed PureB-diodes remains 11 mm^2 , as shown in Fig. 6.7c [29].

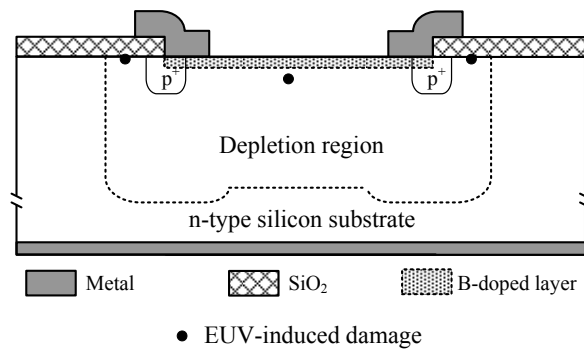


Fig. 6.16 Typical cross-section of a PureB-diode and possible location of the EUV-induced defects [29].

EUV exposure (received EUV dose is 220 kJ/cm^2). Thus, it can be concluded that the ultra-shallow p^+n junction area of PureB-diodes is robust under EUV radiation.

The other possible type of EUV-induced damage is expected at the perimeter of the diode, along the Si-SiO₂ interface [3][5][19][20]. Especially when the diode is under higher reverse bias voltage, the depletion region is extended horizontally along the Si-SiO₂ interface. In this way, radiation-induced defects along the Si-SiO₂ interface can be involved into the extended depletion region along the diode

perimeter. As a result, for diodes with a long perimeter, a significant increase in the dark current can be measured.

To verify this assumption, the following experiment was carried out: PureB-diode arrays on one chip were exposed to prolonged EUV irradiation. The dark current of each diode was measured before and after EUV exposure. The absolute EUV dose received was 6.1 kJ/cm^2 at the highest intensity beam area. As indicated in Table 6.1, after exposure, most of the diodes exhibited an increase in the dark current level from tens of pA to a few nA at a reverse bias of 1 V. This huge increase is believed to be the cross-talk current caused by the EUV-induced carbon contamination layer on the chip surface [24]. A four-hour hydrogen radical (H^*) cleaning was applied to successfully remove the carbon contamination layer [30] (more details about this carbon contamination and the H^* cleaning will be discussed in Chapter 7). After the cleaning step, the measured dark current of all samples dropped to a reasonable value (row no. 4 in Table 6.1), but was still higher than the initial level. As will be discussed in Chapter 7, the H^* cleaning also affects the dark current. However, since the H^* exposure is a uniform process over the $1 \times 0.5 \text{ cm}^2$ chip surface, its effect is expected to be similar for all photodiodes, and not related to the received EUV dose. On the other hand, the measured increased dark current, ΔI_D (shown in row no. 5 in Table 6.1 and Fig. 6.17), was found to be proportional to the received EUV dose and thus should be (at least partly) attributed to the EUV exposure.

One possible reason for this EUV induced damage along the Si-SiO₂ interface on the diode perimeter can be explained by the mechanism presented in Fig. 6.18. EUV radiation can de-passivate the Si-H bond by releasing hydrogen atoms from silicon at the Si-SiO₂ interface (Eq. 6.1) [19], resulting in the formation of Si “dangling-bond” interface states (threefold-coordinated Si atom, D in the equation).

TABLE 6.1 MEASURED DARK CURRENT (A) @ -1V ON PUREB-DIODES WITH NORMAL SiO₂ PASSIVATION LAYER, BEFORE / AFTER EUV EXPOSURE [29].

	Diode #1	Diode #2	Diode #3	Diode #4
Before EUV, I_{D1}	2.70e-11	2.74e-11	2.86e-11	2.56e-11
After EUV, I_{D2}	6.3e-10	1.8e-9	5.2e-9	7.4e-9
After H^* cleaning, I_{D3}	3.59e-11	5.12e-11	9.7e-11	1.12e-10
$\Delta I_D = I_{D3} - I_{D1}$	8.9e-12	23.8e-12	68.4e-12	86.4e-12
Relative EUV dose	0.4	0.7	1.6	1.8

The junction area of the PureB-diodes is $300 \times 300 \text{ }\mu\text{m}^2$.

The absolute EUV dose received was about 6.1 kJ/cm^2 at the highest intensity beam area.

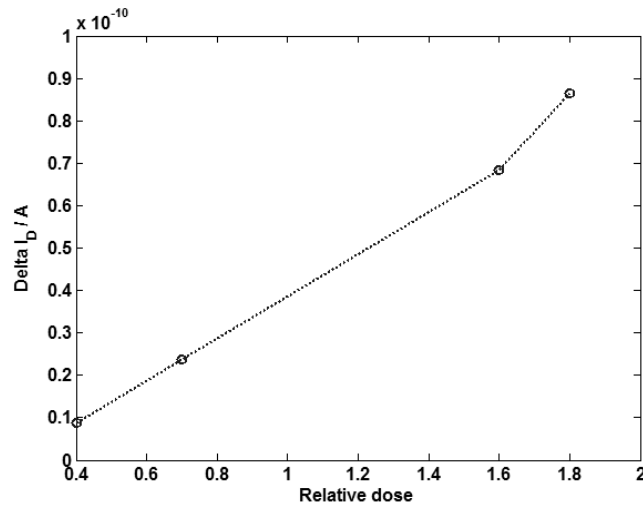


Fig. 6.17. Dark current increase as function of the created relative EUV dose. The junction area of PureB-diodes (DIMES samples) is $300 \times 300 \mu\text{m}^2$ [29].



At the same time, EUV radiation can also release extra hydrogen atoms in the SiO_2 passivation layer [5]; when these hydrogen atoms diffuse to the Si-SiO₂ interface, the Si-H bonds are ruptured from the reaction with the hydrogen atoms (Eq. 6.2), leading to additional interface damage.



The process is illustrated in Fig. 6.19 [31][32][33].

Because of the well-known extremely low diffusion coefficient of hydrogen in nitride materials compared to SiO_2 [34][35][36], a few nanometers of silicon nitride created by a rapid thermal process (RTP) were added to the Si-SiO₂ interface. In this way, the nitride layer was expected to prevent hydrogen atoms released by the EUV photon at the Si-SiO₂ interface from diffusing through the SiO_2 passivation layer and ultimately being lost to the environment. The hydrogen atoms are kept close to the Si-SiO₂ interface and may subsequently recombine with the free silicon “dangling bonds”. In addition, the nitride layer also can prevent the EUV-released hydrogen atoms in the SiO_2 layer from reaching the Si-SiO₂ interface and creating defects along the Si-SiO₂ interface on the diode perimeter. Fig. 6.20 shows the cross-section of PureB-diodes with this new passivation structure. As presented in Table 6.2, compared to diode #4 in Table 6.1 (under the highest EUV intensity beam area, the received absolute EUV dose was about 6.1 kJ/cm^2), after all photodiodes had received an EUV dose of 21.5 kJ/cm^2 (more than three times higher than the highest

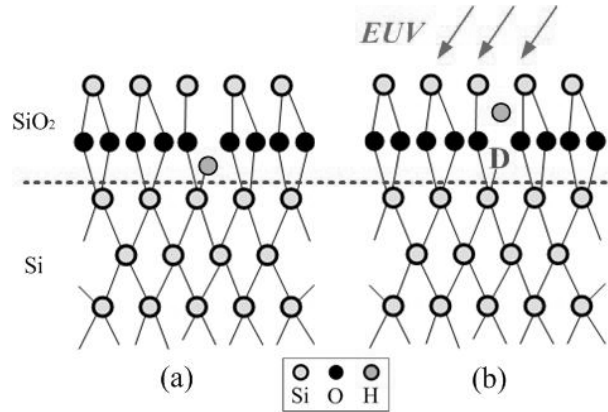


Fig. 6.18 EUV radiation damaging the Si-SiO₂ interface [5]: (a) “Dangling bond” passivated by H atom; (b) EUV irradiation releases H atom.

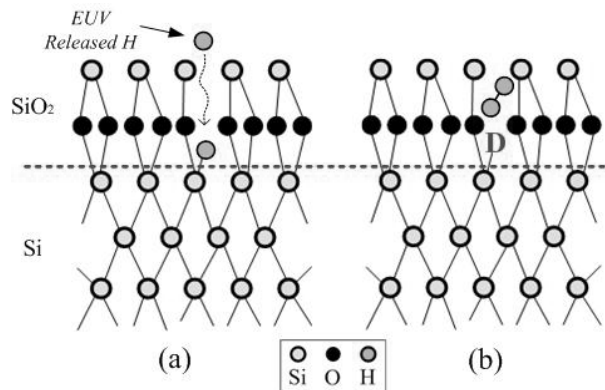


Fig. 6.19 EUV-released H atom damaging the Si-SiO₂ interface [31][32][33]: (a) EUV-released H approaching a passivated “Dangling bond”; (b) “Dangling bond” is de-passivated.

dose in the previous experiment), and after the same H⁺ cleaning, a significantly smaller increase of the dark current was observed.

This result confirms that the main source of the dark current increase after EUV exposure is the EUV-induced damage (Si dangling bonds) at the Si-SiO₂ interface along the diode perimeter. Together with the excellent optical stability, the stable electrical behavior of the PureB-diodes with the additional nitride passivation layer proves that the nanometer-deep boron-doped p⁺n junction and the nanometer-thin α -boron layer are robust to EUV radiation.

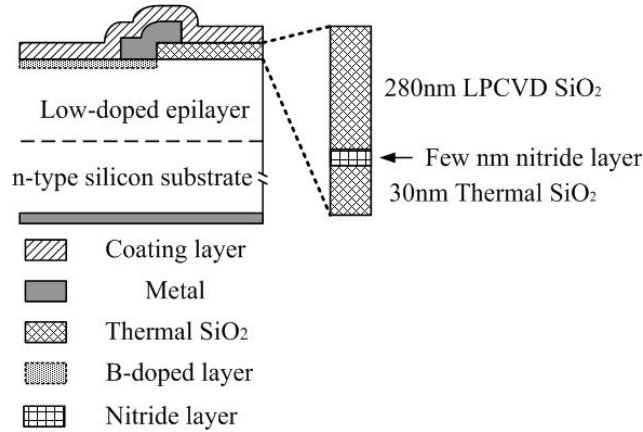


Fig. 6.20 Cross-section of DIMES fabricated PureB-diodes with nitride passivation layer above the Si-SiO₂ interface.

TABLE 6.2 MEASURED DARK CURRENT (A) @ -1V OF PUREB-DIODES WITH NITRIDE PASSIVATION LAYER, BEFORE / AFTER EUV EXPOSURE [29].

	Diode #1	Diode #2	Diode #3	Diode #4	Diode #5
Before EUV, I _{D1}	7.06e-012	3.51e-012	4.75e-012	2.51e-012	5.49e-012
After EUV, I _{D2}	1.69e-009	2.31e-009	3.71e-009	0.001399	4.24e-009
After H [*] cleaning, I _{D3}	31.45e-12	32.95e-12	64.3e-12	43.80e-12	35.65e-12
ΔI _D = I _{D3} - I _{D1}	24.39e-12	29.44e-12	59.55e-12	41.29e-12	30.16e-12

The junction area of the PureB-diodes is 300×300 μm²

The absolute EUV dose received was about 21.5 kJ/cm².

6.4 Summary

The performance stability of PureB-diodes is evaluated. The experimental results prove that the p⁺n junction formed by PureB-CVD technology is stable under DUV/VUV and EUV radiation: after prolonged EUV exposures, no measurable performance degradation caused by the damage to the p⁺n junction itself has been observed. Nevertheless, a surface oxidation, which can be positively charged by photon-emission effect under UV radiation, was found to be the main reason for the measured responsivity degradation in the DUV/VUV and EUV spectral ranges. This charging-induced responsivity loss can be avoided by forming a thicker boron layer or adding a conductive capping layer. The former can eliminate the harmful surface oxidation on PureB-diodes; the latter is helpful in minimizing the surface charge-

accumulation. Moreover, PureB-diodes have also demonstrated good electrical performance stability under intensive EUV radiation when an extra nitride passivation layer is applied to protect the Si-SiO₂ interface along the diode perimeter. The small dark current increase still present can be further scaled down by reducing the reverse bias voltage to the mV range in future applications.

Reference:

- [1] International Technology Roadmap for Semiconductors: Lithography, 2007 Edition. Available at: <http://www.itrs.net>.
- [2] L. Shi, F. Sarubbi, S. N. Nihtianov, L. K. Nanver, T. L. M. Scholtes and F. Scholze, "High performance silicon-based extreme ultraviolet (EUV) radiation detector for industrial application", *Proc. 35th Annual Conference of the IEEE Industrial Electronics Society (IECON)*, pp. 1891-1896, Nov. 2009.
- [3] F. M. Li, O. Nixon and A. Nathan, "Degradation behavior and damage mechanisms of CCD image sensor with deep-UV laser radiation", *IEEE Transactions on Electron Devices*, vol. 51, no. 12, pp. 2229-2236, Dec. 2004.
- [4] T. P. Ma and P. V. Dressendorfer (editors), *Ionizing Radiation Effects in MOS Devices and Circuits*, John Wiley & Sons, Inc., USA, 1989.
- [5] F. M. Li and A. Nathan, *CCD Image Sensors in Deep-Ultraviolet: Degradation Behavior and Damage Mechanisms*, Springer, pp. 96-108, 2004.
- [6] D. K. Schroder, *Semiconductor Material and Device Characterization (Third Edition)*, Wiley-IEEE Press, pp. 251-317, 2006.
- [7] F. Scholze, R. Klein and R. Müller, "Characterization of detectors for extreme UV radiation", *Metrologia*, vol. 43, pp. 6-10, 2006.
- [8] F. Scholze, G. Brandt, P. Müller, B. Meyer, F. Scholz, J. Tümmeler, K. Vogel and G. Ulm, "High-accuracy detector calibration for EUV metrology at PTB", *Proc. SPIE*, vol. 4688, pp. 680-689, 2002.
- [9] R. E. Vest and L. R. Canfield, "Evaluation of Au/GaAsP and Au/GaP Schottky photodiodes as radiometric detectors in the EUV", *Rev. Sci. Instrum.*, vol. 67, pp. 3362, 1996.
- [10] R. Klein et al., "Lifetime testing of EUV optics using intense synchrotron radiation at the PTB radiometry laboratory", *Soft X-Ray and EUV Imaging Systems II, Proc. SPIE*, pp. 105-112, 2001.
- [11] K. Solt et al., "PtSi-n-Si Schottky-barrier photodetectors with stable spectral responsivity in the 120-250 nm spectral range", *Appl. Phys. Lett.*, vol. 69, no. 24, pp. 3662-3664, 1996.
- [12] P. Kuschnerus, H. Rabus, M. Richter, F. Scholze, L. Werner and G. Ulm, "Characterization of photodiodes as transfer detector standards in the 120 nm to 600 nm spectral range", *Metrologia*, vol. 35, pp. 355-362, 1998.
- [13] L. R. Canfield, R. E. Vest, R. Korde, H. Schmidtke and R. Desor, "Absolute silicon photodiodes for 160 nm to 254 nm photons", *Metrologia*, vol. 35, p. 329, 1998.
- [14] F. Scholze, R. Klein and T. Bock, "Irradiation stability of silicon photodiodes for extreme-ultraviolet radiation", *Appl. Opti.*, vol. 42, no. 28, Oct. 2003.

- [15] L. Shi, L. K. Nanver, A. Šakić, S. Nihtianov, A. Gottwald and U. Kroth, “Optical stability investigation of high-performance silicon-based VUV photodiodes”, *Proc. IEEESENSORS2010*, pp. 132-135, Nov. 2010.
- [16] R. E. Vest and L. R. Canfield, “Photoemission from silicon photodiodes and induced changes in the detection efficiency in the far ultraviolet”, *The 10th United States National Conference on Synchrotron Radiation Instrumentation, AIP Conference Proceedings*, vol. 417, pp. 234-240, 1997.
- [17] L. Shi, L. K. Nanver, A. Šakić, S. Nihtianov, T. Knežević, A. Gottwald and U. Kroth, “Series resistance optimization of high-sensitivity Si-based VUV photodiodes”, in *Proc. I2MTC2011*, May 2011.
- [18] L. Shi, S. Nihtianov, S. Xia, L. K. Nanver, A. Gottwald and F. Scholze, “Electrical and optical performance investigation of Si-based ultrashallow junction p+n VUV/EUV photodiodes”, *IEEE Transactions on Instrumentation and Measurement*, vol. 61, no. 5, pp. 1268-1277, May 2012.
- [19] F. Messina and M. Cannas, “Photochemical generation of E centers from Si-H in amorphous SiO₂ under pulsed ultraviolet laser radiation”, *J. Phys.: Condens. Matter*, vol. 18, pp. 9967-9973, 2006.
- [20] G. Barbottin and A. Vapaille (editors), *Instabilities in Silicon Devices: Silicon Passivation and Related Instabilities*, vol. 1 and 2, Elsevier Science Publishers, the Netherlands, 1986.
- [21] Henke data. Available from: http://henke.lbl.gov/optical_constants.
- [22] NIST data. Available from: <http://physics.nist.gov>.
- [23] L. Shi, S. Nihtianov et al., “Stability Characterization of High-Sensitivity Silicon-Based EUV Photodiodes in a Detrimental Environment”, *IEEE Sensors Journal*, vol. 13, no. 5, pp. 1699 – 1707, May 2013.
- [24] R. Garg, A. Wüest, E. Gullikson, S. Bajt and G. Denbeaux, “EUV optics contamination studies in presence of selected hydrocarbons”, *Proc. of SPIE*, vol. 6921, no. 36, 2008.
- [25] Filter Transmission database. Available at: http://henke.lbl.gov/optical_constants/filter2.html.
- [26] L. Shi, S. Nihtianov, L. Haspeslagh, F. Scholze, A. Gottwald and L. K. Nanver, “Surface-Charge-Collection-Enhanced High-Sensitivity High-Stability Silicon Photodiodes for DUV and VUV Spectral Ranges”, *IEEE Trans. on Electron Devices*, vol. 59, no. 11, pp. 2888 – 2894, Nov. 2012.
- [27] K. Kajihara, Y. Ikuta, M. Hirano and H. Hosono, “Power dependence of defect formation in SiO₂ glass by F₂ laser irradiation”, *Appl. Phys. Lett.*, vol. 81, no. 17, pp. 3164-3166, 2002.
- [28] H. Hosono, Y. Ikuta, T. Kinoshita, K. Kajihara and M. Hirano, “Physical disorder and optical properties in vacuum ultraviolet region of amorphous SiO₂”, *Phys. Rev. Lett.*, vol. 87, no. 17, pp. 175 501/1–4, 2001.

- [29] L. Shi, S. Nihtianov, F. Scholze and L. K. Nanver, "Electrical performance stability characterization of high-sensitivity Si-based EUV photodiodes in a harsh industrial application", *Proc. 38th Annual Conference of the IEEE Industrial Electronics Society (IECON)*, pp. 3952-3957, Oct. 2012.
- [30] L. Shi, L. K. Nanver and S. N. Nihtianov, "Stability characterization of high-sensitivity silicon-based EUV photodiodes in a detrimental industrial environment", *Proc. 37th Annual Conference of IEEE Industrial Electronics Society (IECON)*, pp. 2651-2656, Nov. 2011.
- [31] K. L. Brower, "Kinetics of H₂ passivation of Pb centers at the (111) Si- SiO₂ interface", *Phys. Rev. B*, vol. 38, pp. 9657-9666, 1988.
- [32] J. H. Stathis and E. Cartier, "Atomic hydrogen reactions with Pb centers at the (100) Si/SiO₂ interface", *Phys. Rev. Lett.*, vol. 72, pp. 2745-2748, 1994.
- [33] S. N. Rashkeev, D. M. Fleetwood, R. D. Schrimpf and S. T. Pantelides, "Defect generation by hydrogen at the Si- SiO₂ interface", *Phys. Rev. Lett.*, vol. 87, pp. 165506, 2001.
- [34] W. M. Arnoldbik, C. H. M. Marée, A. J. H. Maas, M. J. van den Boogaard and F. H. P. M. Habraken, "Dynamic behavior of hydrogen in silicon nitride and oxynitride films made by low-pressure chemical vapor deposition", *Phys. Rev. B.*, vol. 15; no. 48(8), pp. 5444-5456, Aug. 1993.
- [35] M. McCann, K. Weber and A. Blakers, "An early deposited LPCVD silicon nitride: allowing the possibility of novel cell designs", *Proc. 3rd World Conference on Photovoltaic Solar Energy Conversion*, vol.2, no. 12-16, pp.1135-1138, May 2003.
- [36] R. W. Lee, R. C. Frank and D. E. Swets, "Diffusion of hydrogen and deuterium in fused quartz", *Journal of Chemical Physics*, vol. 36, pp. 1062-1071, 1962.

Chapter 7 Robustness to Detrimental Working Conditions

In VUV- and EUV-related applications, such as synchrotron radiation measurements and next-generation EUV lithography, a periodic cleaning of the surface of the optics (UV detectors, lenses and mirrors) is required to prevent the buildup of carbon contamination layers [1][2]. One effective way to remove this carbon contamination is to use hydrogen radicals (H^*) [1]. In this chapter, the stability of PureB-diodes under H^* exposure is evaluated. A series of surface cleaning tests with different cleaning setups (filament-enhanced H^* and plasma-generated H^*) confirm that the electrical/optical performance of PureB-diodes is stable with negligible performance changes.

7.1 Carbon contamination in vacuum

Hydrocarbon molecules are present in every vacuum chamber [2][3]. They originate from atmospheric contamination, outgassing materials (like printed circuit boards, lubrication, photoresist in IC fabrication, etc.), or can be introduced by the users themselves during specimen handling (e.g. fingerprints). If the molecules are chemically altered under the influence of energetic radiation, for example the VUV/EUV photons, the released carbon can adhere to the irradiated detector surface and form a polymeric carbon layer. This effect is well-known in VUV/EUV optics [2].

As presented in Chapter 6 (Fig. 6.7), after a long-term EUV exposure, an EUV-induced carbon contamination layer was created on the surface of the PureB-diode, and consequently a drop in responsivity was observed. A similar phenomenon is also shown in Fig. 7.1: after a prolonged EUV exposure, a carbon contamination layer was formed on an EUV photodiode array. Besides reducing the responsivity, this EUV-induced carbon layer can also affect the electrical performance of the detectors. It has been found that this carbon contamination layer is conductive enough to create a crosstalk between the neighboring diodes integrated on a single chip. Fig. 7.2 shows the leakage current measured between two isolated bond pads on the chip (in Fig. 7.1) before and after exposure [4][5]. The measured I-V curve presents a ~ 60 pA leakage current through the radiation-induced carbon contamination layer at a 1 V potential difference. Such a level of current could already be larger than the dark current of a single diode at -1 V. Thus, the detector surface needs to be cleaned regularly in real industrial applications not only for minimizing the carbon-induced responsivity drop, but also for avoiding leakage currents due to the conductive contamination layer.

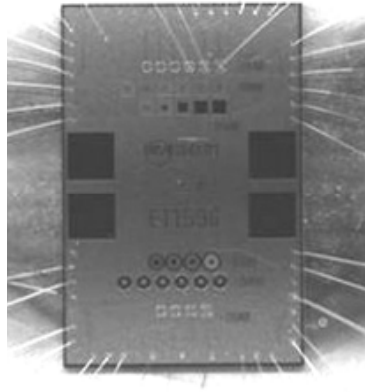


Fig. 7.1 Micro-image of a chip with four 1 mm² PureB-diodes exposed to high-dose EUV irradiation. The dark-gray shadow is from the carbon contamination layer that was formed as a result of the exposure [4][5].

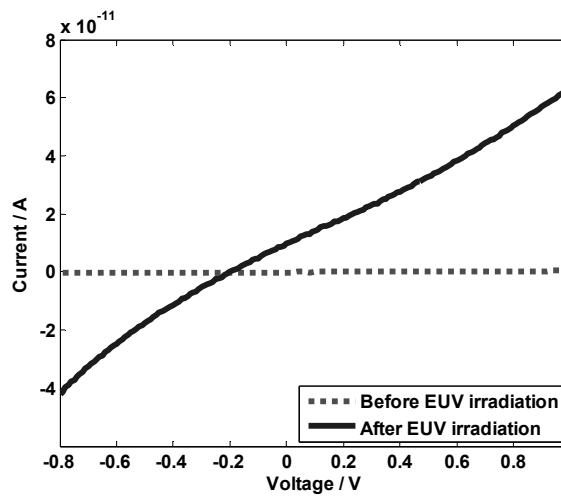


Fig. 7.2 Electrical measurement results before and after EUV radiation. I-V curves were measured between two isolated bond pads on the chip, which is shown in Fig. 7.1 [4].

7.2 Hydrogen radical (H^{*}) cleaning

Aggressive gasses, such as hydrogen radicals (H^{*}), can remove the carbon contamination effectively [1]. However, this kind of cleaning is a destructive process

that could affect the Si-based device itself, especially PureB-diodes whose anodes are only covered by a nanometer-thin boron layer. Fig. 7.3 presents one possible damaging mechanism for Si-based devices under H^* exposure [6]. Therefore, besides the high and stable electrical/optical performance, the hardness of PureB-diodes to such detrimental treatment is equally critical for the implementation of these detectors in real applications.

In this chapter, the experimental results with two H^* cleaning setups are presented to evaluate the hardness of PureB-diodes under this aggressive treatment.

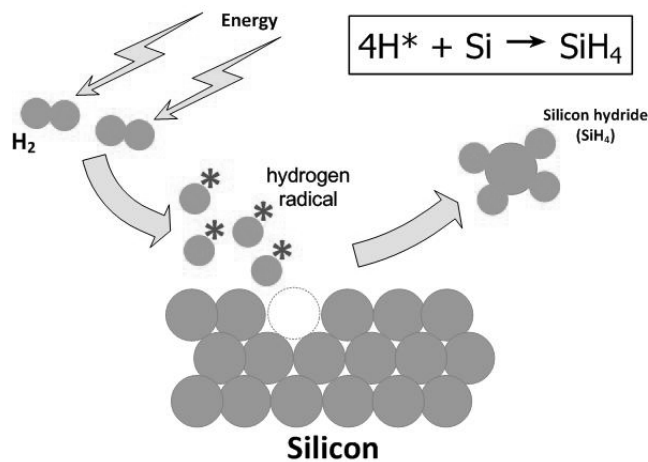


Fig. 7.3 Possible damaging mechanism of Si-based devices under H^* exposure [1][6].

7.2.1 Filament-enhanced H^* generation system

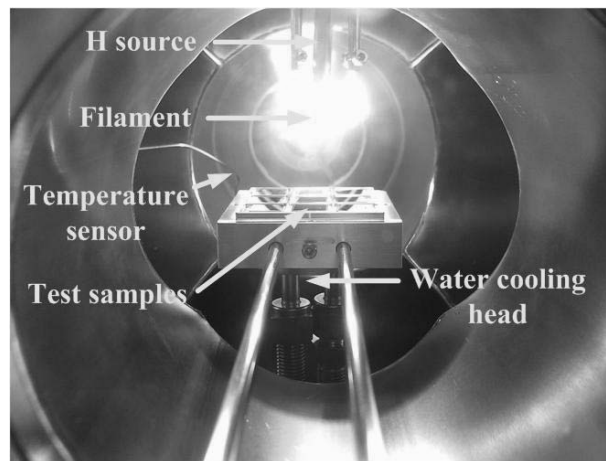
Fig. 7.4 (a) shows a filament-enhanced H^* generation system used for cleaning tests. The pressure in the chamber is 6×10^{-6} mbar. Hydrogen radicals are activated by a filament under the hydrogen source. The filament working temperature is 2000 Kelvin. The distance from the filament to the test samples is fixed at 3 cm. A water cooling system is introduced in the metal holder to prevent the test samples from being overheated by the filament. Furthermore, the filament is programmed to be switched on and off regularly during the cleaning. As illustrated in Fig. 7.4b, the monitored temperature variation of the metal holder during a half-hour cleaning is no more than $34^\circ C$.

The reaction in the vacuum chamber can be expressed with the following equation:

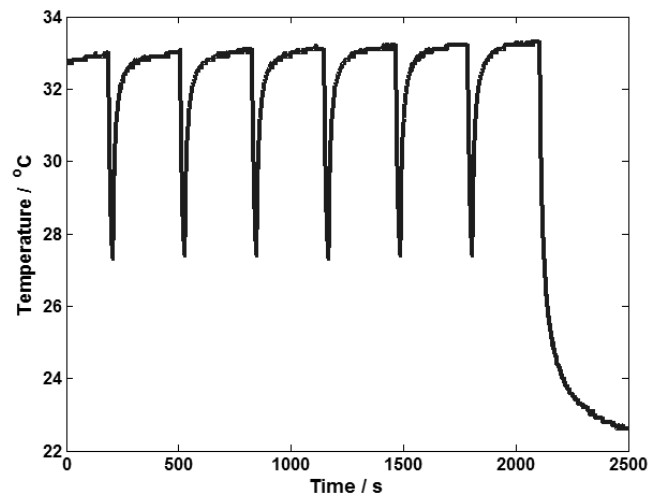


The hydrogen atoms are activated by the high-temperature filament, and become hydrogen radicals [1].

The cleaning rate of this setup was checked in the following way. First, the thickness of the carbon layer deposited on a 1-inch Si wafer was measured by ellipsometry. After a 105-min H^* -cleaning using the above mentioned setup, the carbon layer thickness was measured again. Based on the measurement results

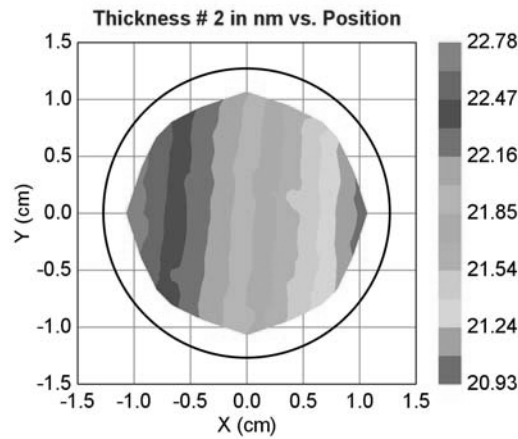


(a)

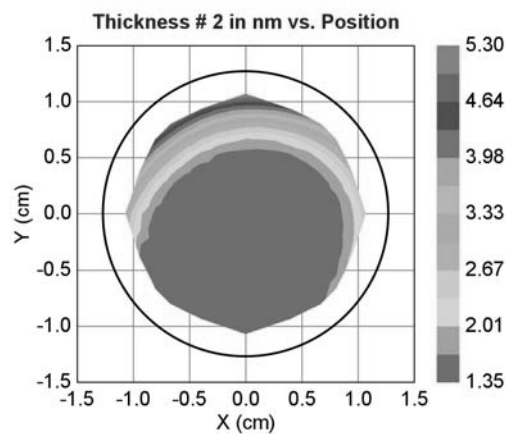


(b)

Fig. 7.4 (a) Filament-enhanced H^* cleaning setup; (b) monitored temperature change of the metal holder during half an hour of H^* cleaning [7].



(a)



(b)

Fig. 7.5 Carbon thickness measurement (a) before, and (b) after H^* cleaning on a 1-inch Si wafer (cleaning time: 105 min; cleaning rate: ~ 0.2 nm/min) [7]. Figures are granted by Ir. Edgar Osorio, ASML.

presented in Fig. 7.5, the cleaning rate was calculated as ~ 0.2 nm / min. [7]

7.2.2 Plasma-generated H^* technique

Fig. 7.6 shows two PureB-diodes packaged in an aluminum box, under plasma-generated H^* exposure. The accepted cleaning rate of this setup is about 1 nm/min over a 6×6 cm² area (much larger cleaning rate than the filament setup), and the temperature during the exposure was not higher than 80 °C. The cleaning was done at the Netherlands Organization for Applied Scientific Research (TNO), in Delft, the

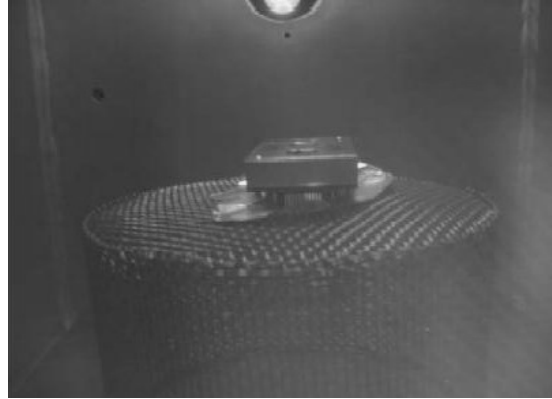


Fig. 7.6 Packaged PureB-diodes during plasma-generated H^* cleaning. The accepted cleaning rate is about 1 nm/min over 6 cm² [4].

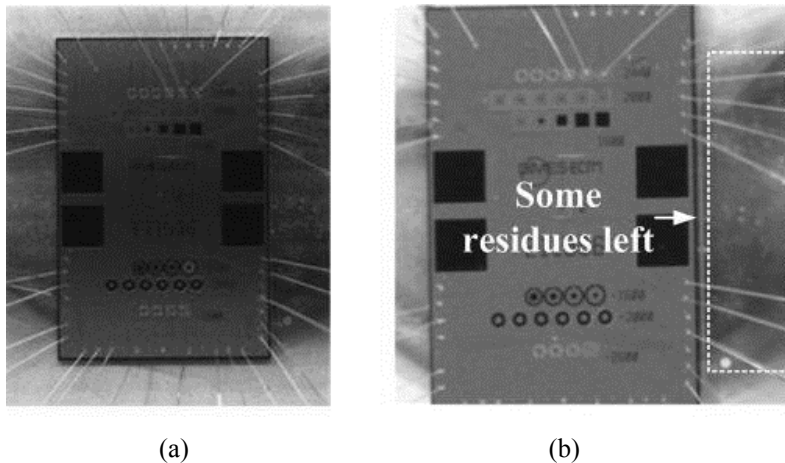


Fig. 7.7 (a) Repeated photograph of Fig. 7.1 for a visual comparison; (b) micro-image of the same sample after a four-hour H^* cleaning in a plasma-generated H^* system [4].

Netherlands [4]. As indicated in Fig. 7.7b, after a four-hour plasma-generated H^* exposure, the radiation-induced contamination layer was completely removed from the die surface [4].

Based on the results presented in Figs. 7.5 and 7.7, it can be seen that both filament-enhanced H^* setup and plasma-generated H^* system can effectively remove the carbon contamination. The main difference between these two methods is the cleaning rate. During the real experiments, owing to the more easy and accessible system as well as the slow and controllable cleaning rate, filament enhanced H^* setup was mainly applied for damaging mechanism analysis. The plasma-generated

H* system, which has a much faster cleaning rate, is used only for the fast cleaning of heavily contaminated samples, for example, the chip shown in Fig. 7.1.

7.3 Stability investigation under H* exposure

As indicated in Table 7.1, after a four-hour H* exposure in the plasma-generated H* system, all cleaned PureB-diodes show an increased dark current.

TABLE 7.1 ELECTRICAL MEASUREMENT RESULTS OF FIVE PUREB-DIODES WITH OXIDE PASSIVATION LAYERS BEFORE AND AFTER A FOUR-HOUR H* CLEANING TEST [4].

Diode #	Dark current (pA)	
	Before H* exposure	After H* exposure
#1	0.05	18.5
#2	0.07	18.3
#3	0.04	18.4
#4	0.06	26.8
#5	0.05	25.7

The junction area of the PureB-diodes is 300×300 μm².

An increase in the dark current level indicates that more defects—which may introduce intermediate energy levels in the forbidden band-gap—are created within the diode depletion region by H* during the exposure. Similar to the study on the radiation-induced dark current increase (in Chapter 6, Section 6.3), two possible locations of H*-induced damage on PureB-diodes are considered: the junction area and the Si-SiO₂ interface along the diode perimeter.

7.3.1 Robustness of the diode active area

First, PureB-diodes with a 1×1 cm² junction area (shown in Chapter 3, Fig. 3.1), and different boron layer thicknesses were used to test the robustness of the

TABLE 7.2 ELLIPSOMETER-MEASURED BORON LAYER THICKNESS BEFORE / AFTER H* EXPOSURE [7].

Diode #	Before H* exposure	After 10-min H* exposure	After 180-min H* exposure
#1	3.9 nm	4.0 nm	3.7 nm
#2	15.1 nm	14.9 nm	14.8 nm

The junction area of the PureB-diodes is 1×1 cm².

nanometer-thin α -boron surface layer. As shown in Table 7.2, based on the ellipsometer measurement results, after the filament-enhanced H^* exposure, there is no measurable change in the boron layer thickness.

Besides the stability of the boron layer, the H^* -induced damage within the underlying boron-doped ultra-shallow p^+n junction was studied by a couple of PureB-diodes with different opening areas in a metal shield on top of the $300 \times 300 \mu m^2$ junction area, as illustrated in Fig. 7.8. From the micro image and the cross-section, it can be seen that outside the opening on the boron layer, the diode surface is protected by a thick aluminum layer ($> 500 \text{ nm}$), and the size of the open area varies from 50×50 to $298 \times 298 \mu m^2$. Table 7.3 shows the dark current of the diodes measured before and after the H^* exposure. No increase of the dark current was observed for any of the photodiodes after all the exposure cycles had been completed.

Moreover, the optical performance stability under the H^* cleaning was checked as well. The measured PureB-diode has an ultra-shallow junction (junction depth $< 10 \text{ nm}$) and a $1 \times 1 \text{ cm}^2$ junction area. As discussed before, any additional defect within the junction area may play a role as an extra “recombination center”, which can lead to the unwanted recombination of the photo-generated charge, and consequently a responsivity degradation. However, as depicted in Fig. 7.9, after a continuous four-hour H^* cleaning in filament-enhanced H^* setup, no measurable drop of the responsivity in the EUV spectral range was detected.

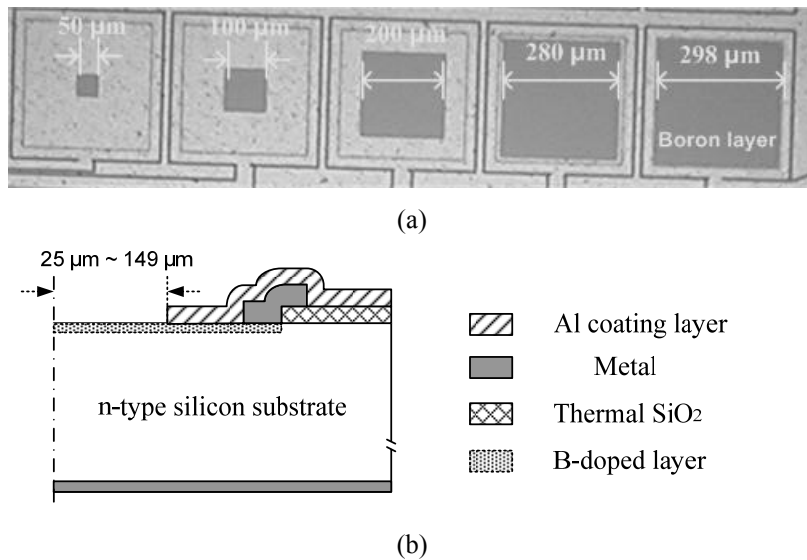


Fig. 7.8 (a) Micro image and (b) cross-section of PureB-diodes with different opening sizes on top of the p - n junction [7].

TABLE 7.3 MEASURED DARK CURRENTS (pA) @ -1V OF PUREB-DIODES WITH DIFFERENT OPENINGS ON THE BORON LAYER BEFORE / AFTER FILAMENT ENHANCED H⁺ EXPOSURE [7].

Opening size on the junction area (μm ²)	Dark current (pA)			
	Before H ⁺ exposure	After 10 min H ⁺ exposure	After 60 min H ⁺ exposure	After 180 min H ⁺ exposure
50×50	0.03	0.02	0.03	0.03
100×100	0.07	0.04	0.04	0.06
200×200	0.08	0.02	0.03	0.05
280×280	0.05	0.02	0.02	0.02
298×298	0.06	0.03	0.03	0.02

The junction area of the PureB-diodes is 300×300 μm².

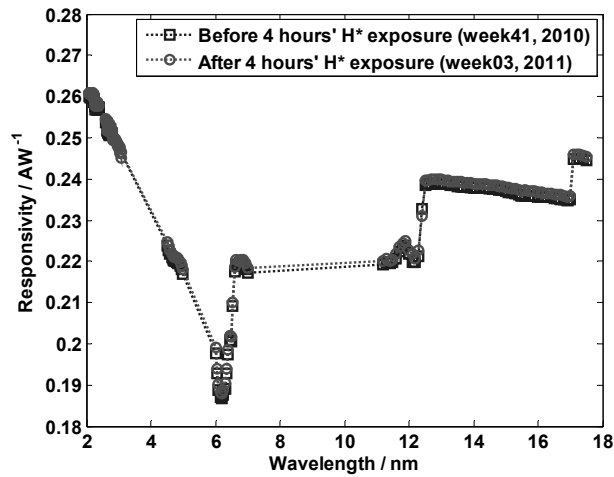


Fig. 7.9 Measured responsivity of the DIMES fabricated PureB-diode (with 1×1 cm² junction area) in the EUV spectral range, before / after a four-hour H⁺-cleaning in the filament-enhanced H⁺ setup [4].

To summarize, the experimental results presented above in Table 7.2, Table 7.3 and Fig. 7.9 show: no change in the boron layer thickness, negligible dark current variation, and good optical performance stability. Based on all these measurement data we can conclude that no H⁺-induced damage is detected within the diode active area. The nanometer-thin boron surface layer, as well as the underlying ultrashallow p⁺n junction, are robust to H⁺ exposure.

7.3.2 H^{*}-induced defects along the diode perimeter

As shown in Fig. 7.10, PureB-diodes with the same open junction area, but gradually changed structure along the perimeter, are applied to study the H^{*}-induced defects out of the diode junction area. As shown in the cross-section, the only difference between these diodes is the varied distance from the p⁺ to n⁺ guard ring. The meshed aluminum coating between the p⁺ and n⁺ guard ring plays a role as a path for H^{*}. Fig. 7.11 presents the measured dark currents at a 1 V reverse bias voltage before and after the filament-enhanced H^{*} exposure. After two short H^{*}

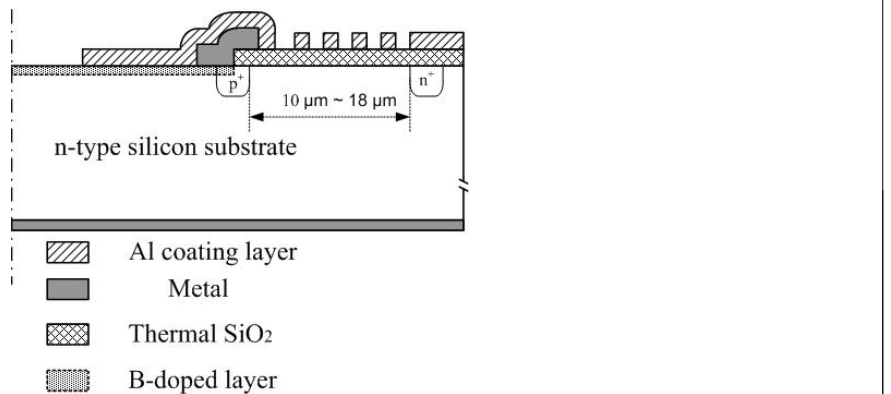


Fig. 7.10 Cross-section of PureB-diodes with different distances from the p⁺ to n⁺ guard ring [7].

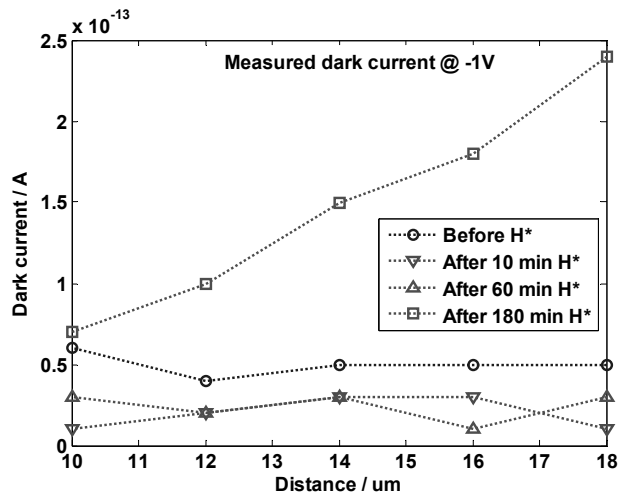


Fig. 7.11 Measured dark currents at a 1 V reverse bias voltage of the PureB-diodes with different distances from the p⁺ guard ring to the n⁺ guard ring (H^{*} cleaning in filament-enhanced setup) [7].

exposures (10 min and 60 min), no significant change in the dark current was detected. However, after a three-hour H^* exposure, a clear dark current increase was observed. The measured dark current increase was proportional to the distance between the p^+ and n^+ guard ring [7]. This result indicates that the H^* -induced damage to PureB-diodes is mainly located along the diode perimeter.

The mechanism behind this electrical degradation was further studied by a couple of gate-control diodes integrated on the same chip with the PureB-diodes arrays mentioned above. A micro-image and cross-section of this kind of device are shown in Fig. 7.12. As indicated in the figure, between two concentric ring-shaped diode areas, which are electrically connected in parallel, there is a metal gate on the oxide layer. The 2- μm -wide gaps in the metal gate act as a path for the hydrogen radicals. The basic principle of operation of these devices is presented in Fig. 7.13. The condition along the Si-SiO₂ interface under this metal gate can be modified by applying a different gate voltage. If there is no gate voltage applied (phase I, in Fig. 7.13), the measured dark current is only a sum of the dark current of the individual diodes. If there is a small negative gate voltage (phase II in Fig. 7.13), an extended depletion region is created along the Si-SiO₂ interface. Under this condition, any H^* -induced damage at the Si-SiO₂ interface will be involved into the depletion region,

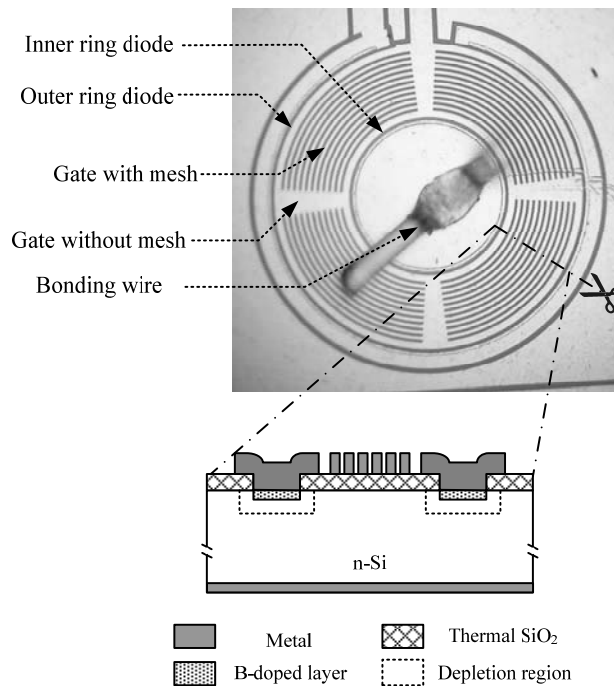


Fig. 7.12 Micro image and cross-section of a gate-controlled PureB-diode with a ring structure [7].

and lead to a higher measured dark current. Up to a certain gate voltage level (threshold voltage, V_T , of the MOS structure), the depletion region along the Si-SiO₂ interface is replaced by an inversion layer (phase III in Fig. 7.13). In this case, defects at the Si-SiO₂ interface are out of the depletion region (they are now in the inversion layer). Therefore, the measured dark current level drops again [8].

From the electrical measurement results presented in Fig. 7.14a, similar to Fig. 7.11, it is hard to see any electrical performance degradation after short filament-enhanced H^{*} exposures (10 min and 60 min). However, after the 180-min H^{*} cleaning step, a significant dark current increase can be observed. To better understand which part under the gate was damaged by the H^{*}, the I-V characteristic of the same kind of device measured in a MOSFET mode (Fig. 7.14b) is compared

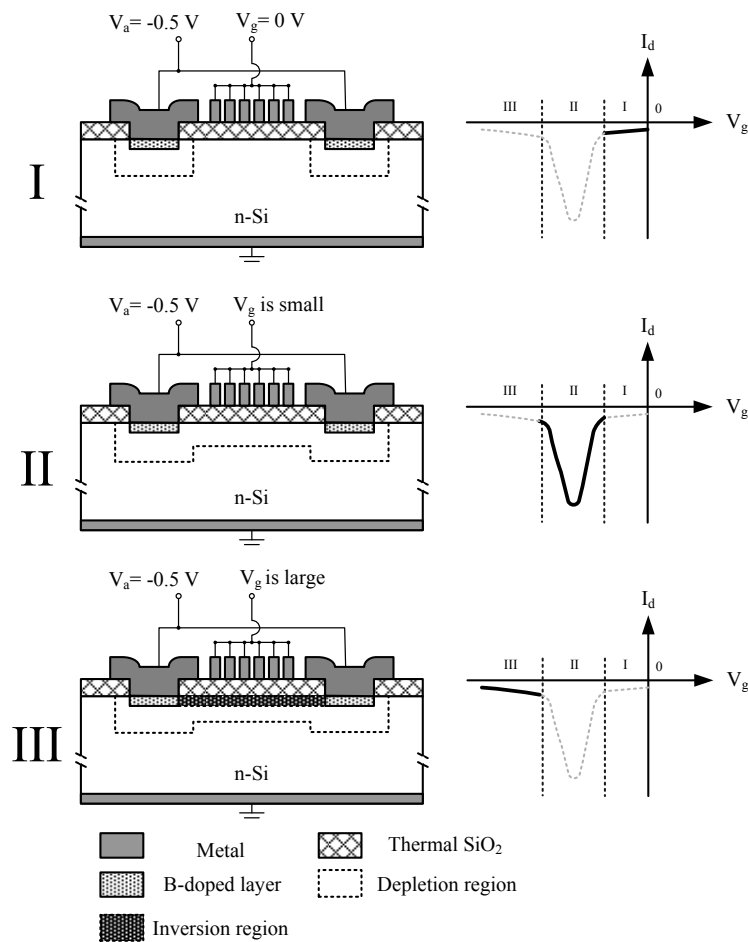


Fig. 7.13 basic principle and operation of the gate-controlled diode [8].

with the gate-controlled diode mode measurement results. As indicated in Fig. 7.15, in a MOSFET operation mode, two PureB-diodes shown in Fig. 7.12 become “source” and “drain”. If the gate voltage is below the threshold voltage (V_T), the MOSFET is turned off and ideally there is no current from the drain to the source, when drain voltage (V_D) is applied. If the gate voltage is above the V_T , similar to phase III in Fig. 7.13, the inverted n-Si under the gate will electrically connect the “source” and “drain”. Therefore, a drain current can be measured.

In Fig. 7.14b, the two measured threshold voltage values (V_{T1} and V_{T2}) can be easily understood as the threshold points of the non-meshed gate area (V_{T1}) and the meshed gate area (V_{T2}), as indicated in Fig. 7.12. The observed peak of the dark

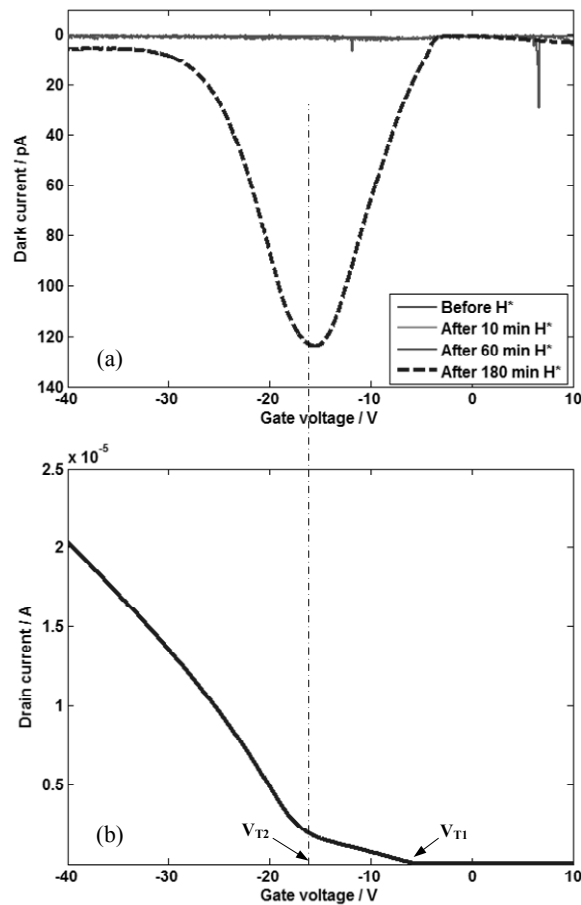


Fig. 7.14 (a) Dark currents of a gate-controlled diode before and after H^+ cleaning; (b) compared with the I-V characteristic measured from the same kind of device in a MOSFET mode [7].

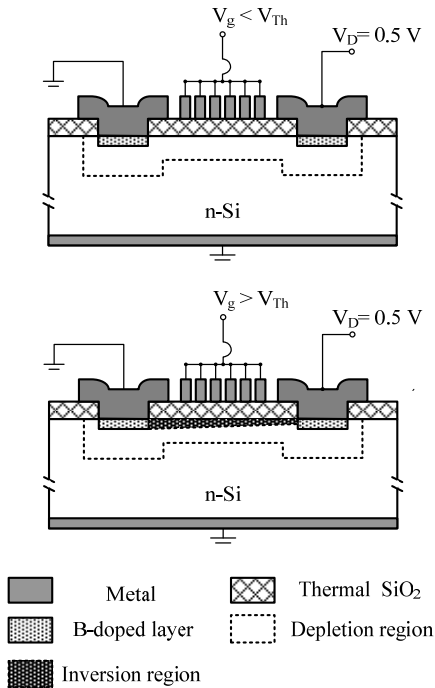
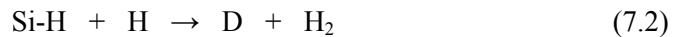


Fig. 7.15 MOSFET mode operation of the gate-controlled diode.

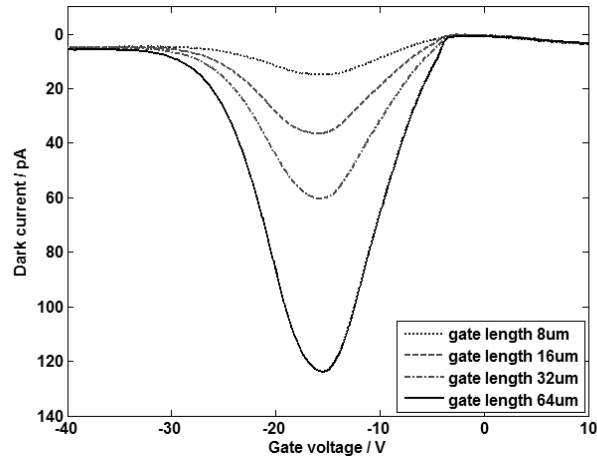
current in Fig. 7.14a fits well with the second threshold point (V_{T2}), which means that after the Si-SiO₂ interface is inverted the measured dark current of the gate-control diode starts to decrease. It is important to mention that, as shown in Fig. 7.16, after both “filament-enhanced” and “plasma-generated” H^{*} exposure, the dark current level was also found to be proportional to the gate area. Based on the measurement results presented above, two conclusions can be made: the H^{*}-induced damage of PureB-diodes is basically located along the diode perimeter; and such damage is probably mainly due to the interface defects along the Si-SiO₂ boundary.

A possible explanation for the observed phenomenon is the following: when there are free hydrogen atoms, an extra hydrogen atom can de-passivate the hydrogen-passivated dangling bond at the Si-SiO₂ interface via the reaction:

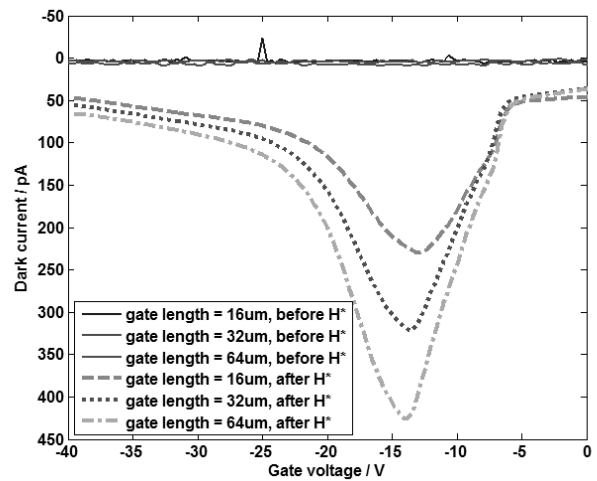


where D is a dangling bond (threefold-coordinated Si atom) [9][10][11].

Furthermore, as shown in Fig. 7.17a, a few weeks after the “filament-enhanced” H^{*} exposure, the measured dark current of the gate-controlled diodes decreased slowly around the threshold point. It is plausible that, just after H^{*} exposure, the excessive free hydrogen atoms were mainly accumulated within the “gap” area



(a)

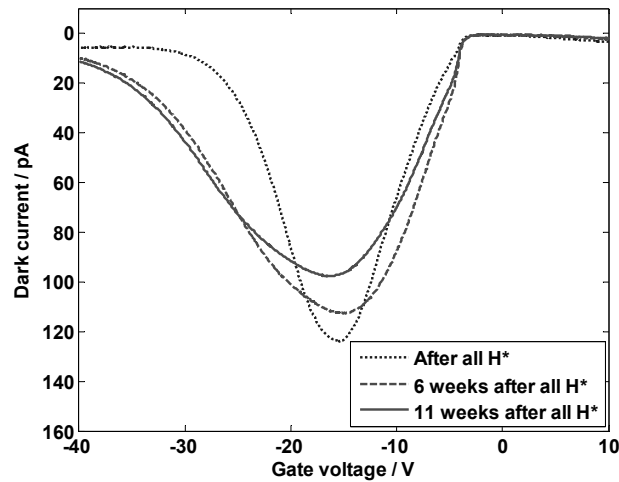


(b)

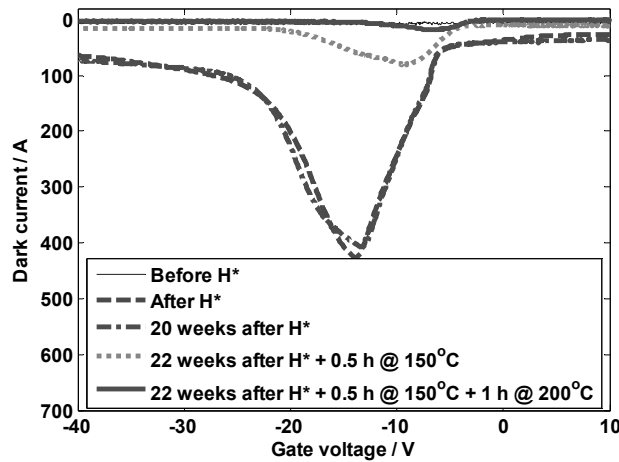
Fig. 7.16 Measured dark currents of gate-controlled diodes with different gate lengths after both filament-enhanced and plasma-generated H^+ exposure; (a) “filament-enhanced” total exposure time: 10 min + 60 min + 180 min [7]; (b) “plasma-generated” total exposure time: about 240 min [4].

under the meshed metal gate. Later, they appear to have diffused to the Si-SiO₂ interface under the metal-covered gate, and have created more defects there. This process leads to a dispersing of the defect-related threshold point of the MOS

structure. However, this phenomenon has not been seen after a four-hour “plasma-generated” H^* exposure. This could be explained as follows: due to the higher cleaning rate (which indicates a more efficient H^* generating rate) and a longer exposure time, more free hydrogen atoms were accumulated along the Si-SiO₂ interface after the “plasma-generated” H^* exposure. The distribution of harmful hydrogen atoms becomes even and no longer depends on the pattern of the metal



(a)



(b)

Fig. 7.17 (a) Measured dark currents change of gate-controlled diode: (a) after filament-enhanced H^* exposure [7]; and (b) after 4 hours plasma-generated H^* exposure [4].

gate. As indicated in Fig. 7.17b, this H^* -induced Si-SiO₂ interface damage is quite stable over time. Twenty weeks after H^* exposure, the measured dark current of the gate-control diode did not change. However, this H^* -induced damage was found to be annealed out by thermal treatment at relatively low temperatures, such as ~ 200 °C. What can also be seen in Fig. 7.17b is that after two hours of baking at 200 °C the dark current level almost went back to its initial value. Therefore, in actual industrial applications, the PureB-diode can be heated regularly to maintain a stable electrical performance.

7.4 Improved passivation

Because of the extremely low diffusion coefficient of hydrogen in silicon nitride (Si₃N₄), compared to SiO₂ [12][13][14], a 100-nm thick layer of silicon nitride is added between two SiO₂ passivation layers on the die surface outside the PureB-diode active area, to protect the Si-SiO₂ interface and Si-bulk (similar to Fig. 6.20). In this way, the nitride layer is expected to prevent hydrogen atoms from diffusing through the SiO₂-Si₃N₄-SiO₂ passivation layer and creating defects along the Si-SiO₂ interface in the area around the diode active surface. Fig. 7.18 shows the cross-section of this new structure [4][7]. As indicated in Table 7.4 and Table 7.5, after receiving the same H^* dose in both “filament-enhanced” and “plasma-generated” setup, no measurable dark current increase can be observed from nitride passivated PureB-diodes. The gate-control diodes, which have this extra silicon nitride in their passivation layer stack, also show a good durability. Compared with SiO₂-passivated devices, negligible electrical performance degradation have been measured (illustrated in Fig. 7.19 and Fig. 7.20).

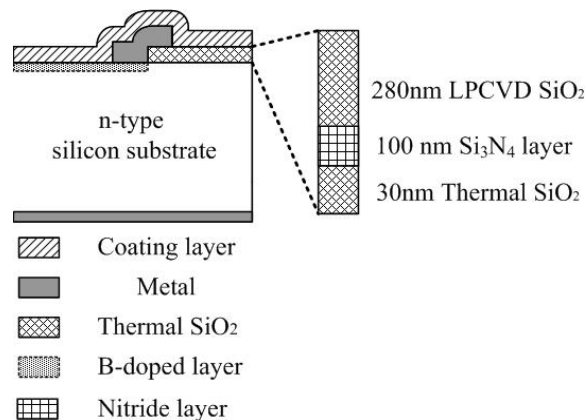


Fig. 7.18 Cross-section of PureB-diode with nitride passivation layer above the Si-SiO₂ interface [4][7].

TABLE 7.4 MEASURED DARK CURRENTS (pA) @ -1V OF PUREB-DIODES (WITH A NITRIDE PASSIVATION LAYER) BEFORE/AFTER “FILAMENT-ENHANCED” H^{*} EXPOSURE [7].

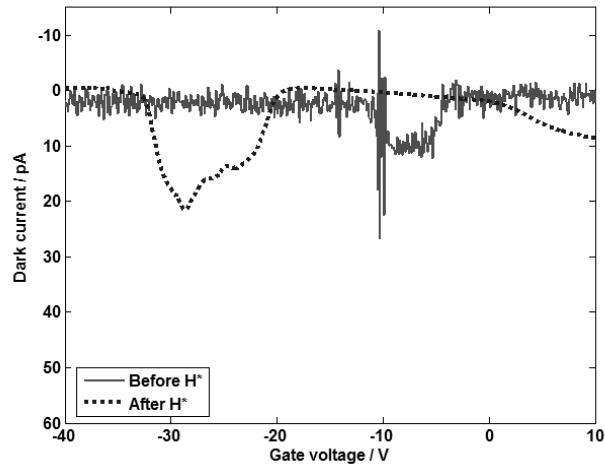
Diode #	Before H [*] exposure	After 10-min H [*] exposure	After 60-min H [*] exposure	After 180-min H [*] exposure
#1	0.01	0.01	0.02	0.04
#2	0.22	0.19	0.19	0.20
#3	0.02	0.01	0.03	0.02
#4	0.02	0.01	0.02	0.02
#5	0.03	0.02	0.01	0.01

The junction area of the PureB-diodes is 300×300 μm².

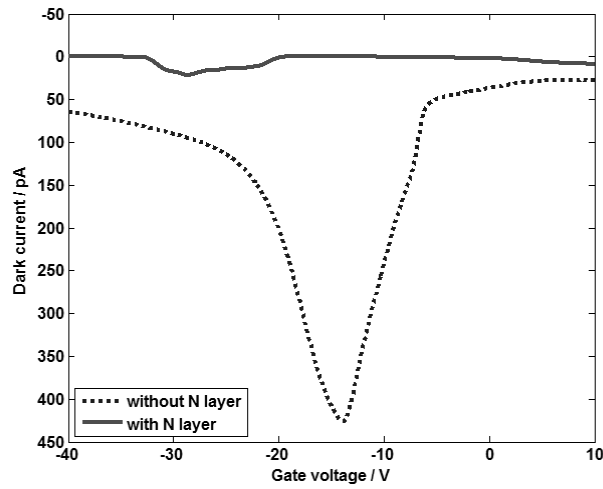
TABLE 7.5 MEASURED DARK CURRENTS (pA) @ -1V OF PUREB-DIODES (WITH A NITRIDE PASSIVATION LAYER) BEFORE/AFTER A FOUR-HOUR “PLASMA-GENERATED” H^{*} EXPOSURE [4].

Diode #	Before H [*] exposure	After H [*] exposure
#1	2.62	3.32
#2	7.08	7.47
#3	1.65	2.65
#4	0.81	1.96
#5	1.68	2.59
#6	2.7	3.3

The junction area of the PureB-diodes is 300×300 μm².



(a)



(b)

Fig. 7.19 Electrical characteristics of gate-controlled diodes with a gate length of $64 \mu\text{m}$ [4]. (a) Measured dark current of diode with extra nitride passivation layer, before and after a four-hour “plasma-generated” H^* cleaning; (b) Comparison of the measured dark current of diodes with/without a nitride passivation layer, after a four-hour “plasma-generated” H^* cleaning.

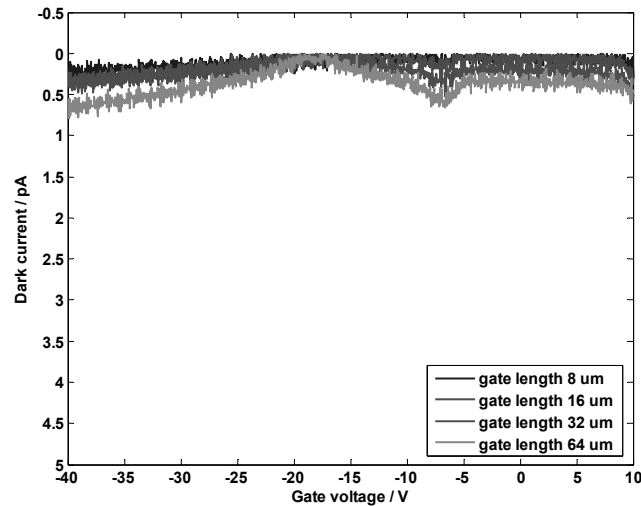


Fig. 7.20 Measured dark currents of nitride-passivated gate-controlled diodes with different gate lengths after “filament-enhanced” H^* cleaning steps (total exposure time: 10 min + 60 min + 180 min) [7].

7.5 Summary

PureB-diodes have demonstrated excellent robustness to H^* cleaning treatment. It was shown that the nanometer-thin α -boron layer and the underlying boron-doped ultra-shallow p^+n junction do not degrade during cleaning with aggressive H^* . In particular, no responsivity drop has been observed after continuous H^* exposure. However, H^* -induced defects created at the Si-SiO₂ interface with only SiO₂ surface passivation may increase the dark current at the diode perimeter under certain biasing conditions. This effect is almost eliminated by either a low-temperature bake (~ 200 °C) or by including a thin Si₃N₄ layer in the passivation layer stack to prevent the H^* radical from reaching the Si-SiO₂ interface.

Due to its high robustness to aggressive carbon-decontamination treatments, the PureB-diode technology shows a high compatibility in vacuum-related working environments, and exhibits a great potential for VUV/EUV radiation detection applications, such as the next-generation 13.5-nm EUV lithography.

Reference:

- [1] K. Motai et al., “Cleaning technology for EUV multilayer mirror using atomic hydrogen generated with hot wire”, *Thin Solid Films*, vol. 516, no. 5, pp. 839-843, January 2008.
- [2] R. Garg, A. Wüest, E. Gullikson, S. Bajt, and G. Denbeaux, “EUV optics contamination studies in presence of selected hydrocarbons”, *Proc. of SPIE.*, vol. 6921, no. 36, 2008.
- [3] Tom Levesque, “Review of plasma cleaning technology for decontamination in FIB, SEM and TEM”, *MICROSCOPY AND ANALYSIS*, vol. 25, no. 6, September 2011.
- [4] L. Shi, S. Nihtianov et al., “Stability Characterization of High-Sensitivity Silicon-Based EUV Photodiodes in a Detrimental Environment”, *IEEE Sensors Journal*, vol. 13, no. 5, pp. 1699 – 1707, May 2013.
- [5] L. Shi, S. Nihtianov, F. Scholze and L. K. Nanver, “Electrical performance stability characterization of high-sensitivity Si-based EUV photodiodes in a harsh industrial application”, *Proc. 38th Annual Conference of the IEEE Industrial Electronics Society (IECON)*, pp. 3952-3957, Oct. 2012.
- [6] H. Nagayoshi, S. Nishimura, K. Terashima and A. Ulyashin, “Texturing mechanism of Si using hydrogen radicals”, *Proc. IEEE 4th World Conference on Photovoltaic Energy Conversion*, pp. 1411-1414, May 2006.
- [7] L. Shi, L. K. Nanver and S. N. Nihtianov, “Stability characterization of high-sensitivity silicon-based EUV photodiodes in a detrimental industrial environment”, *Proc. 37th Annual Conference of IEEE Industrial Electronics Society (IECON)*, pp. 2651-2656, Nov. 2011.
- [8] D. K. Schroder, *Semiconductor Material and Device Characterization (Third Edition)*, Wiley-IEEE Press, pp. 429-432, 2006.
- [9] K. L. Brower, “Kinetics of H₂ passivation of Pb centers at the (111) Si-SiO₂ interface”, *Phys. Rev. B*, vol. 38, pp. 9657–9666, 1988.
- [10] J. H. Stathis and E. Cartier, “Atomic hydrogen reactions with Pb centers at the (100) Si/SiO₂ interface”, *Phys. Rev. Lett.*, vol. 72, pp. 2745-2748, 1994.
- [11] S. N. Rashkeev, D. M. Fleetwood, R. D. Schrimpf and S. T. Pantelides, “Defect generation by hydrogen at the Si- SiO₂ interface”, *Phys. Rev. Lett.*, vol. 87, pp. 165506, 2001.
- [12] W. M. Arnoldbik, C. H. M. Marée, A. J. H. Maas, M. J. van den Boogaard and F. H. P. M. Habraken, “Dynamic behavior of hydrogen in silicon nitride and oxynitride films made by low-pressure chemical vapor deposition”, *Phys. Rev. B.*, vol. 15, no. 48(8), pp. 5444-5456, Aug. 1993.
- [13] M. McCann, K. Weber and A. Blakers, “An early deposited LPCVD silicon nitride: allowing the possibility of novel cell designs”, *Proc. of 3rd World Conference on Photovoltaic Solar Energy Conversion*, vol. 2, no. 12-16, pp. 1135-1138, May 2003.

- [14] R. W. Lee, R. C. Frank and D. E. Swets, "Diffusion of hydrogen and deuterium in fused quartz", *Journal of Chemical Physics*, vol. 36, pp. 1062-1071, 1962.

Chapter 8 Conclusions

In this final chapter, a short overview of the UV photodiode design strategies is offered and a summary of the major contributions of this research work is presented. Next, the on-going work and potential extensions are shortly discussed.

8.1 Strategies for creating high-performance Si-based photodiodes

Based on the performance characterization of PureB-diodes, as well as the comparative study of several representative commercially available Si-based UV photodiodes, the strategies to design high-performance Si-based UV photodiodes which can meet the key requirements defined in Chapter 1, are summarized as follows:

High sensitivity

A shallow p-n junction and a beneficial surface electric field have been found helpful in reducing the depth of the effective charge collection zone, and consequently in enhancing the photodiode sensitivity. In addition, a defect-free doping technique and a sufficiently wide depletion region are essential.

High operational speed

The time constant, which is a product of the series resistance (R_s) and the junction capacitance (C_j), sets the major limitation of the diode's response time, and consequently the operational speed. A high conductivity surface (which can be realized by a deeper junction or a conductive capping layer) is required to reduce R_s of the photodiodes, especially when the diode has a large junction area (few mm^2 or more). At the same time, once the junction area is fixed, a wider depletion zone means a smaller C_j .

High stability

An oxide-free capping layer can minimize not only the photoelectron emission induced positive charge on the diode surface, but also the radiation-induced damage along the Si-SiO₂ interface.

The above-presented design strategies are summarized in Fig. 8.1, which shows the design targets and the related determining factors. By knowing the design strategies and adhering to different application requirements, the trade-offs between different device structures can be made more effectively.

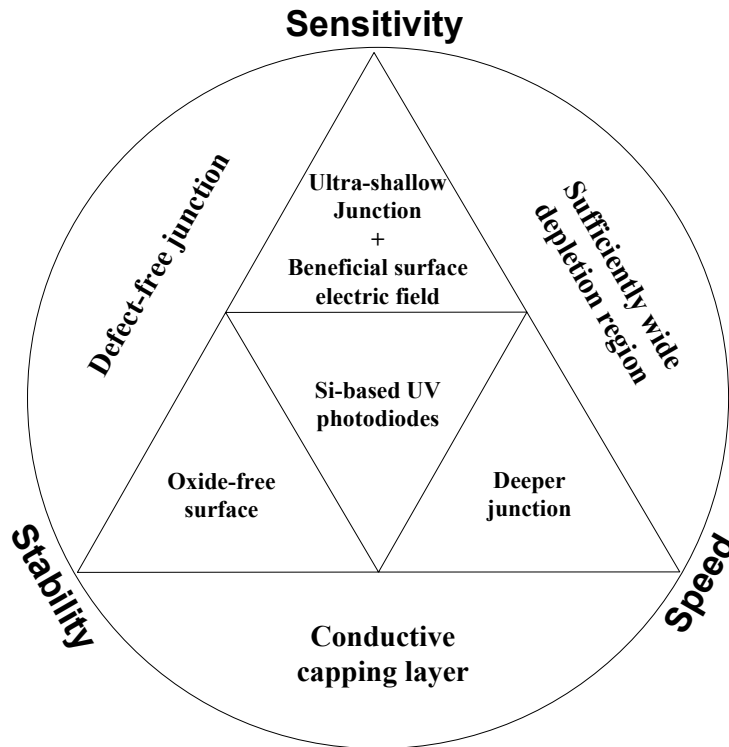


Fig. 8.1 Relations between three key performance factors and related obligatory structure characteristics of UV photodiodes.

8.2 Major research achievements

The major achievements of this research work are:

- Optical performances of commercially available state-of-the-art Si-based UV photodetectors are reviewed, and their advantages and drawbacks are summarized.
- The outstanding EUV responsivity and the superior DUV/VUV responsivity of PureB-diodes have been investigated. A distinctive doping-profile-induced surface charge-collection process in the highly-doped p^+ region has been validated.
- The electrical and optical stability of PureB-diodes are explored by prolonged UV exposure. Improvements have been proposed for increasing the UV radiation hardness of the device.

- Regarding specific challenging industrial application requirements, the robustness of PureB-diodes in detrimental working environment is evaluated.
- Based on the key performance requirements (high sensitivity, high stability and high operational speed) defined in Chapter 1, strategies for designing high-performance Si-based UV photodiodes are presented.

8.3 Ongoing and potential future work

1. Investigation of surface conditions

As discussed in Chapter 3 and Chapter 6, the main reason for the responsivity degradation of PureB-diodes is a surface oxidation. Therefore, in order to predict the oxidation mechanism, and eradicate this harmful factor, it is necessary to understand the species (silicon oxide or boron oxide), location (on top or below the nanometer-thin boron layer), structure (complete film or just islands) and quantity (thickness or density) of the oxide content. Then, the optical stability of PureB-diodes will be further improved.

However, due to the lack of a sub-nanometer surface analysis technique, this surface oxidation phenomenon has not yet been fully investigated and understood. Recently, a couple of X-ray Photoelectron Spectroscopy (XPS) measurements have been carried out to measure the surface chemical components of PureB-diodes. As a first step, the species and quantity of the surface oxide were detected. Further analysis, with the help of a high-resolution Transmission Electron Microscopy (HRTEM) and other techniques, will focus on the location and structure of the surface oxide.

As discussed in Chapter 4 and Chapter 6, a high and stable surface charge-collection efficiency of PureB-diodes relies on critical surface conditions, such as a steep doping profile without roll-off at the surface, a defect-free doping method and an oxide-free capping layer. Thus, an accurate sub-nanometer surface condition investigation could be also helpful in further understanding the surface charge-collection phenomenon of PureB-diode.

2. Investigation of Bipolar/CMOS compatibility

Obviously, as a Si-based process, Pure-B CVD technology has an inherent potential to achieve Bipolar/CMOS compatibility. The observed high surface charge-collection efficiency, which can guarantee a high DUV/VUV and EUV responsivity of thermally annealed PureB-diodes (at 900°C), makes the chance even bigger.

A full Bipolar/CMOS compatibility will give an opportunity to integrate PureB-diodes together with electronic interface circuits and other sensors on a single chip.

In this way, smart sensor systems or even CCD or CMOS UV image sensors, can be realized [1].

An early-phase demonstration on the IC-compatibility of PureB-diode technology is shown in Fig. 8.2. The PureB-diode and a bipolar transistor-based temperature sensor were successfully integrated on a single chip [2]. The distance between the diode active area and the temperature sensor is only 75 μm [2]. This temperature sensor is built up of two npn bipolar transistors working in differential mode. From Fig. 8.3, it can be seen that the measured ΔV_{be} of the two transistors is very linear in

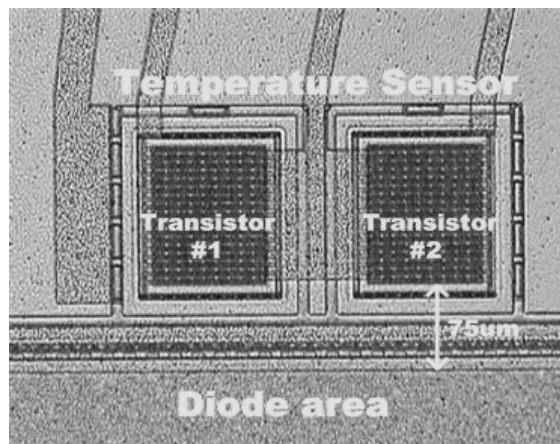


Fig. 8.2 Micro-image of an integrated temperature sensor and the neighboring photodiode. [2]

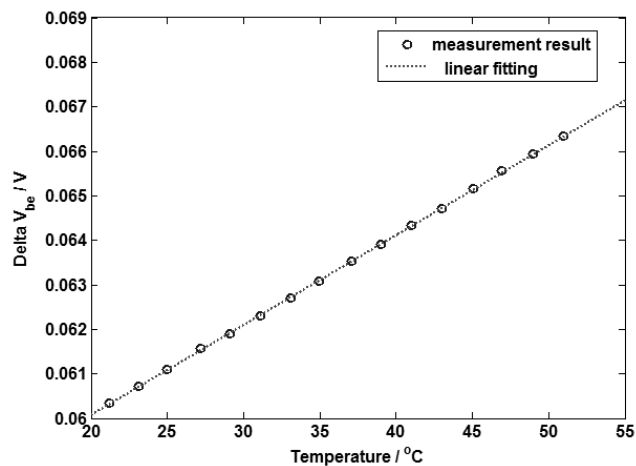


Fig. 8.3 The voltage offset ΔV_{be} as a function of temperature for two transistors with bias currents of 100 μA and 10 μA , respectively. [2]

the temperature range from 20 °C to 50 °C. The sensitivity of this temperature sensor is 0.2 mV/ °C [2]. Since the temperature coefficient of the PureB-diode is well defined in the EUV spectral range (the measured temperature coefficients, from 30 °C to 80 °C, of the responsivity at 13.5-nm and 11.5-nm radiation wavelengths are 0.018% and 0.022% per Kelvin, respectively [1]), the information from this on-chip real-time temperature sensor can be used for further improvements to the optical measurement accuracy.

Reference:

- [1] L. Shi, F. Sarubbi, S. N. Nihtianov, L. K. Nanver, T. L. M. Scholtes and F. Scholze, “High performance silicon-based extreme ultraviolet (EUV) radiation detector for industrial application”, *Proc. 35th Annual Conference of the IEEE Industrial Electronics Society (IECON)*, pp. 1891-1896, Nov. 2009.
- [2] L. Shi, S. Nihtianov et al., “Stability Characterization of High-Sensitivity Silicon-Based EUV Photodiodes in a Detrimental Environment”, *IEEE Sensors Journal*, vol. 13, no. 5, pp. 1699 – 1707, May 2013.

Summary

This thesis presents a performance investigation of newly-developed ultra-shallow junction photodiodes (PureB-diodes) for ultraviolet (UV) radiation detection. The photodiodes are fabricated by pure boron chemical vapor deposition (PureB CVD) technology, which can provide nanometer-thin boron capping layer and nanometer-deep defect-free p^+n junction. Due to its unique features, the PureB-diode technology is considered to be a promising solution for developing advanced UV photodetectors.

Chapter 1 presents the motivation and the objectives of the research work. In view of one of the most demanding UV-related industrial applications: deep-UV (DUV) and extreme-UV (EUV) lithography; the major challenges for designing high-performance UV photodetectors are defined.

In Chapter 2, the results of a comparative study of the existing ultraviolet (UV) photodetectors are presented, based on the performance requirements defined in Chapter 1. The subsequent analyses are restricted to silicon-based devices, due to their superior characteristics: high sensitivity, simplicity, low costs, and IC-compatibility. The optical performance of state-of-the-art Si-based UV photodiode is reviewed, and their advantages and drawbacks are summarized in comparison with a proposed ideal structure of Si-based UV photodiode. Owing to the nanometer-deep junction and the nanometer-thin α -boron capping layer, PureB-diodes have an ultra-thin front absorption window which can greatly reduce the unwanted photon loss, consequently achieve a near-theoretical responsivity at 13.5-nm wavelength in the EUV spectral range. This unique feature indicates that PureB-diodes can potentially provide better sensitivity than any other commercially available Si-based photodetector over the full UV spectral range. Therefore, photodiodes fabricated by the PureB CVD technology was chosen as the main candidate to design high-sensitivity, high-stability photodiodes for UV radiation detection.

In Chapter 3, for proper interpretation and analysis of the reported optical experimental data in this thesis, the fabrication process and the device structure of PureB-diodes are introduced. Due to the limited attenuation length (penetration depth) of DUV/VUV photons in silicon, the surface conditions of Si-based photodiodes play an important role in their optical performance. The surface structure and properties of PureB-diodes are discussed in detail.

In Chapter 4, a superior DUV/VUV optical performance of PureB-diodes has been presented. A doping-profile-induced surface charge-collection effect is validated as an additional important factor for achieving the high DUV/VUV sensitivity, especially when the junction depth is significantly increased by extra thermal treatment. It has been demonstrated that, along with the ultra-shallow junction, an optimized surface-layer doping profile plus a damage-free doping technique could be an alternative way to reduce the equivalent thickness of the pre-absorption layer on top of the effective charge-collection zone of the photodiode. The observed doping-profile-enhanced effect of surface charge-collection offers significant opportunities for designing a high-sensitivity photodiode for the case that an “ultra-shallow junction” is difficult to apply; for instance, when a low surface sheet resistance is the primary goal. At the same time, this doping-profile-enhanced effect of surface charge-collection also enhances the compatibility of PureB CVD technology with standard Si processing, and becomes one of the inherent advantages of these silicon-based photodiodes when it comes to fabricating fully-integrated UV smart-sensor systems.

In Chapter 5, two potential negative effects related to a high surface sheet resistance of PureB-diodes have been studied: unpredictable response times and high series resistance. With respect to the response time, it has been demonstrated experimentally that, when PureB-diodes have a high surface sheet resistance, as well as a large active area (in the order of mm^2), their response time is only slightly affected by variations of the size and location of the incident light spot. In most of the practical applications, this influence is negligible. Yet, for achieving a shorter response time, it makes sense to reduce the series resistance. This can be achieved, for instance, by improving the structure of the PureB-diodes either by creating an extended anode with the help of an aluminum grid, or by extra thermal annealing. Although PureB-diodes with an aluminum grid have a higher responsivity for the same series resistance value, the local non-uniformity of the sensitivity limits the applications of this method. Alternatively, a low series resistance can also be achieved with a deeper junction of the PureB-diodes. Due to the high efficiency of collecting charge at the surface, PureB-diodes with a deeper junction still maintain a good VUV/EUV responsivity and an excellent uniformity.

In Chapter 6, the performance stability of PureB-diodes is evaluated. The experimental results prove that the p^+n junction formed by PureB CVD technology is stable under DUV/VUV and EUV radiation: after prolonged exposures, no performance degradation caused by the damage to the junction itself has been observed. Nevertheless, a surface oxidation, which can be positively charged by the photoelectron emission effect under UV radiation, was found to be the main reason for the small responsivity degradation that was measured after receiving some

Summary

VUV/DUV and EUV radiation. This charging-induced responsivity loss can be avoided by forming a thicker boron layer or adding a conductive capping layer. The former can eliminate the harmful surface oxidation on PureB-diodes; the latter is helpful in minimizing the charge-accumulation on the diode surface. Moreover, PureB-diodes have also demonstrated good electrical performance stability under intensive EUV radiation when an extra nitride passivation layer is applied to protect the Si-SiO₂ interface along the diode perimeter. The still observed small dark current increase can be further scaled down by reducing the reverse bias voltage to the mV range in future applications.

In Chapter 7, the durability of PureB-diodes in detrimental environments (under aggressive cleaning) is evaluated. Experimental results prove that PureB-diodes have excellent robustness to hydrogen radical (H^{*}) cleaning treatment: the nanometer-thin α -boron layer and the underlying boron-doped ultra-shallow p⁺n junction do not degrade during cleaning with aggressive H^{*}. In particular, no responsivity drop has been observed after continuous H^{*} exposure. However, H^{*}-induced defects created at the Si-SiO₂ interface with only SiO₂ surface passivation outside the photodiode sensitive area, nearby the diode perimeter, increase the dark current at certain biasing conditions. This effect is almost eliminated by either a low-temperature bake (~ 200 °C) or by including a thin Si₃N₄ layer in the passivation layer stack to prevent the hydrogen from reaching the Si-SiO₂ interface.

In Chapter 8, a short overview of the UV photodiode design strategies is offered and a summary of the major contributions of this research is presented. Next, the ongoing work and potential extensions are shortly discussed.

Samenvatting

Dit proefschrift beschrijft de resultaten van het onderzoek naar de kwaliteiten van een pasontwikkelde fotodiode met een ultradunne junctie (PureB-diode), die wordt gebruikt voor de detectie van ultraviolette (UV) straling. De fotodioden worden vervaardigd met gebruikmaking van de technologie van chemische dampdepositie van zuiver borium (PureB CVD). Hiermee worden nanometer-dunne afdekklagen en nanometer-diepe defectvrije p⁺n juncties vervaardigd. Dank zij deze unieke mogelijkheden wordt de PureB-diode technologie beschouwd als een veelbelovend voor de ontwikkeling van geavanceerde UV fotodetectoren.

Hoofdstuk 1 beschrijft de motivatie en de doelstellingen van het onderzoek. Met het oog op een van de meest veeleisende industriële UV toepassingen: deep-UV (DUV) en extreme-UV (EUV) lithografie; worden de belangrijkste uitdagingen vastgesteld voor het ontwerp van UV fotodetectoren met hoge kwaliteit.

In hoofdstuk 2 worden de resultaten weergegeven van een vergelijkende studie van bestaande UV fotodetectoren; welke gebaseerd is op de kwaliteitseisen die in hoofdstuk 1 zijn vastgesteld. De achtereenvolgende analyses zijn beperkt tot detectoren die met siliciumtechnologie zijn vervaardigd. Deze detectoren hebben namelijk superieure kwaliteiten, zoals: een hoge gevoeligheid, eenvoud, lage kosten, en IC compatibiliteit. De optische kwaliteiten van eigentijdse Si-gebaseerde UV fotodioden worden besproken, waarbij een samenvatting wordt gegeven van hun voor- en nadelen in vergelijking met die van de ideale structuur voor een Si-gebaseerde UV fotodiode die in dit proefschrift wordt voorgesteld. Dankzij de nanometer-diepe junctie en de nanometer-dunne α -borium afdeklaag, hebben PureB-dioden een ultradun absorptievenster, hetgeen ongewenst fotonenverlies ten zeerste reduceert. Hierdoor wordt er voor de 13,5 nm golflengte van het EUV spectrum een lichtgevoeligheid bereikt die bijna gelijk is aan de theoretisch waarde. Deze unieke eigenschap laat zien dat PureB-dioden in aanleg, over het gehele UV bereik, een beter gevoeligheid hebben dan commercieel verkrijgbare Si-gebaseerde UV fotodioden. Daarom is de fotodiode vervaardigd met PureB CVD technologie gekozen als de belangrijkste kandidaat voor het ontwerp van UV detectoren met hoge gevoeligheid en hoge stabiliteit.

Ten behoeve van de interpretatie en analyse van gerapporteerde optische experimentele gegevens, worden in hoofdstuk 3 het fabricatieproces en de structuur van de PureB-dioden besproken. Als gevolg van de beperkte indringingsdiepte van DUV/VUV fotonen in silicium, spelen oppervlakte-effecten in Si-gebaseerde fotodioden een belangrijke rol met betrekking tot de optische kwaliteiten. De oppervlaktestructuur en de daarmee samenhangende eigenschappen van PureB-dioden worden daarom in detail besproken.

In hoofdstuk 4 worden de superieure optische kwaliteiten van PureB-dioden gepresenteerd. Het blijkt dat de hoge DUV/VUV gevoeligheid mede te danken is aan het verzamelen van oppervlaktelading, hetgeen wordt bevorderd door het doteringsprofiel. Dit gebeurt met name als de junctiediepte wordt vergroot middels thermische behandeling. Er wordt aangetoond dat, tezamen met optimalisering van het doteringsprofiel, het gebruik van schadevrije doteringstechnologie een alternatieve manier verschaffen voor het verminderen van de equivalente dikte van de voor-absorptielaag die zich bovenop de effectieve verzamelzone voor lading bevindt. Vooral als, bijvoorbeeld omwille van een lagere laagweerstand, het lastig is om een ultradunne junctie te gebruiken, dan biedt het waargenomen ladingsverzameleffect aantrekkelijke mogelijkheden voor het ontwerp van fotodioden met een hoge gevoeligheid. Tegelijkertijd verbetert het ook de compatibiliteit van PureB CVD technologie met standaard Si bewerking. Dit opent de mogelijkheden om deze Si-gebaseerde fotodioden op te nemen in volledig geïntegreerde UV smart-sensor systems.

In hoofdstuk 5 worden twee potentiële nadelige effecten bestudeerd die te maken hebben met de hoge weerstand van de oppervlaktelaag, welke de oorzaak zou kunnen zijn van onvoorspelbaarheid van de responsietijd en van een hoge serieweerstand. Met betrekking tot de responsietijd is experimenteel aangetoond dat bij PureB-dioden met hoge oppervlaktelaagweerstand en een groot actief gebied (in de orde van enige mm^2) de responsietijd nauwelijks wordt beïnvloed door variaties in de afmetingen en de plaats van belichtingsplek. Toch heeft het zin om de serieweerstand te verkleinen omdat die tot een kortere responsietijd leidt. Dit kan worden bereikt door het verbeteren van de structuur van de PureB-dioden. Een middel middelen hiertoe is het uitbreiden van de anode met een aluminium rooster. Ook kan tijdens de fabricage een extra uitgloeistap worden toegepast, waardoor de

Samenvatting

laagweerstand vermindert. Ofschoon PureB-dioden met een aluminium rooster bij dezelfde weerstand een hogere lichtgevoeligheid hebben, beperkt de lokale niet-uniformiteit van de gevoeligheid de toepasbaarheid van deze methode. Als gevolg van de hoge doelmatigheid van het verzamelen van lading aan het oppervlak, hebben PureB-dioden met een diepere junctie toch nog een goede DUV/VUV lichtgevoeligheid en een uitstekende uniformiteit.

In hoofdstuk 6 worden de eigenschappen van PureB-dioden ten aanzien van de stabiliteit geëvalueerd. Experimentele resultaten tonen aan dat de p^+n junctie, die wordt gevormd met PureB CVD technologie, stabiel is onder condities van DUV/VUV en EUV straling: Ook bij langdurige belichting wordt geen afname van de kwaliteit als gevolg van schade aan de junctie waargenomen. Wel is er oppervlakteoxidatie waargenomen welke positief geladen kan worden als gevolg van foto-elektron emissie onder UV straling. Dit effect vormde de belangrijkste reden voor de kleine afname van de lichtgevoeligheid in het spectrale bereik voor DUV/VUV en EUV straling. Deze achteruitgang kan worden voorkomen door een dikkere boriumlaag te vormen of door een geleidende toplaag toe te voegen. Eerstgenoemde maatregel voorkomt de vorming van de schadelijke oppervlakteoxidatie op de PureB-dioden. Laatstgenoemde maatregel helpt om ladingsopslag aan het diodeoppervlak te minimaliseren. Verder vertonen PureB-dioden een goede stabiliteit van het elektrische gedrag bij EUV straling als er een extra nitride passivatielaag wordt toegepast, teneinde de Si-SiO₂ interface rondom de omtrek van de diode te beschermen.

In hoofdstuk 7 wordt de duurzaamheid geëvalueerd van PureB-dioden in schadelijke omgevingen (bijvoorbeeld bij agressief schoonmaken). Experimentele resultaten tonen aan dat PureB-dioden een uitstekende robuustheid hebben bij een reinigingsbehandeling met waterstof radicalen (H^{*}): de nanometer-dunne α -boriumlaag en de onderliggende borium-gedoopte ultra-ondiepe p^+n junctie desintegreren niet bij schoonmaken met het agressieve H^{*}. In het bijzonder wordt er geen vermindering van de lichtgevoeligheid gevonden na voortdurende blootstelling aan H^{*}. Echter doen door H^{*} geïnduceerde defecten op de Si-SiO₂ overgang, met slechts een SiO₂ oppervlakte-passivatie buiten het fotogevoelige gebied, vlakbij de diodeomtrek, de donkerstroom onder bepaalde condities toenemen. Dit effect wordt bijna geheel geëlimineerd door ofwel een bakstap bij lage-temperatuur (~ 200 °C),

Samenvatting

of door een dunne Si_3N_4 laag aan de passivatielaag toe te voegen, om te voorkomen dat waterstof de Si-SiO₂ interface bereikt.

In hoofdstuk 8 wordt een kort overzicht gepresenteerd van de ontwerpstrategieën voor fotodioden. Tevens wordt een samenvatting gegeven van de belangrijkste bijdragen van het onderzoek. Tot slot worden het lopend werk en mogelijke uitbreidingen daarvan kort besproken.

Appendix

DIVISIONS OF THE UV SPECTRAL RANGE

Sub-range	Wavelength limits (nm)
Near-UV (NUV)	400 - 300
Middle-UV (MUV)	300 - 200
Far-UV (FUV)	200 - 100
Deep-UV (DUV)	350 - 190
Vacuum-UV (VUV)	200 - 10
Extreme-UV (EUV)	100 - 10

These appear to be the most commonly used names and wavelength ranges, but other terminology can be found as well.

List of Publications

Journal Papers

L. Shi and S. Nihtianov, “Comparative Study of Silicon-Based Ultraviolet Photodetectors”, *IEEE Sensors Journal*, vol. 12, no. 7, pp. 2453 – 2459, July 2012.

L. Shi, S. Nihtianov, S. Xia, L. K. Nanver, A. Gottwald and F. Scholze, “Electrical and Optical Performance Investigation of Si-Based UltraShallow Junction p+n VUV/EUV Photodiodes”, *IEEE Trans. Instrumentation and Measurement*, vol. 61, no. 5, pp. 1268 – 1277, May 2012.

L. Shi, S. Nihtianov, L. Haspeslagh, F. Scholze, A. Gottwald and L. K. Nanver, “Surface-Charge-Collection-Enhanced High-Sensitivity High-Stability Silicon Photodiodes for DUV and VUV Spectral Ranges”, *IEEE Trans. on Electron Devices*, vol. 59, no. 11, pp. 2888 – 2894, Nov. 2012.

L. Shi, S. Nihtianov, L. K. Nanver, and F. Scholze, “Stability Characterization of High-Sensitivity Silicon-Based EUV Photodiodes in a Detrimental Environment”, *IEEE Sensors Journal*, vol. 13, no. 5, pp. 1699 – 1707, May 2013.

Conference proceedings

L. Shi, F. Sarubbi, S. N. Nihtianov, L. K. Nanver, T. L. M. Scholtes and F. Scholze, “High performance silicon-based extreme ultraviolet (EUV) radiation detector for industrial application”, *Proc. 35th Annual Conference of IEEE Industrial Electronics Society (IECON)*, pp. 1891-1896, Nov. 2009.

L. Shi, F. Sarubbi, L. K. Nanver, U. Kroth, A. Gottwald and S. Nihtianov, “Optical performance of B-layer ultra-shallow-junction silicon photodiodes in the VUV spectral range”, *Proc. Euroensors XXIV*, Sept. 2010.

L. Shi, L. K. Nanver, A. Šakić, S. Nihtianov, A. Gottwald and U. Kroth, “Optical Stability Investigation of High-Performance Silicon-Based VUV Photodiodes,” *Proc. IEEE SENSORS2010*, pp. 132-135, Nov. 2010.

L. Shi, L. K. Nanver, A. Šakić, S. Nihtianov, T. Knežević, A. Gottwald and U. Kroth, “Series resistance optimization of high-sensitivity Si-based VUV

List of Publications

photodiodes”, *Proc. 2011 IEEE Instrumentation and Measurement Technology Conference (I2MTC)*, May 2011. **(Best paper award)**

L. Shi, L. K. Nanver, C. Laubis, F. Scholze and S. Nihtianov, “Electrical performance optimization of a silicon-based photodiode with near-theoretical quantum efficiency”, *Proc. TRANSDUCERS2011*, Jun. 2011.

L. Shi, S. Nihtianov, L. K. Nanver, F. Scholze, and A. Gottwald, “High-sensitivity high-stability silicon photodiodes for DUV, VUV and EUV spectral ranges,” *Proc. SPIE*, vol. 8145, pp. 21-25, Aug. 2011.

L. Shi, L. K. Nanver and S. N. Nihtianov, “Stability characterization of high-sensitivity silicon-based EUV photodiodes in a detrimental industrial environment”, *Proc. 37th Annual Conference of IEEE Industrial Electronics Society (IECON)*, pp. 2651-2656, Nov. 2011

L. Shi, S. Nihtianov, F. Scholze and L. K. Nanver, “Electrical Performance Stability Characterization of High-Sensitivity Si-Based EUV Photodiodes in a Harsh Industrial Application”, *Proc. 38th Annual Conference of the IEEE Industrial Electronics Society (IECON)*, pp. 3952-3957, Oct. 2012.

L. Shi, S. Xia, F. Sarubbi, R. Naulaerts, S. Nihtianov, L. Nanver, “Response time of shallow junction silicon photodiodes”, *Proc. ELECTRONICS’ 2008*, pp. 21-26, Sep, 2008.

L. K. Nanver, T. L. M. Scholtes, F. Sarubbi, W. B. de Boer, G. Lorito, A. Šakić, S. Milosavljević, C. Mok, **L. Shi**, S. Nihtianov, K. Buisman, “Pure-boron chemical-vapor-deposited layers: A new material for silicon device processing”, *Proc. 18th International Conference on Advanced Thermal Processing of Semiconductors (RTP2010)*, pp. 136-139, Oct. 2010.

Workshop contributions

L. Shi, F. Sarubbi, S. N. Nihtianov, L. K. Nanver and F. Scholze, “Stability investigation of high performance silicon-based DUV/EUV photodiodes”, *Proc. 12th Annual Workshop on Semiconductor Advances for Future Electronics and Sensors (SAFE)*, pp. 530-533, Nov. 2009. **(Special presentation)**

L. Shi, S. Nihtianov, L. K. Nanver, U. Kroth, “VUV Performance Characterization of a Silicon-Based Ultrashallow-Junction Photodiode”, *Proc. 13th Annual Workshop*

List of Publications

on Semiconductor Advances for Future Electronics and Sensors (SAFE), pp. 158-161, Nov. 2010. **(Special presentation)**

Invited presentation

L. Shi, EUV detector radiation and environmental hardness, *Book of Abstracts, 262nd PTB Seminar, EUV Metrology*, 27-28 October 2011, Berlin, Germany.

Acknowledgements

This research work has been supported by the Dutch technology Foundation (STW) under project number: 10024. Their support is gratefully acknowledged.

Many people have offered me valuable help during the last four and half years. Without their support, I could not have finished my dissertation successfully. A complete story, which shows all their names and how great their help is, could be another chapter of this book. Therefore, I would like to briefly summarise my acknowledgements in the following table.

I would like to take this opportunity to express my gratitude to	
Supervisor	Dr. Stoyan Nihtianov;
Promoter	Prof. Albert Theuwissen;
Guidance and/or support in scientific research	Dr. Stoyan Nihtianov; Prof. Lis K. Nanver; Dr. Francesco Sarubbi; Dr. Frank Scholze; Dr. Alexander Gottwald; Dr. L. Haspeslagh;
Device fabrication	Prof. Lis K. Nanver and her group; Specially to T. L. M. Scholtes; S. Milosavljevic; Dr. A. Šakić; V. Mohammadi; Other staff of the DIMES-ICP clean rooms; Dr. L. Haspeslagh;
Experiment	Ir. Zu-yao Chang; Ir. P.J.F. Swart; L.A. Steenweg; W. van der Vlist; J. van Hartingsveldt; Ir. Edgar Osorio; Other staff of the DIMES measurement room; T. Knežević; Ing. F. Molkenboer; R. Naulaerts; Sha Xia;
Optical measurement	Dr. F. Scholze; Dr. A. Gottwald; C. Laubis; U. Kroth;
User committee member of STW project (project nr.: 10024)	ASML; FEI; PTB; ASM; TNO;
Owner of the reprinted figures	American Institute of Physics; IOP Publishing; Dr. Raj Korde; Dr. K. Solt; Dr. F. Scholze; Prof. Lis K. Nanver;
Other staff members of the EI Lab	Kofi; Paddy; Michiel; Joyce; Karen; Willem; Piet; Jeroen; Ger; Jeff; Antoon; etc.

Acknowledgements

English review and Dutch translation	Sarah von Galambos; Prof. G.C.M. Meijer;
Help besides scientific research	Dr. Stoyan Nihtianov; Prof. Lis K. Nanver; Prof. GuoQi Zhang; Prof. P.M. Sarro;
Colleagues and friends	Mohammad; Sha and Jie; Ruimin and Chi; Zili and Shubin; Chung-Kai; Ning; Zhichao; Agung; Darko; Caspar; Yue Chen; Lukasz; Sharma; Ali Heidary; Maureen; Deva; Qinwen and Jia Wei; Vahid; Agata; Huaiwen; Kamran; Jiaming; Yang Xu; Zeyu; Jawei Xu; Rao; Lin Qi; Negin; Yujian; Gianpaolo; Amir; Caroline; Dr. Li and Dr. Wang; etc.
Love and encouragement	Family Guo: Qian and Cheng, Specially to Youyou and Hehe; Family Su: Mengmeng and Yanliang, Specially to Qiaoqiao; My cousin's Family: Xin and Zhen, Specially to Youzi; My parents.

About the Author



Lei Shi was born in Harbin, China. He got his bachelor degree in Electrical Engineering, at Harbin Engineering University, China, in 2003; and received his master degree in Microelectronics, at Delft University of Technology, the Netherlands, in 2007. He is currently a Ph.D. candidate in the Electronics Instrumentation Laboratory of Delft University of Technology. His research mainly focuses on Semiconductor-based UV photodetectors.

